Two neuronal peptides encoded from a single transcript regulate mitochondrial complex III in *Drosophila*

Justin A. Bosch[1,*], Berrak Ugur[2,†], Israel Pichardo-Casas[1], Jorden Rabasco[1], Felipe Escobedo[1], Zhongyuan Zuo[2], Ben Brown[3], Susan Celniker[3], David A. Sinclair[1], Hugo Bellen[2,4-6], and Norbert Perrimon[1,6,*].

1) Department of Genetics, Blavatnick Institute, Harvard Medical School, Boston, MA.
2) Department of Molecular and Human Genetics, BCM, Houston, TX 77030, USA
3) Lawrence Berkeley National Laboratory, Berkeley, CA.
4) Jan and Dan Duncan Neurological Research Institute, Texas Children's Hospital, Houston, TX 77030, USA
5) Department of Neuroscience, BCM, Houston, TX 77030, USA
6) Howard Hughes Medical Institute

[†]Current address: Departments of Neuroscience and Cell Biology, Howard Hughes Medical Institute, Yale University School of Medicine, New Haven, Connecticut 06510, USA

***Corresponding authors:**

Justin A. Bosch and Norbert Perrimon (lead contact)
Harvard Medical School
77 Avenue Louis Pasteur
Dept. of Genetics, NRB 336
Boston, MA 02115
617-432-7672
Email: perrimon@genetics.med.harvard.edu (lead contact)
jabosch@hms.harvard.edu

Summary:

Naturally produced peptides (<100 amino acids) are important regulators of physiology, development, and metabolism. Recent studies have predicted that thousands of peptides may be translated from transcripts containing small open reading frames (smORFs). Here, we describe two peptides in *Drosophila* encoded by conserved smORFs, Sloth1 and Sloth2. These peptides are translated from the same bicistronic transcript and share sequence similarities, suggesting that they encode paralogs. Yet, Sloth1 and Sloth2 are not functionally redundant, and loss of either peptide causes animal lethality, reduced neuronal function, impaired mitochondrial function, and neurodegeneration. We provide evidence that Sloth1/2 are highly expressed in neurons, imported to mitochondria, and regulate mitochondrial complex III assembly. These results suggest that phenotypic analysis of smORF genes in *Drosophila* can provide a wealth of information on the biological functions of this poorly characterized class of genes.

Keywords: smORF, peptide, paralogs, mitochondria, complex III, bicistronic transcript, neurodegeneration, *Drosophila*, CRISPR/Cas9

Introduction

Naturally produced peptides are regulators of metabolism, development, and physiology. Well-known examples include secreted peptides that act as hormones (PEARSON *et al.* 1993), signaling ligands (KATSIR *et al.* 2011), or neurotransmitters (SNYDER AND INNIS 1979). This set of peptides are produced by cleavage of larger precursor proteins (FRICKER 2005), peptides can also be directly translated from a transcript with a small open reading frame (smORF) (COUSO AND PATRAQUIM 2017; PLAZA *et al.* 2017; HSU AND BENFEY 2018; YEASMIN *et al.* 2018). Due to their small size (<100 codons), smORFs have been understudied. For example, smORFs are underrepresented in genome annotations (BASRAI *et al.* 1997), are theoretically a poor target for EMS mutagenesis, and are often ignored in proteomic screens. Consequently, there is growing interest in this class of protein-coding gene as a potentially rich source of novel bioactive peptides (MUDGE *et al.* 2022).

A major obstacle in identifying smORFs that encode functionally important peptides is distinguishing them from the enormous number of smORFs present in the genome by chance (e.g. 260,000 in yeast) (BASRAI *et al.* 1997). Many groups have identified and categorized smORFs with coding potential using signatures of evolutionary conservation, ribosomal profiling, and mass spectrometry (SAGHATELIAN AND COUSO 2015; COUSO AND PATRAQUIM 2017; PLAZA *et al.* 2017). Together, these approaches suggest there may be hundreds, possibly thousands, of unannotated smORF genes. However, these “omics” methods do not tell us which smORFs encode peptides with important biological functions.

Functional characterization of smORF genes in cell lines and model organisms has the potential to confidently identify novel peptides. Historically, unbiased genetic screens and gene cloning led to the fortuitous identification and characterization of smORF peptides (e.g. POLARIS (CASSON *et al.* 2002), RpL41 (SUZUKI *et al.* 1990), Nedd4 (KUMAR *et al.* 1993), *Drosophila* pri/tal (GALINDO *et al.* 2007)). More recently, candidate bioinformatically-predicted smORF-encoded peptides (aka SEPs) have been targeted for characterization (e.g., DWORF (NELSON *et al.* 2016), Elabela/toddler (CHNG *et al.* 2013; PAULI *et al.* 2014), Myomixer (BI *et al.* 2017), Myoregulin (ANDERSON *et al.* 2015), and Sarcolamban (MAGNY *et al.* 2013), and Hemotin (PUEYO *et al.* 2016)). Collectively, these studies have been invaluable for assigning biological functions to smORF peptides. Therefore, continued functional characterization is needed to tackle the enormous number of predicted smORF peptides.

Here, through an effort to systematically characterize human-conserved smORF genes in *Drosophila* (in preparation), we identified two previously unstudied smORF peptides CG32736-PB and CG42308-PA that we named Sloth1 and Sloth2 based on their mutant phenotypes. Remarkably, both peptides are translated from the same transcript and share amino acid sequence similarity, suggesting that they encode paralogs. Loss of function analysis revealed that

each peptide is essential for viability, and mutant animals exhibit defective neuronal function and photoreceptor degeneration. These phenotypes can be explained by our finding that Sloth1 and Sloth2 localize to mitochondria and play an important role in complex III assembly. Finally, we propose that both peptides bind in a shared complex. These studies uncover two new components of the mitochondria and demonstrate how functional characterization of smORFs will lead to novel biological insights.

Results

sloth1 and *sloth2* are translated from the same transcript and are likely distantly related paralogs

Current gene annotations for *sloth1* and *sloth2* (aka *CG32736* and *CG42308*, respectively) indicate that they are expressed from the same transcript (Flybase, Figure 1A), known as a bicistronic (or dicistronic) gene (BLUMENTHAL 2004; CROSBY *et al.* 2015; KARGINOV *et al.* 2017). For example, nearby transcription start sites (Figure 1A) are predicted to only generate a single transcript (HOSKINS *et al.* 2011). In addition, a full-length transcript containing both smORFs is present in the cDNA clone RE60462 (GenBank Acc# AY113525), which was derived from an embryonic library (STAPLETON *et al.* 2002), and we detected the full-length bicistronic transcript by RT-PCR amplification from total RNA from 3rd instar larvae, adult flies, and S2R+ cells (Supplemental Figure 1). In addition, the encoded peptides Sloth1 and Sloth2 have subtle sequence similarity (27%), are similar in size (79aa and 61aa, respectively), and each contain a predicted single transmembrane domain (Figure 1B). While this type of gene structure is relatively rare in eukaryotes (BLUMENTHAL 2004; KARGINOV *et al.* 2017), there are known cases in *Drosophila* of multicistronic transcripts encoding smORF paralogs – the *pri*/*tal* locus (GALINDO *et al.* 2007) and the *Sarcolamban* locus (MAGNY *et al.* 2013). Furthermore, it is well known that paralogs are often found adjacent to each other in the genome due to tandem duplication (TAYLOR AND RAES 2004). Therefore, we propose that *sloth1* and *sloth2* are paralogs translated from the same transcript.

Sloth1 and Sloth2 closely resemble their human orthologs (SMIM4 and C12orf73*)*, based on sequence similarity, similar size, and presence of a transmembrane domain (Figure 1B). Like Sloth1 and Sloth2, SMIM4 and C12orf73 also have subtle amino acid sequence similarity to each other (Figure 1B). In addition, *sloth1* and *sloth2* are conserved in other eukaryotic species (Figure 1C). Remarkably, *sloth1* and *sloth2* orthologs in choanoflagelate, sea squirt, and lamprey exhibit a similar bicistronic gene architecture as *Drosophila* (Figure 1C, Supplemental File 1). In contrast, *sloth1* and *sloth2* orthologs in jawed vertebrates (e.g. mammals) are located on different chromosomes (e.g. human Chr.3 and Chr.12, respectively). Interestingly, we only found one ortholog similar to *sloth2* in the evolutionarily distant *Plasmodium*, and two orthologs similar to *sloth2* in *Arabidopsis*, which are located on different chromosomes

231 (Figure 1C). Therefore, we hypothesize that the *sloth1* and *sloth2* ORFs
232 duplicated from an ancient single common ancestor ORF and became unlinked
233 in animals along the lineage to jawed vertebrates.
234
235 We next investigated *sloth1* and *sloth2* translation parameters and efficiency,
236 since their ORFs are frameshifted relative to each other (Figure 1A) and they are
237 not separated by an obvious internal ribosome entry site (IRES) (VAN DER KELEN
238 *et al.* 2009). Remarkably, only five nucleotides separate the stop codon of the
239 upstream ORF (*sloth1*) and the start codon of the downstream ORF (*sloth2*)
240 (Figure 1A). Therefore, *sloth1* should be translated first and inhibit translation of
241 *sloth2*, similar to the functions of so-called upstream ORFs (uORFs) (THOMPSON
242 2012). However, *sloth1* has a non-optimal Kozak sequence 5' to the start codon
243 (*ACACATG*) and *sloth2* has an optimal Kozak (*CAAAATG*) (CAVENER 1987).
244 Therefore, scanning ribosomes may occasionally fail to initiate translation on
245 *sloth1*, in which case they would continue scanning and initiate translation on
246 *sloth2*, known as "leaky scanning" translation (THOMPSON 2012).
247
248 To test this translation model, we constructed an expression plasmid with the
249 *Renilla Luciferase* (*RLuc*) reporter gene downstream of *sloth1* (*sloth1-RLuc*),
250 while retaining non-coding elements of the original transcript (5' UTR, Kozak
251 sequences, 5bp intervening sequence) (Figure 1D). By transfecting this reporter
252 plasmid into *Drosophila* S2R+ cells, along with a *Firefly Luciferase* (*FLuc*) control
253 plasmid, we could monitor changes in translation of the downstream ORF by the
254 ratio of RLuc/FLuc luminescence. Using derivatives of the reporter plasmid with
255 Kozak or ATG mutations, we found that translation of the downstream ORF
256 increased when translation of *sloth1* was impaired (Figure 1E). Reciprocally,
257 translation of the downstream ORF was decreased when *sloth1* translation was
258 enhanced with an optimal Kozak. These results suggest that *sloth1* inhibits
259 translation of *sloth2*, and that balanced translation of both smORFs from the
260 same transcript might be achieved by suboptimal translation of *sloth1*.
261
262 **_sloth1_ and _sloth2_ are essential in _Drosophila_ with non-redundant function**
263
264 To determine if *sloth1* and *sloth2* have important functions in *Drosophila*, we
265 used in vivo loss of function genetic tools. We used RNA interference (RNAi) to
266 knock down the *sloth1-sloth2* bicistronic transcript. Ubiquitous expression of an
267 shRNA targeting the *sloth1* coding sequence (Figure 2A) lead to significant
268 knockdown of the *sloth1-sloth2* transcript in 3rd instar larvae (Figure 2B), as
269 determined by two different primer pairs that bind to either the *sloth1* or *sloth2*
270 coding sequence. Ubiquitous RNAi knockdown of *sloth1-sloth2* throughout
271 development lead to reduced number of adult flies compared to a control (Figure
272 2C). This reduced viability was largely due to adult flies sticking in the food after
273 they eclosed from their pupal cases (Figure 2D). Escaper knockdown flies were
274 slow-moving and had 30% climbing ability compared to control flies (Figure 2E).
275 RNAi knockdown flies also had short scutellar bristles (Figure 2F).
276

277 We confirmed our RNAi results using CRISPR/Cas9 to generate somatic
278 knockout (KO) flies. By crossing flies ubiquitously expressing Cas9 (*Act-Cas9)*
279 with flies expressing an sgRNA that targets the coding sequence of either *sloth1*
280 or *sloth2* (Figure 2A, Supplemental Figure 2A), the resulting progeny will be
281 mosaic for insertions and deletions (indels) that cause loss of function in somatic
282 cells (PORT *et al.* 2014; XUE *et al.* 2014). Both *sloth1* and *sloth2* somatic KO flies
283 had significantly reduced viability compared to controls (Figure 2G). Furthermore,
284 escaper adults had short scutellar bristles (Figure 2H) and frequently appeared
285 sluggish. Importantly, similar phenotypes were observed when targeting either
286 *sloth1* or *sloth2*.
287
288 Next, we further confirmed our loss of function results using CRISPR/Cas9 in the
289 germ line to generate KO lines for *sloth1* and *sloth2*. These reagents are
290 particularly important to test if *sloth1* and *sloth2* have redundant function by
291 comparing the phenotypes of single and double null mutants. We generated four
292 KO lines (Figure 2A, Supplemental Figure 2A-C): 1) a frameshift indel in *sloth1*
293 (*sloth1*-KO), 2) a frameshift indel in *sloth2* (*sloth2*-KO), 3) a 552 bp deletion of
294 the *sloth1* and *sloth2* reading frames (dKO), and 4) a knock-in of the reporter
295 gene *Gal4* that removes *sloth1* and *sloth2* coding sequences (*Gal4-KI*). Since
296 *sloth1* and *sloth2* are on the X-chromosome, we analyzed mutant hemizygous
297 male flies. All four mutant lines were hemizygous lethal, which were rescued by a
298 genomic transgene (Figure 2I,), ruling out off-target lethal mutations on the X-
299 chromosome. Like RNAi and somatic KO results, rare mutant adult escaper flies
300 had slower motor activity (Figure 2J) and short scutellar bristles (Figure 2K).
301 Furthermore, the short scutellar bristle phenotype and slower motor activity could
302 be rescued by a genomic transgene (Figure 2J, K).
303
304 The phenotypic similarity of single and double mutants suggests that *sloth1* and
305 *sloth2* are not functionally redundant. However, since both ORFs are encoded on
306 the same transcript, it is unclear if mutating one ORF will affect the other. For
307 example, a premature stop codon can induce non-sense mediated decay of an
308 entire transcript (NICKLESS *et al.* 2017). To address this possibility, we performed
309 additional fly lethality rescue experiments. First, transheterozygous female flies
310 (*sloth1-KO*/+, *sloth2-KO*/+) were viable and had normal scutellar bristles.
311 Second, we created single ORF versions of a genomic rescue transgene –
312 *{Δsloth1-sloth2}* and {*sloth1*-Δ*sloth2*} (Supplemental Figure 2A). We found that
313 *sloth1-KO* lethality could only be rescued by {*sloth1*-Δ*sloth2*}, and vice versa,
314 *sloth2-KO* lethality could only rescued by {Δ*sloth1-sloth2*} (Figure 2L).
315 Furthermore, single ORF rescue transgenes were unable to rescue the lethality
316 of *dKO* and *Gal4-KI* lines (Figure 2L). Third, we used the Gal4/UAS system
317 (BRAND AND PERRIMON 1993) to rescue mutant lethality with ubiquitously
318 expressed cDNA transgenes. These results showed that single ORF KOs could
319 only be rescued by expression of the same ORF (Figure 2L). Similar results were
320 found by expressing cDNAs encoding the human orthologs (Figure 2L). In all,
321 these results show that both *sloth1* and *sloth2* are essential, have similar loss of

322 function phenotypes, are not functionally redundant with one another, and are
323 likely to retain the same function as their human orthologs.
324
325 **Loss of *sloth1* and *sloth2* leads to defective neuronal function and**
326 **degeneration**
327
328 Since loss of *sloth1* and *sloth2* caused reduced adult mobility and climbing
329 defects (Figure 2E, J), we speculated that the two peptides normally play an
330 important role in the brain or muscle. To determine where *sloth1* and *sloth2* are
331 expressed, we used the *Gal4-KI* line as an in vivo transcriptional reporter. *Gal4-*
332 *KI* mobility defects and lethality could be rescued by expressing the entire
333 bicistronic transcript (*UAS-sloth1-sloth2*) (Figure 2J, L), or coexpression of both
334 smORFs as cDNA (*UAS-sloth1* and *UAS-sloth2)* (Figure 2L). Thus, the *Gal4-KI*
335 line is likely an accurate reporter of *sloth1* and *sloth2* expression. By crossing
336 *Gal4-KI* flies with a *UAS-GFP* fluorescent reporter, we observed strong GFP
337 expression in larval (Figure 3A, B) and adult brains (Figure 3C). In addition, *Gal4-*
338 *KI* is expressed in motor neurons at the larval neuromuscular junction (NMJ)
339 (Figure 3D) and in larval brain cells that are positive for the neuronal marker Elav
340 (Figure 3E).
341
342 We then tested if *sloth1* and *sloth2* were important for neuronal function by
343 measuring neuronal electrical activity in *dKO* animals. Electrical recordings taken
344 from the larval NMJ showed that *dKO* motor neurons have normal excitatory
345 junction potential (EJP) under resting conditions at 0.75 mM Ca^{2+} (Supplemental
346 Figure 3). However, under high frequency stimulation (10hz), *dKO* NMJs could
347 not sustain a proper response (Figure 4A), indicating that there is a defect in
348 maintaining synaptic vesicle pools. Importantly, this phenotype is rescued by a
349 genomic transgene. To test if a similar defect is present in the adults, we
350 assessed phototransduction and synaptic transmission in photoreceptors via
351 electroretinogram (ERG) recordings (WU AND WONG 1977; HARDIE AND RAGHU
352 2001). ERGs recorded from young (1-3 days old) *dKO* photoreceptors showed
353 an amplitude similar to that of genomic rescue animals (Figure 4B). However,
354 upon repetitive light stimulation, ERG amplitudes were significantly reduced
355 (Figure 4B), suggesting a gradual loss of depolarization. Similar results were
356 observed when young flies were raised in 24hr dark (Figure 4C). Moreover, ERG
357 traces also showed a progressive loss of “on” and “off” transients (Figure 4B, C),
358 which is indicative of decreased synaptic communication between the
359 photoreceptor and the postsynaptic neurons. ERG phenotypes are rescued by a
360 full-length genomic rescue transgene, but not by single ORF rescue transgenes
361 (Figure 4B, C). To test if loss of both *sloth1* and *sloth2* lead to
362 neurodegeneration, we aged the animals for 4-weeks in 12hr light/dark cycle or
363 constant darkness and recorded ERGs. Similar to young animals, aged animals
364 raised in light/dark conditions also displayed a reduction in ERG amplitude upon
365 repetitive stimulation (Figure 4E). These results indicate that both *sloth1* and
366 *sloth2* are required for sustained neuronal firing in larval motor neurons and adult
367 photoreceptors. Interestingly, similar mutant phenotypes in the NMJ and

368 photoreceptors are known to be due to defects in ATP production (VERSTREKEN
369 *et al.* 2005; SANDOVAL *et al.* 2014; JAISWAL *et al.* 2015).
370
371 In addition to measuring neuronal activity, we analyzed *dKO* neurons for changes
372 in morphology and molecular markers. Confocal imaging of the NMJ in *dKO* 3rd
373 instar larvae did not reveal obvious changes in synapse morphology or markers
374 of synapse function (Supplemental Figure 4). In contrast, using transmission
375 electron microscopy (TEM) of sectioned adult eyes, we observed reduced
376 photoreceptor number and aberrant morphology such as enlarged
377 photoreceptors and thinner glia in *dKO* animals (Figure 5A-C), suggestive of
378 degeneration. These phenotypes were rescued by a genomic transgene, but not
379 with single ORF rescue constructs (Figure 5A-C, Supplemental Figure 5).
380 Furthermore, these phenotypes were similar between young and aged flies, as
381 well as aged flies raised in the dark (Figure 5A-C, Supplemental Figure 5). It is
382 known that mutations affecting the turnover of Rhodopsin protein (Rh1) can lead
383 to photoreceptor degeneration (ALLOWAY *et al.* 2000; JAISWAL *et al.* 2015). To test
384 if this mechanism is occurring in *dKO* photoreceptors, we imaged Rh1 protein
385 levels using confocal microscopy. We observed Rh1 accumulation in
386 degenerating *dKO* photoreceptors in 4 week aged flies exposed to light (Figure
387 5D). However, Rh1 accumulation was milder in 4 week aged flies raised in the
388 dark (Supplemental Figure 6). These results point out that light stimulation, and
389 hence activity, enhance degeneration due to Rh1 accumulation in *dKO* animals.
390
391 **Sloth1 and Sloth2 localize to mitochondria and their loss impairs normal**
392 **respiration and ATP production**
393
394 Mitochondrial dysfunction in *Drosophila* is known to cause phenotypes that are
395 reminiscent of loss of *sloth1* and *sloth2*, such as pupal lethality, reduced neuronal
396 activity, photoreceptor degeneration, and Rh1 accumulation in photoreceptors
397 (JAISWAL *et al.* 2015). Therefore, we investigated the possible role of Sloth1 and
398 Sloth2 in mitochondria.
399
400 Prior to our work, a large-scale study of human protein localization suggested
401 that SMIM4 and C12orf73 localize to mitochondria in cultured cells (THUL *et al.*
402 2017). SMIM4 has a predicted mitochondrial targeting sequence using MitoFates
403 (FUKASAWA *et al.* 2015) (0.842), but C12orf73, Sloth1, and Sloth2 do not (.0016,
404 0.016, 0.009, respectively). In addition, SMIM4 and Sloth1 are predicted to
405 localize to the mitochondrial inner membrane using DeepMito (0.93 and 0.73,
406 respectively), but C12orf73 and Sloth2 are not (0.66 and 0.49, respectively)
407 (SAVOJARDO *et al.* 2020). To test if Sloth1/2 localize to mitochondria in
408 *Drosophila*, we transfected S2R+ cells with Sloth1-FLAG or Sloth2-FLAG. Both
409 Sloth1 and Sloth2 proteins colocalized with the mitochondrial marker ATP5α
410 (Figure 6A). Furthermore, Sloth1-FLAG and Sloth2-FLAG were enriched in
411 mitochondrial fractions relative to cytoplasmic fractions (Figure 6B). Similar
412 results were observed using stable S2R+ cell lines that express streptavidin

binding peptide (SBP) tagged Sloth1 or Sloth2 under a copper inducible promoter (*MT-Sloth1-SBP* and *MT-Sloth2-SBP*) (Figure 6C).

Next, we raised antibodies to Sloth1/2 to determine their endogenous localization. Using two independently generated antibodies for each peptide, immunolocalization in larval brains from wild-type or *sloth1/2* dKO animals showed no overlapping signal with a mitochondrial marker and no clear signal above background (Supplemental Figure 7). Furthermore, we did not detect Sloth1 or Sloth2 bands of the expected molecular weight on western blots from wild-type S2R+ whole cell lysates or isolated mitochondria using anti-Sloth1, anti-Sloth2, anti-SMIM4, or anti-C12orf73 (Supplemental Figure 8A-C). In contrast, anti-Sloth1 western blots of mitochondria isolated from 3rd instar larvae and adult thoraxes showed a <15kDa band that is absent from *sloth1/2* KO or RNAi samples (Supplemental Figure 8D), suggesting this band corresponds to endogenous Sloth1. Unfortunately, anti-Sloth2 failed to detect a similar band under the same conditions (Supplemental Figure 8D).

Since our Sloth1/2 antibodies may not be sensitive enough to detect the endogenous peptides, we generated a stable S2R+ cell line expressing *sloth1/2* transcript under a copper inducible promoter (*MT-sloth1/2*) and induced expression for 16hrs. Anti-Sloth1 and anti-Sloth2 western blots of mitochondria isolated from *MT-sloth1/2* cells detected <15kDa bands that did not appear in wild-type S2R+ cells, and thus are likely Sloth1 and Sloth2 peptides translated from the overexpressed *sloth1/2* transcript (Supplemental Figure 8B). Furthermore, Sloth1 and Sloth2 were enriched in *MT-sloth1/2* mitochondrial fractions relative to cytoplasmic fractions (Figure 6D), similar to the results obtained with FLAG and SBP-tagged peptides (Figures 6B-C). Based on their amino acid sequence, Sloth1 and Sloth2 are predicted to run at 9.3kDa and 6.7kDa, respectively. While Sloth1 does appear to run larger than Sloth2, both peptides run ~2kDa larger than expected (Figure 6D).

A method of assaying defects in mitochondrial function is measuring cellular oxygen consumption from live cells with a Seahorse stress test. Since this typically involves assaying a monolayer of cells, we generated KO S2R+ cell lines using CRISPR/Cas9. Compared to control cells, single KO and double KO S2R+ cells (Supplemental Figure 9A, B) had reduced basal respiration (Figure 7A, B), ATP production (Supplemental Figure 9C), and proton leaks (Supplemental Figure 9D). Results were similar for single KO and dKO lines. These results suggest that both *sloth1* and *sloth2* are required to support normal mitochondrial respiration in S2R+ cells.

Next, we assayed *sloth1* and *sloth2* mutant flies for defects in mitochondrial function. ATP levels are an important indicator of mitochondrial function (KANN AND KOVACS 2007; GOLPICH *et al.* 2017) and mutations in *Drosophila* mitochondrial genes can lead to reduced ATP levels (JAISWAL *et al.* 2015). Indeed, *dKO* larvae had ~60% ATP compared to control larvae, which was

459 rescued by a genomic transgene (Figure 7C). Impaired mitochondrial function
460 can also lead to cellular stress responses, such as increased expression of the
461 mitochondrial chaperone Hsp60 (PELLEGRINO *et al.* 2013). Western blot analysis
462 showed that *Drosophila* Hsp60 was elevated in lysates from mutant larval brains
463 compared to control, and this effect was rescued by a genomic transgene (Figure
464 7D). Finally, mitochondrial dysfunction can cause changes in mitochondrial
465 morphology and number (TREVISAN *et al.* 2018). There were no obvious changes
466 in mitochondrial morphology in mutant larval motor neurons (Supplemental
467 Figure 4, Supplemental Figure 9E), and adult mutant photoreceptors contained
468 mitochondria with normal cristae (Figure 7E). In contrast, mitochondrial number
469 was increased in mutant photoreceptors in aged animals (Figure 7E,
470 Supplemental Figure 10A) and decreased in mutant photoreceptors in young
471 animals (Figure 7F, Supplemental Figure 10B). In all, these data suggest that
472 Sloth1 and Sloth2 localize to mitochondria and are important to support
473 respiration and ATP production.
474
475 **Sloth1/2 regulate respiratory complex III assembly**
476
477 While our study was in preparation, two studies demonstrated that human
478 SMIM4 and C12orf73 are inner mitochondrial membrane peptides important for
479 complex III assembly and physically interact with complex III subunits (ZHANG *et*
480 *al.* 2020; DENNERLEIN *et al.* 2021). If Sloth1 or Sloth2 have similar roles in
481 *Drosophila*, this could explain why *sloth1/2* mutant flies have reduced ATP
482 production.
483
484 To test for a role in Sloth1/2 in respiratory complex assembly, we visualized the
485 relative abundance of individual complexes and subunits in wild-type vs *sloth1/2*
486 loss of function animals. First, we resolved native respiratory complexes using
487 blue native polyacrylamide gel electrophoresis (BN-PAGE). Using mitochondria
488 isolated from adult thorax, we identified the five respiratory complexes (CI, CII,
489 CIII, CIV, CV) based on molecular weight and a previous study that established
490 this protocol (GARCIA *et al.* 2017). Importantly, a ~600kDa band corresponding to
491 complex III was diminished in mitochondria isolated from thoraxes with *sloth1/2*
492 knockdown (Figure 8A). Similarly, the complex III band was diminished in
493 mitochondria isolated from *sloth1/2* knockout 3rd instar larvae (Figure 8B). This
494 change was rescued by a wild-type genomic transgene, but not single paralog
495 transgenes (Figure 8B). Next, we detected individual respiratory subunits by
496 SDS-PAGE and western blotting of isolated mitochondria. Using antibodies that
497 recognize UQCR-C2, the fly homolog of human complex III subunit UQCRC2, we
498 found that the ~40kDa band corresponding to UQCR-C2 was diminished in
499 mitochondria isolated from *sloth1/2* RNAi adult thoraxes (Figure 8C), as well as
500 *sloth1/2* knockout 3rd instar larvae (Figure 8D).
501
502 To test whether Sloth1/2 physically interact with subunits of mitochondrial
503 complex III, we performed co-immunoprecipitation experiments in transfected
504 S2R+ cells. SMIM4 and C12orf73 interact with complex III subunits UQCC1 and

505 UQCRFS1, respectively (ZHANG *et al.* 2020; DENNERLEIN *et al.* 2021). Therefore,
506 we tested if Sloth1 or Sloth2 could immunoprecipitate the fly homologs CG10075
507 (dUQCC1) or RFeSP (dUQCRFS1). Using Sloth1-FLAG as bait, we detected
508 CG10075-HA (Figure 8E) and RFeSP-HA (Figure 8F) binding to anti-FLAG
509 beads. In contrast, Sloth2-FLAG pulled-down CG10075-HA and RFeSP-HA
510 weakly or was at background levels (Figure 8E,F). Together, these results
511 suggest that Sloth1/2 are required for proper complex III assembly, mediated
512 through physical interaction with complex III subunits.
513
514 **Sloth1 and Sloth2 act in a stoichiometric complex**
515
516 We speculated that Sloth1 and Sloth2 could physically interact, based on the
517 observation that both share the same loss of function phenotypes and subcellular
518 localization. Indeed, some paralogs bind to the same protein complex
519 (SZKLARCZYK *et al.* 2008) and there is a tendency for proteins in the same
520 complex to be co-expressed (PAPP *et al.* 2003). To confirm this putative
521 interaction between Sloth1 and Sloth2, we used co-immunoprecipitation and
522 western blotting. This revealed that Sloth1-FLAG could immunoprecipitate
523 Sloth2-HA (Figure 9A), and reciprocally Sloth2-FLAG (Figure 9B) could
524 immunoprecipitate Sloth1-HA. Interestingly, the levels of tagged peptide in cell
525 lysates were higher when the opposite peptide was overexpressed (Figure 9A,B).
526 Proteins in a complex commonly have important stoichiometry and unbound
527 proteins can be degraded to preserve this balance (PAPP *et al.* 2003; SOPKO *et*
528 *al.* 2006; VEITIA *et al.* 2008; PRELICH 2012; BERGENDAHL *et al.* 2019).
529 Furthermore, imbalanced protein complex stoichiometry can lead to
530 haploinsufficient or dominant negative phenotypes (PAPP *et al.* 2003; SOPKO *et*
531 *al.* 2006; VEITIA *et al.* 2008; PRELICH 2012; BERGENDAHL *et al.* 2019).
532
533 To test this possibility for Sloth1/2, we overexpressed either *sloth1* or *sloth2* in
534 vivo. Low-level ubiquitous overexpression (using *da-Gal4*) of either *UAS-sloth1*
535 or *UAS-sloth2* cDNA had no effect on adult fly viability (Figure 2L). To increase
536 expression levels, we used the strong ubiquitous driver *tub-Gal4*. Whereas
537 *tub>sloth1* flies were viable as adults, *tub>sloth2* animals were 100% pupal lethal
538 (Figure 9C). However, *tub>sloth2* animals could be rescued to adulthood by co-
539 expression of *sloth1*. Importantly, this rescue was not due to dilution of the Gal4
540 transcription factor on two *UAS* transgenes, since co-expression of *UAS-*
541 *tdtomato* did not rescue *tub>sloth2* lethality. Finally, *tub-Gal4* overexpression of
542 the entire *sloth1-sloth2* bicistronic transcript resulted in viable adult flies. In all,
543 these results suggest that Sloth1 and Sloth2 interact in a complex where their
544 stoichiometric ratio is important for normal function.
545
546 **Discussion**
547
548 Here, we have assigned new functions to two previously uncharacterized smORF
549 peptides. Sloth1 and Sloth2 appear to be distantly-related paralogs, yet each is
550 important to support mitochondrial and neuronal function in *Drosophila*. We

propose a model where Sloth1 and Sloth2 peptides are translated from the same transcript, imported into mitochondria where they interact with each other and complex III to promote its assembly (Figure 10). Our results are supported by two recent studies published during preparation of this manuscript, in which human Sloth1 (SMIM4) and Sloth2 (C12orf73/Brawnin) were discovered as novel mitochondrial complex III assembly factors in cultured human cells and zebrafish (ZHANG *et al.* 2020; DENNERLEIN *et al.* 2021).

Muti-cistronic genes are relatively rare in eukaryotes, but some have been characterized in *Drosophila* (GALINDO *et al.* 2007; MAGNY *et al.* 2013) and mammals (KARGINOV *et al.* 2017). Similar to operons in prokaryotes, it is thought that multicistronic transcripts allow for coordinated expression of proteins in the same pathway or complex (KARGINOV *et al.* 2017). Indeed, the similarity of loss of function phenotypes between *sloth1* and *sloth2* suggest that they function together in the same pathway/complex. Interestingly, 44/196 annotated bicistronic genes in *Drosophila* contain two ORFs with homology to each other (Flybase, DIOPT), and a recent study suggests that human bicistronic genes containing a smORF frequently encode physically interacting peptide/protein pair (CHEN *et al.* 2020). Therefore, related peptides encoded on the same transcript may be a prevalent phenomenon in eukaryotes. ORF translation in multicistronic transcripts can occur by different mechanisms, such as re-initiation of translation, IRES, or leaky ribosome scanning (VAN DER KELEN *et al.* 2009). Our data and observations support leaky scanning, and we propose a model whereby both peptides are translated because *sloth1* contains a non-optimal Kozak sequence.

The presence of *sloth1* and *sloth2* orthologs in many eukaryotic species suggest that their function is likely broadly conserved. Indeed, we could rescue the lethality of *sloth1* and *sloth2* mutant flies by expressing their human counterparts. Interestingly, *Plasmodium* and *Arabidopsis* only have homologs with similarity to *sloth2*. Perhaps *sloth2* maintained functions more similar to its common ancestor with *sloth1*. We were unable to identify homologs in some eukaryotes such as yeast, though their amino acid sequence may simply be too diverged for detection using bioinformatic programs such as BLAST.

The physical interactions of Sloth1-Sloth2, Sloth1-RFeSP, and Sloth1-CG10075, and complex III assembly defects in *sloth1/2* loss of function animals, suggest that Sloth1/2 together regulate complex III assembly. Indeed, Sloth1 is bioinformatically predicted to localize to the mitochondrial inner membrane (DeepMito), and Sloth1 and Sloth2 have predicted transmembrane domains (TMHMM 2.0), suggesting they interact with complex III at the inner membrane. This is supported by data showing SMIM4 and C12orf73 are integral membrane proteins in the mitochondrial inner membrane (ZHANG *et al.* 2020; DENNERLEIN *et al.* 2021). In addition, our data suggests that Sloth1 and Sloth2 interact in a stoichiometric manner, explaining why single mutants have the same phenotype as double mutants. This is supported by the finding that SMIM4 protein levels are dependent on the presence of C12orf73 and vice versa (DENNERLEIN *et al.* 2021).

597 Perhaps maintenance of the proper ratio of Sloth1/2 is an important factor for
598 optimal complex III assembly. Future experiments could address whether Sloth1
599 and Sloth2 directly bind each other, or if they require complex III subunits for
600 physical association.
601
602 Several observations and experiments suggest that Sloth1/2 peptides do not
603 have equivalent function. The two peptides have weak homology to each other
604 (27% identity) and Sloth1 has 18aa (30%) more than Sloth2, suggesting
605 divergence of function. Unlike Sloth1, Sloth2 does not have a clear
606 mitochondrial-targeting signal. Perhaps Sloth2 has a cryptic signal that is not
607 recognized by prediction software, or Sloth2 may be co-imported with Sloth1.
608 Furthermore, we could not detect robust immunoprecipitation of RFeSP or
609 CG10075 using Sloth2 as bait. Perhaps Sloth2 binds complex III indirectly
610 through Sloth1, or Sloth 2 binds a different complex III subunit. More likely is that
611 both Sloth1 and Sloth2 need to be present for binding to complex III, and the
612 endogenous Sloth1 present under conditions of Sloth2-FLAG overexpression is
613 insufficient for co-IP assays. Sloth2 may also be less stable than Sloth1, which
614 could potentially explain why were unable to detect endogenous Sloth1 using
615 anti-Sloth1 antibodies. Interestingly, only strong overexpression of Sloth2, and
616 not Sloth1, was lethal to flies. Future studies may elucidate the mechanism
617 explaining these functional differences in Sloth1/2.
618
619 Neurons have a high metabolic demand and critically depend on ATP generated
620 from mitochondria to support processes such as neurotransmission (VERSTREKEN
621 *et al.* 2005; KANN AND KOVACS 2007). Therefore, it is not unexpected that
622 neurodegenerative diseases are frequently associated with mitochondrial
623 dysfunction (GOLPICH *et al.* 2017). We find similar results in *Drosophila*, where
624 loss of *sloth1* and *sloth2* leads to defects in mitochondrial function, impaired
625 neuronal function, photoreceptor degeneration, and Rh1 accumulation in
626 photoreceptors. Despite finding that the *Gal4-KI* reporter was strongly expressed
627 in neurons and could rescue *sloth1/2* lethality, it is likely these peptides play
628 important roles in other cell types. For example, publicly available RNA-seq data
629 suggest that they are ubiquitously expressed (Flybase). In addition, neuronal
630 expression of *sloth1* or *sloth2* was unable to rescue mutant lethality (Figure 2L).
631 Furthermore, we observed *sloth1/2* loss of function phenotypes in dissected adult
632 thoraxes, which are composed of mostly muscle. At present, there are no
633 reported human disease-associated mutations in *SMIM4* and *C12orf73*.
634 Mutations in these genes might not cause disease, or they might cause lethality.
635 It is also possible that the lack of functional information on these genes has
636 hampered identification of disease-associated mutations.
637
638 There is great interest in identifying the complete mitochondrial proteome (CALVO
639 *et al.* 2016), so it is remarkable that Sloth1/2 have been largely missed in
640 proteomic or genetic screens for mitochondrial components. For example, they
641 are not present in bioinformatic and proteomic datasets of fly mitochondrial
642 proteins (SARDIELLO *et al.* 2003; CHEN *et al.* 2015), nor in genetic screens of

lethal mutations on the X-chromosome affecting nervous system maintenance (YAMAMOTO *et al.* 2014). It is possible that the small size of these peptides lead to this discrepancy; due to less frequent mutations in these ORFs, or fewer tryptic products for MS. It is also possible that these peptides form weak interactions with mitochondrial proteins, preventing their immunoprecipitation. Recently, human SMIM4 was identified in a proteomic screen (DENNERLEIN *et al.* 2021), human C12orf73 was identified in two proteomics screens (LIU *et al.* 2018; ANTONICKA *et al.* 2020) and a bioinformatic screen (ZHANG *et al.* 2020), and mouse SMIM4 was identified in a proteomics screen (BUSCH *et al.* 2019).

Our discovery of *sloth1* and *sloth2* highlights the effectiveness of loss of function genetics for identifying smORF genes with important biological functions. Recent technical advances such as genome engineering (e.g. CRISPR/Cas9) and massively parallel profiling have the potential to rapidly assign functions to many uncharacterized smORFs (GUO *et al.* 2018; CHEN *et al.* 2020). For example, investigation of uncharacterized smORF genes may yield additional important mitochondrial components. Indeed, there is a greater tendency for annotated human smORF peptides to localize to mitochondria (72/719, 10%) compared to the whole proteome (1228/20351, 6%) (UniProt). Interestingly, ~40 smORF peptides function at the human mitochondrial inner membrane (UniProt), such as the Complex III member UQCRQ (82aa) (USUI *et al.* 1990) and the recently described Mitoregulin/MoxI (56aa) that regulates the electron transport chain and fatty acid β-oxidation (MAKAREWICH *et al.* 2018; STEIN *et al.* 2018; CHUGUNOVA *et al.* 2019). Therefore, modulation of protein complexes in the inner mitochondrial membrane may be a common function of smORF peptides. As functional annotation of hundreds, perhaps thousands, of smORF genes is becoming easier, many new biological insights are likely to emerge from their analyses.

Acknowledgements:

We thank the TRiP and DRSC for help generating transgenic flies, Dr. Marcia Haigis for use of a Seahorse XF analyzer, Claire Hu, Tera Levin, and Dan Richter for bioinformatics help, Lucy Liu for assistance mounting larvae to image the NMJ, Thai LaGraff for help with qPCR, and Rich Binari and Cathryn Murphy for general assistance. We thank members of the BDGP for discussions. We also thank the HMS MicRoN (Microscopy Resources on the North Quad) Core. J.A.B. was supported by the Damon Runyon Foundation. This work was supported by NIH grants R01GM084947, R01GM067761, R24OD019847, and NHGRI HG009352 (S.E.C). N.P. is an investigator of the Howard Hughes Medical Institute.

Author Contributions:

Conceptualization, J.A.B., B.U., I.P., B.B., S.C., H.B., N.P.; Methodology, J.A.B., B.U., I.P., N.P.; Investigation, J.A.B., B.U., I.P., J.R., F.E., Z.Z.; Writing – Original Draft, J.A.B.; Writing – Review & Editing, J.A.B., B.U., I.P., J.R., F.E., Z.Z., S.C.,

H.B., N.P.; Supervision, B.B., S.C., D.A.S., H.B., N.P.; Funding acquisition, J.A.B., B.B., S.C., N.P.

Declaration of Interests:

D.A.S is a consultant to, inventor of patents licensed to and in some cases board member of and owner of equity in MetroBiotech, Cohbar, EdenRoc and Life Biosciences. For more information and affiliations see https://genetics.med.harvard.edu/sinclair

Figure titles and legends:

Figure 1: Bicistronic gene structure of the smORFs *sloth1* and *sloth2.* A. Bicistronic gene model for *sloth1* and *sloth2*. Zoom in shows intervening sequence (*GCAAA*) between *sloth1* stop codon and *sloth2* start codon. **B.** Comparison of protein structure, amino acid length size, and amino acid percent identity between *Drosophila* and Human orthologs. Shaded rectangle indicates predicted transmembrane (TM) domain. **C.** Phylogenetic tree of *sloth1* and *sloth2* orthologs in representative eukaryotic species. Linked gene structure (candidate bicistronic transcript or adjacent separate transcripts) is indicated by a black line connecting red and blue squares. **D.** Plasmid reporter structure of *pMT-sloth1-Rluc* and derivatives. Kozak sequences upstream of start codon are underlined. Mutations indicated with shaded grey box. pMT= Metallothionein promoter. RLuc = Renilla Luciferase. **E.** Quantification of RLuc luminescence/Firefly Luciferase, normalized to *pMT-sloth1-Rluc*, for each construct. Significance of mutant plasmid luminescence was calculated with a T-Test comparing to *pMT-sloth1-Rluc*. Error bars are mean with SEM. **** P≤0.0001. N=4 biological replicates.

Figure 2: *sloth1* and *sloth2* loss of function analysis. A. *sloth1-sloth2* transcript structure with shRNA and sgRNA target locations, primer binding sites, in/del locations, and knock-in Gal4 transgene. **B.** qPCR quantification of RNAi knockdown of the *sloth1-sloth2* transcript. Significance of fold change knockdown was calculated with a T-Test comparing to *da>attP40* for PD43265 and PD43573. Error bars show mean with SEM. P-values *** P≤0.001. N=6. **C.** Quantification of adult fly viability from *sloth1-sloth2* RNAi knockdown. Fly cross schematic (left) and graph (right) with percentage of progeny with or without the CyO balancer. Ratios of balancer to non-balancer were analyzed by Chi square test, **** P≤0.0001. Sample size (N) indicated on graph. **D.** Pictures of fly food vials, focused on the surface of the food. *da>shRNA* flies are frequently found stuck in the fly food. **E.** Quantification of adult fly climbing ability after *sloth1* and *sloth2* RNAi. Significance calculated with a T-test, **** P≤0.0001. Error bars show mean with SD. N=3 biological replicates. **F.** Stereo microscope images of adult fly thorax to visualize the scutellar bristles. RNAi knockdown by *da-Gal4* crossed with either *attP40* or *UAS-shRNA*^{JAB200}*.* Arrowheads point to the two longest scutellar bristles. **G.** Quantification of adult fly viability from *sloth1-sloth2* somatic knockout. Fly cross schematic (left) and graph (right) with percentage of

735 progeny with or without the CyO balancer. Ratios of balancer to non-balancer
736 were analyzed by Chi square test, **** P≤0.0001. Sample size (N) indicated on
737 graph. **H.** (Left) Stereo microscope images of adult fly thorax to visualize the
738 scutellar bristles. Somatic knockout performed by crossing *Act-Cas9* to sgRNAs.
739 (Right) Quantification of the frequency of adult flies with at least one short
740 scutellar bristle after somatic KO of *sloth1* or *sloth2.* Sample sizes indicated on
741 graph. Arrowheads point to the two longest scutellar bristles. **I.** Quantification of
742 adult fly viability from *sloth1-sloth2* hemizygous knockout in males and rescue
743 with a genomic transgene or *UAS-sloth1-sloth2* transgene. Fly cross schematic
744 (left) and graph (right) with percentage of male progeny with or without the FM7c
745 balancer. Sample size (N) indicated on graph. **J.** Still images from video of adult
746 flies inside plastic vials. Images are 5 seconds after vials were tapped. Adult flies
747 climb upward immediately after tapping. All flies are males. Each vial contains 10
748 flies, except dKO, which contains 5 flies. **K.** Stereo microscope images of adult
749 male fly thorax to visualize the scutellar bristles. *attP40* is used as a negative
750 control. Arrowheads point to the two longest scutellar bristles. **L.** Hemizygous
751 mutant male genetic rescue experiments.
752
753 **Figure 3. *sloth1-sloth2* are expressed in neurons A.** Fluorescent stereo
754 microscope images of 3rd instar larvae expressing GFP with indicated genotypes.
755 **B.** Fluorescent compound microscope image of 3rd instar larval brain expressing
756 *UAS-GFP*. DAPI staining labels nuclei. **C.** Confocal microscopy of adult brain
757 with indicated genotypes. Anti-HRP staining labels neurons. **D.** Confocal
758 microscopy of the 3rd instar larval NMJ at muscle 6/7 segment A2 expressing
759 *UAS-GFP*. Anti-FasII staining labels the entire NMJ. **E.** Confocal microscopy of
760 the 3rd instar larval ventral nerve cord (VNC) expressing *Gal4-KI*, *UAS-GFP-nls*.
761 GFP-nls is localized to nuclei. Anti-Elav stains nuclei of neurons. Arrow indicates
762 example nuclei that expresses UAS-GFP and is positive for Elav.
763
764 **Figure 4. *sloth1-sloth2* are important for neuronal function. A.** Traces of
765 electrical recordings from 3rd instar larval NMJ in control, *dKO*, and
766 *dKO+genomic rescue* animals over 10 minutes under high frequency stimulation
767 (10 Hz). Graph on right is a quantification of the relative excitatory junction
768 potential (EJP) for indicated genotypes. Error bars show mean with SD. N ≥ 5
769 larvae per genotype. Significance for each genotype was calculated with a T-Test
770 comparing to control flies. **B-D.** Traces of electroretinogram (ERG) recordings
771 from adult eye photoreceptors upon repetitive stimulation with light (left) and
772 quantification of the relative ERG amplitude for indicated genotypes (right). Error
773 bars show mean with SD. N ≥ 6 larvae per genotype. ** P≤0.01, *** P≤0.001.
774 Significance for each genotype was calculated with a T-Test comparing to control
775 flies. **B.** Recordings were taken from 1-3 days post-eclosion animals that were
776 raised in a 12hr light/dark cycle. “On” and “Off” transients indicated by closed and
777 open arrowhead, respectively. **C.** Recordings were taken from 1-3 days post-
778 eclosion animals that were raised in a 24hr dark. **D.** Recordings were taken from
779 four week aged animals that were raised in a 12hr light/dark cycle.
780

781 **Figure 5. Loss of *sloth1-sloth2* causes neurodegeneration. A-C.**
782 Transmission electron microscopy (TEM) images of sectioned adult eye
783 photoreceptors (left) and quantification of photoreceptor number and aberrant
784 photoreceptors (right). Scalebar is 2μm. Filled red arrows indicate dead or dying
785 photoreceptors. Open red arrows indicate unhealthy photoreceptors. Error bars
786 show mean with SD. N ≥ 8 ommatidium per genotype. **A.** 4 weeks old raised in a
787 12hr light/dark cycle. **B.** 3 days old raised in a 12hr light/dark cycle. **C.** 4 weeks
788 old raised in 24hr dark. **D.** Confocal microscopy of adult eye photoreceptors
789 stained with phalloidin (green) and anti-Rh1 (red). Animals were 4 weeks old and
790 raised in a 12hr light/dark cycle. Arrowheads indicate photoreceptors with higher
791 levels of Rh1.
792
793 **Figure 6. Sloth1 and Sloth2 localize to mitochondria. A.** Confocal microscopy
794 of S2R+ cells transfected with Sloth1-FLAG or Sloth2-FLAG and stained with
795 anti-FLAG (green) and anti-ATP5alpha (red). DAPI (blue) stains nuclei. **B-D.**
796 SDS-PAGE and western blotting of S2R+ cellular fractions. WCL = Whole Cell
797 Lysate, cyto. = cytoplasmic lysate, mito. = mitochondrial lysate. Mitochondrial
798 control = ATP5alpha, cytoplasmic control = alpha-tubulin. Each lane loaded
799 equal amounts of protein (15μg/lane). Blots were stripped and reprobed after
800 detection of each antigen. **B.** Transfected Sloth1-FLAG or Sloth2-FLAG. **C.**
801 Stable cells expressing copper-inducible Sloth1-SBP or Sloth2-SBP. **D.** Stable
802 cells expressing copper-inducible Sloth1-SBP or Sloth2-SBP.
803
804 **Figure 7. *sloth1-sloth2* are important for mitochondrial function. A.**
805 Seahorse mitochondrial stress report for wildtype S2R+ and dKO #1 cells. Error
806 bars show mean with SD. N=6 for each genotype. **B.** Quantification of basal OCR
807 (timepoint 3) in panel A and including data from single KO and additional dKO
808 cell lines. Significance of KO lines was calculated with a T-test compared to
809 S2R+. Error bars show mean with SD. **** P≤0.0001. N=6 for each genotype. **C.**
810 Quantification of ATP levels in 3rd instar larvae. Error bars show mean with SEM.
811 N = 3 experiments. **D.** Western blot from lysates of 3rd instar larval brains. **E-F.**
812 TEM images of sectioned adult photoreceptors (left) and quantification of
813 mitochondria number (right). Mitochondria are indicated with red dots. Error bars
814 show mean with SD. Sample size indicated on graph. **E.** Adult flies are 4 weeks
815 old and raised in a 12hr light/dark cycle. **F.** Adult flies are 3 days old and raised in
816 a 12hr light/dark cycle.
817
818 **Figure 8. Sloth1 and Sloth2 physically interact with complex III and regulate**
819 **its assembly. A-B.** Blue native PAGE gel of mitochondria isolated from **A.** 10
820 adult thoraxes and **B.** 10 whole 3rd instar larvae of indicated genotype. Bands
821 corresponding to native respiratory complexes are indicated with arrowheads. **C-**
822 **D.** SDS-PAGE and western blotting of mitochondria isolated from **C.** adult thorax
823 and **D.** whole 3rd instar larvae of indicated genotype. Each lane loaded equal
824 amount of protein (15μg). Blots were stripped and reprobed after detection of
825 each antigen. **E-F.** Western blots from co-immunoprecipitation experiments in
826 transfected S2R+ cells using Sloth1-FLAG and Sloth2-FLAG as bait and either **E.**

827 RFeSP-HA or **F.** CG10075-HA as prey. Blots were striped and reprobed after
828 detection of each antigen. Arrowheads indicated expected band, asterisks
829 indicate unknown bands.
830
831 **Figure 9. Sloth1 and Sloth2 act in a stoichiometric complex. A-B.** Western
832 blots from co-immunoprecipitation experiments in transfected S2R+ cells. **A-B.**
833 Immunoprecipitation using Sloth1-FLAG and Sloth2-FLAG as bait and either **A.**
834 Sloth1-HA or **B.** Sloth2-HA as prey. Blots were striped and reprobed after
835 detection of each antigen. Arrowheads indicated expected band, asterisks
836 indicate unknown bands. **C.** Developmental viability assay using *tub-Gal4* to
837 overexpress indicated transgenes throughout development. Crosses resulting in
838 no viable adults are scored as lethal (black box).
839
840 **Figure 10. Model for Sloth1 and Sloth2 bicistronic translation and function**
841 **in mitochondria**
842
843 **Methods**
844
845 **Molecular cloning**
846
847 Plasmid DNAs were constructed and propagated using standard protocols.
848 Briefly, chemically competent TOP10 *E.coli.* (Invitrogen, C404010) were
849 transformed with plasmids containing either Ampicillin or Kanamycin resistance
850 genes and were selected on LB-Agar plates with 100µg/ml Ampicillin or 50µg/ml
851 Kanamycin. Oligo sequences are in Supplemental File 2.
852
853 *sloth1-sloth2* expression reporters: *pMT-sloth1-RLuc* was constructed by Gibson
854 (NEB E2611) assembly of two DNA fragments with overlapping sequence, 1)
855 5'UTR, *sloth1* coding sequence, and intervening sequence (*GCAAA*) were
856 amplified from S2R+ genomic DNA. 2) Plasmid backbone was amplified from
857 *pRmHa-3-Renilla* (ZHOU *et al.* 2008), which contains a *Metallothionein* promoter
858 and coding sequence for Renilla luciferase. *pMT-sloth1-RLuc* derivatives were
859 constructed by a PCR-based site directed mutagenesis (SDM) strategy.
860
861 shRNA expression vector for in vivo RNAi: *pValium20-sloth1-sloth2* (aka *UAS-*
862 *shRNA*, or *JAB200*) was constructed by annealing complementary oligos and
863 ligating into *pValium20* (NI *et al.* 2011) digested with NheI and EcoRI. See
864 Supplemental Figure 1 for location of target site.
865
866 sgRNA expression vectors for CRISPR/Cas9: Plasmids encoding two sgRNAs
867 were constructed by PCR amplifying an insert and ligating into *pCFD4* (PORT *et*
868 *al.* 2014) digested with BbsI. sgRNAs constructed: *pCFD4-sloth1* (aka JAB203),
869 *pCFD4-sloth2* (aka GP01169), *pCFD4-sloth1-sloth2* (aka JAB205, for dKO). See
870 Supplemental Figure 1 for location of target sites.
871 Gal4 HDR donor plasmid: *pHD-sloth1-sloth2-Gal4-SV40-loxP-dsRed-loxP* was
872 assembled by digesting *pHD-DsRed-attP* (GRATZ *et al.* 2014) with EcoRI/XhoI

873 and Gibson assembling with four PCR amplified fragments: 1) Left homology arm
874 from genomic DNA from *nos-Cas9[attP2]* flies. 2) *Gal4-SV40* from *pAct-FRT-*
875 *stop-FRT3-FRT-FRT3-Gal4 attB* (BOSCH *et al.* 2015). 3) *loxP-dsRed-loxP* from
876 *pHD-DsRed-attP*. 4) Right homology arm from genomic DNA from *nos-*
877 *Cas9[attP2]* flies.
878
879 Custom pEntr vectors: Construction of pEntr vectors (for Gateway cloning) was
880 performed by Gibson assembly of PCR amplified backbone from pEntr-dTOPO
881 (Invitrogen C4040-10) and PCR amplified gene coding sequence (when
882 appropriate, with or without stop codon). List of plasmids: *pEntr_sloth1* (from
883 S2R+ cDNA), *pEntr_sloth2* (from S2R+ cDNA), *pEntr_hSMIM4* (from IDT
884 gBlock), *pEntr_hC12orf73* (from IDT gBlock), *pEntr_sloth1-sloth2* transcript (from
885 S2R+ cDNA), *pEntr_sloth1-sloth2* genomic (from S2R+ genomic DNA), and
886 *pEntr_BFP* (from *mTagBFP2*). Derivatives of *pEntr_sloth1-sloth2* genomic that
887 lack *sloth1* or *sloth2* coding sequence, or derivatives of *pEntr_sloth1* or
888 *pEntr_sloth2* with or without only the N-terminal signal sequence, were generated
889 by PCR amplifying the plasmid and reassembling the linearized plasmid (minus
890 the desired sequence) by Gibson.
891
892 Custom gateway expression vectors: *pMT-GW-SBP* was constructed by
893 digesting *pMK33-SBP-C* (YANG AND VERAKSA 2017) and *pMK33-GW* (Ram
894 Viswanatha) with XhoI/SpeI and ligating the GW insert into digested *pMK33-*
895 *SBP-C* using T4 ligase.
896
897 Gateway cloning LR reactions: Gateway cloning reactions were performed using
898 LR Clonase II Enzyme mix (Invitrogen 11791-020). See Supplemental File 3 for
899 plasmids constructed by Gateway reactions. Additional plasmids obtained were
900 *pEntr_RFeSP* (DmCD00481962), *pEntr_CG10075* (DmCD00473802) (The FlyBi
901 Consortium; https://flybi.hms.harvard.edu/), *pAWF* and *pAWH* (Carnegie
902 Science/Murphy lab), *pWalium10-roe* (PERKINS *et al.* 2015), and *pBID-G* (WANG
903 *et al.* 2012).
904
905 **Fly genetics**
906
907 Flies were maintained on standard fly food at 25˚C. Wild-type (WT) or control
908 flies refers to *yw*. The *yv; attP40* strain is used as a negative control for
909 experiments involving an shRNA or sgRNA transgene inserted into *attP40*.
910
911 Fly stocks were obtained from the Perrimon lab collection, Bloomington Stock
912 center (indicated with BL#), or generated in this study (see below). Bloomington
913 Stocks: *yw* (1495), *yv; P{y[+t7.7]=CaryP}attP40* (36304), *yv,P{y[+t7.7]=nos-*
914 *phiC31\int.NLS}X; P{y[+t7.7]=CaryP}attP40* (25709), *P{y[+t7.7]=nos-*
915 *phiC31\int.NLS}X, y[1] sc[1] v[1] sev[21]; P{y[+t7.7]=CaryP}attP2* (25710),
916 *w[1118]; Dp(1;3)DC166, PBac{y[+mDint2] w[+mC]=DC166}VK00033* (30299),
917 *y[1] M{w[+mC]=Act5C-Cas9.P}ZH-2A w[*]* (54590), *y[1] sc[*] v[1] sev[21];*
918 *P{y[+t7.7] v[+t1.8]=nos-Cas9.R}attP2* (78782), *w[*]; P{w[+mC]=UAS-*

2xEGFP}AH2 (6874), *w[1118]; P{w[+mC]=UAS-GFP.nls}14* (4775), *y1 w*; P{tubP-GAL4}LL7/TM3, Sb1 Ser1* (5138), *MN-Gal4*, *UAS-mitoGFP* (42737), *MN-Gal4*, *UAS-nSybGFP* (9263), *UAS-tdTomato* (92759), *elav-Gal4* (8760). Perrimon Lab stocks: *w; da-Gal4*, *lethal/FM7-GFP*.

Transgenic flies using PhiC31 integration were made by injecting attB-containing plasmids at 200ng/ul into integrase-expressing embryos that contained an attP landing site (attP40 or attP2). Injected adults were outcrossed to balancer chromosome lines to isolate transgenic founder flies and eventually generate balanced stocks. *pCFD4-sloth1[attP40]* (aka JAB203), *pCFD4-sloth2[attP40]* (aka GP01169), *pCFD4-sloth1-sloth2[attP40]* (aka JAB205, for dKO), *pValium20-sloth1-sloth2[attP40]* (aka *UAS-shRNA*, or *JAB200*) lines were selected with *vermillion+*. *pWalium10-sloth1[attP2]*, *pWalium10-sloth2[attP2]*, *pValium10-sloth2[attP40]*, *pWalium10-hSMIM4[attP2]*, *pWalium10-hC12orf73[attP2]*, *pWalium10-sloth1-sloth2*transcript*[attP2]*, *pBID-{sloth1-sloth2}[attP40]*, *pBID-{Δsloth1-sloth2}[attP40]*, *pBID-{sloth1-Δsloth2}[attP40]* were selected with *white+.*

sloth1-KO, *sloth2-KO,* and *dKO* fly lines were made by crossing sgRNA-expressing transgenic lines to *nos-Cas9[attP2]* flies, outcrossing progeny to *FM7-GFP* balancer flies, and screening progeny founder flies for deletions by PCR and Sanger sequencing.

Gal4-KI flies were made by injecting sgRNA plasmid (JAB205) and *pHD-sloth1-sloth2-Gal4-SV40-loxP-dsRed-loxP*, each at 200ng/ul, into embryos expressing Cas9 in the germ line (*nos-Cas9*). Injected adults were outcrossed to *FM7-GFP* flies, progeny were screened for RFP+ expression, and RFP+ founder lines were confirmed by PCR for a correct knock-in.

Knockdown crosses were performed by crossing *da-Gal4* with *pValium20-sloth1-sloth2[attP40]*/*CyO* (aka *UAS-shRNA*, or *JAB200*) or *attP40/CyO* as a negative control. Quantification of viability was performed by counting the number of progeny with or without the CyO balancer. A Chi-square test was used to determine if the ratio of non-balancer flies (CyO^-) to balancer flies (CyO^+) was significantly altered in shRNA crosses compared to control crosses. Data was analyzed using Excel and Prism.

For climbing assays, *da-Gal4/shRNA or da-Gal4/attP40* adult progeny were aged 1 week after eclosion and 10 flies were transferred into empty plastic vials without use of CO2. Climbing ability was quantified by tapping vials and recording the number of flies that climb to the top of the vial within 10 seconds, using video analysis. Climbing assays with the same 10 flies were performed three times and averaged. Three biological replicates were performed for each genotype. A T-Test was used to calculate statistical significance. Data was analyzed using Excel and Prism.

965 Somatic knockout crosses were performed by crossing *Act-Cas9* to
966 *sgRNA[attP40]/CyO* or *attP40/CyO* as a negative control. *Act-*
967 *Cas9/sgRNA[attP40]* female and male progeny were analyzed for phenotypes.
968 Quantification of viability was performed by counting the number of progeny with
969 or without the *CyO* balancer. A Chi-square test was used to determine if the ratio
970 of non-balancer flies (CyO^-) to balancer flies (CyO^+) was significantly altered in
971 somatic knockout crosses compared to control crosses. Male and female
972 progeny were analyzed separately because they differ in the number of copies of
973 the endogenous *sloth1-sloth2* loci on the X-chromosome. Data was analyzed
974 using Excel and Prism.
975
976 Mutant and genomic rescue crosses were performed by crossing *mutant/FM7-*
977 *GFP* females to genomic rescue constructs or *attP40* as a negative control.
978 *mutant/Y* hemizygous male progeny were analyzed for phenotypes.
979 Quantification of viability was performed by counting the number of *mutant/Y* vs
980 *FM7GFP* male progeny. Gal4/UAS rescue crosses were performed by crossing
981 *mutant/FM7-GFP;; da-Gal4* females to *UAS-X* lines. Additionally, *Gal4-KI/FM7-*
982 *GFP* females were crossed to *UAS-X*. Rare *sloth1*-KO, *sloth2-KO, dKO,* and
983 *Gal4-KI* hemizygous adult males normally die by sticking to the fly food after they
984 eclose. To collect these rare mutants for further analysis (scutellar bristle images,
985 climbing assays), we inverted progeny vials so that mutant adults fell onto the dry
986 cotton plug once they eclose.
987
988 Overexpression crosses were performed by crossing *tub-Gal4/TM3* females to
989 *UAS-X* lines. At least 100 *tub-Gal4/UAS-X* progeny were analyzed for
990 phenotypes.
991
992 **Cell fractionation and mitochondrial isolation**
993
994 To isolate mitochondria from S2R+ cells, cell pellets were resuspended in 1.1ml
995 hypotonic buffer (10 mM NaCl, 1.5 mM MgCl2, 10 mM Tris- HCl pH 7.5),
996 transferred to cold glass dounce on ice, and incubated for 10min to induce cell
997 swelling. Cells were homogenized with 10 strokes using pestle B (tight pestle),
998 followed by addition of 800µl of 2.5x homogenization buffer (525mM mannitol,
999 175 mM sucrose, 12.5 mM Tris-HCl pH 7.5 and 2.5 mM EDTA). Homogenates at
1000 this step are considered whole cell lysate (WCL). WCL was centrifuged at 1,300g
1001 for 5min at 4˚C, supernatant transferred to a new tube, repeated centrifugation.
1002 Supernatant was transferred to a new tube and centrifuged at 17,000g for 15min
1003 at 4˚C. Supernatant was removed (cytoplasmic fraction) and 2ml 1x
1004 Homogenization buffer (210 mM mannitol, 70 mM sucrose, 5 mM Tris-HCl pH 7.5
1005 and 1 mM EDTA) was added to the pellet. The centrifugation was repeated and
1006 250µl 1x Homogenization buffer was added to the pellet (mitochondrial fraction).
1007 For SDS-PAGE comparisons of cell fractions, WCL, cytoplasmic, and
1008 mitochondria were lysed in RIPA buffer and protein concentration normalized by
1009 BCA assay (Thermo Fischer, 23227).
1010

1011 Mitochondrial isolation from 7 day old adult thoraxes and whole 3rd instar larvae
1012 was modified from (GARCIA *et al.* 2017). Briefly, dissected adult male thoraxes or
1013 whole 3rd instar male larvae were placed into 100µl mitochondrial isolation buffer
1014 (250mM Sucrose, 150mM MgCl2, 10mM Tris-HCl pH 7.4) on ice. Thoraxes were
1015 ground using a blue pestle and a motorized pestle holder. 400µl mitochondrial
1016 isolation buffer was added to homogenized thoraxes and samples were
1017 centrifuged at 500g at 4˚C for 5min to pellet debris and tissues. Supernatant was
1018 transferred to a new tube and the centrifugation repeated. Supernatant was
1019 transferred to a new tube and centrifuged at 5000g at 4˚C for 5min to pellet
1020 mitochondria. The mitochondrial pellet was washed 2x by adding 1ml
1021 mitochondrial isolation buffer and repeating centrifugation at 5000g at 4˚C for
1022 5min. For BN-PAGE experiments, 10 thoraxes or 10 whole 3rd instar larvae were
1023 used. For SDS-PAGE, 30 thoraxes or 30 whole 3rd instar larvae were used, and
1024 mitochondria were lysed in RIPA buffer and protein concentration normalized by
1025 BCA assay (Thermo Fischer, 23227).
1026
1027 **Blue Native PAGE (BN-PAGE) of mitochondrial respiratory complexes**
1028
1029 Native mitochondrial respiratory complexes were visualized by Blue Native PAGE
1030 (BN-PAGE) gels following the manufacturer's instructions protocols (Nativepage
1031 12% Bis Tris Protein Gels, 1.0 mm, 15 well, Thermo Fisher Scientific
1032 BN1003BOX). Mitochondrial pellets from 10 thoraxes or 10 larvae were
1033 resuspended in 20ul sample buffer cocktail (5µl sample buffer, 8µl 5% digitonin,
1034 7µl H20, 2µl 5% Coomassie G-250 sample additive). 15µl sample ran on each
1035 lane.
1036
1037 **Cell culture**
1038
1039 *Drosophila* S2R+ cells (YANAGAWA *et al.* 1998), or S2R+ cells stably expressing
1040 Cas9 and a mCherry protein trap in *Clic* (known as PT5/Cas9) (VISWANATHA *et al.*
1041 2018), were cultured at 25˚C using Schneider's media (21720-024,
1042 ThermoFisher) with 10% FBS (A3912, Sigma) and 50 U/ml penicillin strep
1043 (15070-063, ThermoFisher). S2R+ cells were transfected using Effectene
1044 (301427, Qiagen) following the manufacturer's instructions.
1045
1046 For generating stable cell lines MT-Sloth1-SBP, MT-Sloth2-SBP, and MT-
1047 Sloth1/2, S2R+ cells were seeded in 6-well plates and transfected with *pMK33*
1048 expression plasmids (see Supplemental File 3). *pMK33* derived plasmids contain
1049 a Hygromycin resistance gene and a *Metallothionein* promoter to induce gene
1050 expression. After 4 days, transfected cells were selected with 200µg/ml
1051 Hygromycin in Schneider's medium for approximately 1 month. For induction of
1052 gene expression, cells were cultured with 500 µM CuSO4 in Schneider's medium
1053 for 16hrs.
1054
1055 For generating KO cell lines, S2R+Cas9 cells were transfected with *tub-GFP*
1056 plasmid (gift of Steve Cohen) and an sgRNA-expressing plasmid (*pCFD4-*

1057 *sloth1[attP40]* (aka JAB203), *pCFD4-sloth2[attP40]* (aka GP01169), or *pCFD4-*
1058 *sloth1-sloth2[attP40]* (aka JAB205, for dKO)). 48hrs after transfection, cells were
1059 resuspended in fresh media, triturated to break up cell clumps, and pipetted into
1060 a cell straining FACS tube (352235 Corning). Single GFP+ cells were sorted into
1061 single wells of a 96 well plate containing 50% conditioned media using an Aria-
1062 594 instrument at the Harvard Medical School Division of Immunology's Flow
1063 Cytometry Facility. Once colonies were visible by eye (3-4 weeks), they were
1064 expanded and analyzed by PCR and Sanger sequencing.
1065
1066 For co-immunoprecipitation experiments, S2R+ cells were transfected in 100mm
1067 petri dishes. Four days after transfection, cells were resuspended and
1068 centrifuged at 1000g for 10min at 4˚C. Cell pellets were washed once with ice-
1069 cold 1x PBS, re-centrifuged, and flash frozen in liquid nitrogen. Cell pellets were
1070 subjected to mitochondrial isolation (described above) and mitochondrial pellets
1071 were flash frozen in liquid nitrogen. Mitochondrial pellets were resuspended in
1072 250µl mitochondrial lysis buffer (~.5-1ug/ul final protein concentration), incubated
1073 on ice for 30min and centrifuged at 13,000g for 10min at 4˚C. The supernatant
1074 was incubated with 20µl magnetic anti-FLAG beads (Sigma-Aldrich M8823) for
1075 2hr at 4˚C with gentle rocking. Beads were washed 3x in mitochondrial lysis
1076 buffer using a magnetic stand and eluted for 30min at 4˚C with 20ul 3xFLAG
1077 peptide diluted at 1mg/ml in mitochondrial lysis buffer. Mitochondrial lysis buffer:
1078 50 mM Tris-HCl pH 7.4, 150 mM NaCl, 10% glycerol (v/v), 20 mM MgCl2, 1%
1079 digitonin (v/w) (Sigma D141), protease inhibitor (Pierce 87786), and 2 mM PMSF
1080 added immediately before use.
1081
1082 To measure mitochondrial respiration in S2R+ cells, we performed a Mito Stress
1083 Test on a Seahorse XFe96 Analyzer (Agilent, 103015-100). 50,000 cells were
1084 seeded into Seahorse XF96 tissue culture microplates and incubated at 25˚C
1085 overnight. 1hr before analysis, cell culture media was replaced with serum-free
1086 Schneider's media and drugs were loaded into the Seahorse XFe96 Sensor
1087 Cartridge (Final concentrations: Oligomycin 1µM, Bam15 .5µM, 1µM
1088 Antimyzin/Rotenone "R/A"). Seahorse analysis was performed at room
1089 temperature. Mitochondrial respiration recordings were normalized to cell number
1090 using CyQUANT (Thermo Fisher C7026) fluorescence on a plate reader. Data
1091 analysis was performed using Seahorse Wave Desktop Software 2.6, Excel, and
1092 Prism. N=6 wells for each condition. Significance was calculated using a T-Test.
1093
1094 To measure *MT-sloth1-RLuc* reporter expression, S2R+ cells were transfected in
1095 white opaque-bottom 96 well plates with *MT-sloth1-RLuc* (or derivatives) and
1096 *MT-FLuc* (Firefly Luciferase) (ZHOU *et al.* 2008) as an internal control. Briefly, to
1097 each well, 10ng of plasmid mix was added, then 10µl Enhancer mix (.8µl
1098 Enhancer + 9.2µl EC buffer), and was incubated for 2-5min at room temperature.
1099 20µl of Effectene mix (2.5µl Effectene + 17.5µl EC buffer) was added and
1100 incubated for 5-10min at room temperature. 150µl of S2R+ cells (at 3.3x10^5
1101 cells/ml) was added gently to each well and incubated at 25˚C. After 3 days
1102 incubation, 200µM CuSO4 was added. After 24 hours incubation, media was

1103 gently removed from the wells by pipetting and cell luminescence was measured
1104 using the Dual-Glo assay (Promega E2920). Two luminescence normalizations
1105 were performed. First, for each sample, Renilla luminescence was normalized to
1106 Firefly luminescence (Rluc/Fluc). Next, Rluc/Fluc ratios for each sample were
1107 normalized to Rluc/Fluc ratios for wild-type *MT-sloth1-RLuc* (aka fold change
1108 Rluc/Fluc to WT). For each genotype, N=4. Significance was calculated using a
1109 T-test. Data was analyzed using Excel and Prism.
1110
1111 **Western blotting**
1112
1113 Protein or cell samples were denatured in 2x SDS Sample buffer (100mM Tris-
1114 CL pH 6.8, 4% SDS, .2% bromophenol blue, 20% glycerol, .58 M β-
1115 mercaptoethanol) by boiling for 10 min. For western blots using glycine-based
1116 gels (Figure 7D, Figure 8C-F, Figure 9A-B, Supplemental Figure 8A,B,D),
1117 denatured proteins and Pageruler Prestained Protein Ladder (Thermo Fisher
1118 Scientific 26616) were loaded into 4–20% Mini-PROTEAN TGX gels (Biorad
1119 4561096) using running buffer (25 mM Tris, 192 mM glycine, 0.1% SDS, pH 8.3).
1120 For western blots using tricine-based gels (Figure 6B-D, Supplemental Figure 8C
1121) (to improve resolution of small peptides), denatured proteins and Precision Plus
1122 Protein™ Dual Xtra Prestained Protein Standards (Biorad 1610377) were loaded
1123 into 16.5% Mini-PROTEAN® Tris-Tricine Gels (Biorad 4563066) using
1124 Tris/Tricine/SDS Running buffer (Biorad 1610744). Gels were ran at 100-200V in
1125 a Mini-PROTEAN Tetra Vertical Electrophoresis Cell (Biorad 1658004). Proteins
1126 were transferred to Immobilon-FL PVDF (Millipore IPFL00010) in transfer buffer
1127 (25 mM Tris, 192 mM glycine) using a Trans-Blot Turbo Transfer System (Biorad
1128 1704150) (Standard SD program). Resulting blots were incubated in TBST (1x
1129 TBS + .1% Tween20) for 20min on an orbital shaker, blocked in 5% non-fat milk
1130 in TBST for 1 hour at room temperature, and incubated with primary antibody
1131 diluted in blocking solution overnight at 4˚C. Blots were washed with TBST and
1132 incubated in secondary antibody in blocking solution for 4 hours at room
1133 temperature. Blots were washed in TBST before detection of proteins. HRP-
1134 conjugated secondary antibodies were visualized using ECL (34580,
1135 ThermoFisher). Blots were imaged on a ChemiDoc MP Imaging System
1136 (BioRad)**.** Antibody complexes were reprobed by incubating blots with stripping
1137 buffer (Thermo Scientific 46430) following the manufacturer's instructions, re-
1138 blocked in 5% non-fat milk in TBST, and incubated with primary antibody
1139 overnight as described.
1140
1141 For western blots from larval brains, 3rd instar larval brains were dissected in ice
1142 cold PBS buffer with protease and phosphatase inhibitors. 10 brains per
1143 genotype were homogenized in RIPA buffer and protein concentration was
1144 measured by BCA assay (Thermo Fischer, 23227). Equal amounts of protein
1145 samples were mixed with 1X Sample buffer (BioRad, 161-0747), boiled for 5 min,
1146 and loaded into 4-20% Mini-PROTEAN® TGX gel (Bio-Rad). Gels were then
1147 transferred to nitrocellulose membranes using Bio-Rad Trans-Blot SD Semi-Dry
1148 Transfer system. Western blots using anti-Hsp60 likely recognize Hsp60A, as

1149 opposed to Hsp60B/C/D, because only Hsp60A is expressed in the larval brain
1150 (flyrnai.org/tools/dget/web).
1151
1152 Commercially available or published antibodies used for western blotting: rat anti-
1153 HA (1:2000, Roche 11867423001) (Figure 9A,B), chicken anti-HA (1:1000, ET-
1154 HA100, Aves) (Figure 8E,F), mouse anti-FLAG (1:1000, Sigma F1804), mouse
1155 anti-SBP (1:1000, Santa Cruz sc-101595), mouse anti-a-Tubulin (1:20000,
1156 Sigma T5168), rabbit anti-GFP (1:5000, Invitrogen A-6455), rabbit anti-Hsp60
1157 antibody (Abcam ab46798), mouse anti-actin (MP Biomedicals 08691002), anti-
1158 actin Rhodamine (Biorad 12004163), rabbit anti-SMIM4 (1:10,000, HPA047771),
1159 anti-UQCR-C2 (1:1000, (MURARI *et al.* 2020)), anti-SdhA (1:1000, (MURARI *et al.*
1160 2020)), rabbit anti-C12orf73 (1:1000, HPA038883), anti-mouse HRP (1:3000,
1161 NXA931, Amersham), anti-rat HRP (1:3000, Jackson 112-035-062), anti-rabbit
1162 HRP (1:3000, Amersham NA934), anti-chicken HRP (1:1000, Sigma
1163 SAB3700199), anti-mouse 800 (only used in Figure 8E,F to detect mouse anti-
1164 FLAG) (1:5000, Invitrogen A32730). Anti-Sloth1 and Anti-Sloth2 antibodies
1165 (1:1000) were raised in rabbits (Genscript, PolyExpress Silver Package).
1166 Epitopes used: Anti-Sloth1 #1: RRLLDSWPGKKRFGC, Anti-Sloth1 #2:
1167 CEQQHLQARAANNTN, Anti-Sloth2 #1: CHSTQVDPTAKPPES, Anti-Sloth2 #2:
1168 CYKPLEDLRVYIEQE
1169
1170 **Molecular biology**
1171
1172 S2R+ cell genomic DNA was isolated using QuickExtract (QE09050, Lucigen).
1173 Fly genomic DNA was isolated by grinding a single fly in 50µl squishing buffer
1174 (10 mM Tris-Cl pH 8.2, 1 mM EDTA, 25 mM NaCl) with 200µg/ml Proteinase K
1175 (3115879001, Roche), incubating at 37˚C for 30 min, and 95˚C for 2 minutes.
1176 PCR was performed using Taq polymerase (TAKR001C, ClonTech) when
1177 running DNA fragments on a gel, and Phusion polymerase (M-0530, NEB) was
1178 used when DNA fragments were sequenced or used for molecular cloning. DNA
1179 fragments were run on a 1% agarose gel for imaging or purified on QIAquick
1180 columns (28115, Qiagen) for sequencing analysis. Sanger sequencing was
1181 performed at the DF/HCC DNA Resource Core facility and chromatograms were
1182 analyzed using Lasergene 13 software (DNASTAR).
1183
1184 For RT-qPCR analysis of *sloth1-sloth2* RNAi knockdown, *da-Gal4* was crossed
1185 with *attP40* or *UAS-shRNA* and ten 3rd instar larvae progeny of each genotype
1186 were flash frozen in liquid nitrogen. Frozen larvae were homogenized in 600µl
1187 Trizol (Invitrogen 15596026) and RNA extracted using a Direct-zol RNA Miniprep
1188 kit (Zymo Research, R2050). cDNA was generated using the iScript Reverse
1189 Transcription Supermix (BioRad 1708840). cDNA was analyzed by RT-qPCR
1190 using iQ SYBR Green Supermix (BioRad 170-8880). qPCR primer sequences
1191 are listed in Supplemental File 2. Each qPCR reaction was performed with two
1192 biological replicates, with three technical replicates each. Data was analyzed
1193 using Bio-Rad CFX Manager, Excel, and Prism. Data from *sloth1-sloth2* specific
1194 primers were normalized to primers that amplify *GAPDH* and *Rp49*. Statistical

1195 significance was calculated using a T-Test.

1196 **Bioinformatic analysis**

1197

1198 Protein similarity between fly and human Sloth1 and Sloth2 orthologs was
1199 determined using BLASTP (blast.ncbi.nlm.nih.gov) by defining the percent amino
1200 acid identity between all four comparisons. Homologs in other organisms and
1201 their gene structure were identified using a combination of BLASTP, Ensembl
1202 (www.ensembl.org), HomoloGene (www.ncbi.nlm.nih.gov/homologene), and
1203 DIOPT (www.flyrnai.org/diopt). Protein accession numbers: Human *SMIM4*
1204 NP_001118239.1, Human *C12orf73* NP_001129042.1, Mouse *SMIM4*
1205 NP_001295020.1, Mouse *C12orf73 homolog* NP_001129039.1, Zebrafish
1206 *SMIM4* NP_001289975.1, Zebrafish *C12orf73 homolog* NP_001129045.1,
1207 Lamprey *SMIM4* XP_032827557.1, Lamprey *C12orf73 homolog*
1208 XP_032827559.1, *D.melanogaster CG32736* NP_727152.1, *D.melanogaster*
1209 *CG42308* NP_001138171.1, *Arabidopsis AT5G57080* NP_200518.1, *Arabidopsis*
1210 *AT4G26055* NP_001119059.1, *Plasmodium PF3D7_0709800* XP_002808771.1,
1211 Choanoflagellate (*Salpingoeca urceolata*) *m.92763* (RICHTER *et al.* 2018),
1212 Choanoflagellate (*Salpingoeca urceolata*) *sloth2* homolog is unannotated but
1213 present in comp15074_c0_seq2 (RICHTER *et al.* 2018). Sea squirt (*C. intestinalis*)
1214 *sloth1* and *sloth2* homologs are unannotated but present in *LOC100183920*
1215 XM_018812254.2. Genomic sequences for *sloth1/2* ORFs in *D.melanogaster*,
1216 Lamprey, Choanoflagellate, and Sea squirt are shown in Supplemental File 1.

1217

1218 Amino acid sequence of fly and human Sloth1/Sloth2 were analyzed for
1219 predicted domains using the following programs: MitoFates
1220 (http://mitf.cbrc.jp/MitoFates/cgi-bin/top.cgi), DeepMito
1221 (http://busca.biocomp.unibo.it/deepmito/), TMHMM 2.0
1222 (http://www.cbs.dtu.dk/services/TMHMM/).

1223

1224 Amino acid sequences were aligned using Clustal Omega
1225 (https://www.ebi.ac.uk/Tools/msa/clustalo/) and visualized using Jalview
1226 (https://www.jalview.org/).

1227

1228 **Imaging**

1229

1230 For imaging adult scutellar bristles, adult flies were frozen overnight and
1231 dissected to remove their legs and abdomen. Dissected adults were arranged on
1232 a white surface and a focal stack was taken using a Zeiss Axio Zoom V16. Focal
1233 stacks were merged using Helicon Focus 6.2.2.

1234

1235 For imaging larval brains, wandering 3rd instar larvae were dissected in PBS and
1236 carcasses were fixed in 4% paraformaldehyde for 20min. Fixed carcasses were
1237 either mounted on slides in mounting medium (see below), or permeabilized in
1238 PBT, blocked for 1hr in 5% normal goat serum (S-1000, Vector Labs) at room
1239 temperature, and incubated with primary antibody (anti-Elav) overnight at 4˚C,
1240 washed with PBT, incubated with secondary antibody (anti-mouse 633) for 4hr at

1241 room temperature, washed with PBT and PBS, and incubated in mounting media
1242 (90% glycerol + 10% PBS) overnight at 4˚C. Larval brains were dissected from
1243 carcasses and mounted on a glass slide under a coverslip using vectashield (H-
1244 1000, Vector Laboratories Inc.). Images of larval brains were acquired on a Zeiss
1245 Axio Zoom V16 or a Zeiss 780 confocal microscope. Images were processed
1246 using Fiji software.
1247
1248 For imaging the larval NMJ, wandering 3rd instar larvae were dissected as
1249 previously described (BRENT *et al.* 2009). Briefly, larvae were pinned to a
1250 Sylgard-coated (Dow 4019862) petri dish, an incision was made along their
1251 dorsal surface, their cuticle was pinned down to flatten the body wall muscles,
1252 and were fixed in 4% paraformaldehyde for 20min. Fixed carcasses were
1253 permeabilized in PBT, blocked for 1hr in 5% normal goat serum (S-1000, Vector
1254 Labs) at room temperature, and incubated with primary antibody overnight at
1255 4˚C, washed with PBT, incubated with secondary antibody for 4hr at room
1256 temperature, washed with PBT and PBS, and incubated in mounting media (90%
1257 glycerol + 10% PBS) overnight at 4˚C. Whole carcasses mounted on a glass
1258 slide under a coverslip using vectashield (H-1000, Vector Laboratories Inc.).
1259 Images of the NMJ were acquired on a Zeiss Axio Zoom V16 or a Zeiss 780
1260 confocal microscope. Images were taken from muscle 6/7 segment A2. Images
1261 were processed using Fiji software. Quantification of bouton number from NMJ
1262 stained with anti-HRP and anti-Dlg1 was performed by manual counting of
1263 boutons in an entire NMJ for wild-type (N=8) and dKO animals (N=7). A T-test
1264 was used to determine significance.
1265
1266 For imaging whole larvae, wandering 3rd instar larvae were washed with PBS and
1267 heat-killed for 5min on a hot slide warmer to stop movement. Larvae were
1268 imaged using a Zeiss Axio Zoom V16 fluorescence microscope.
1269
1270 For imaging the adult brain, ~1 week old adult flies were dissected in PBS and
1271 whole brains were fixed in 4% paraformaldehyde for 20min. Fixed brains were
1272 permeabilized in PBT, blocked for 1hr in 5% normal goat serum (S-1000, Vector
1273 Labs) at room temperature, incubated with anti-HRP 647 overnight at 4˚C,
1274 washed with PBT and PBS, and incubated in mounting media (90% glycerol +
1275 10% PBS) overnight at 4˚C. Adult brains were mounted on glass slides under a
1276 coverslip using vectashield (H-1000, Vector Laboratories Inc.). Images of adult
1277 brains were acquired on a Zeiss 780 confocal microscope. Images were
1278 processed using Fiji software.
1279
1280 For confocal microscopy of adult photoreceptors, the proboscis was removed
1281 and the head was pre-fixed with 4% formaldehyde in PBS for 30 min. After pre-
1282 fixation, eyes were removed from the head and fixed an additional 15 minutes.
1283 Fixed eyes were washed with PBS 3x for 10 min each and permeabilized in 0.3%
1284 Triton X-100 in PBS for 15 min. Permeabilized, fixed samples were blocked in 1X
1285 PBS containing 5% normal goat serum (NGS) and 0.1% Triton X-100 for 1 h
1286 (PBT). Samples were incubated in primary antibody diluted in PBT overnight at

1287 4°C, washed 3x with PBT, and incubated in secondary antibodies in NGS for 1hr
1288 at room temp the next day. Following secondary antibody incubation, samples
1289 were washed with PBS and were mounted on microscope slides using
1290 vectashield. Samples were imaged with LSM710 confocal with 63X objective and
1291 processed using Fiji software.
1292
1293 S2R+ cells transfected with Sloth1-FLAG or Sloth2-FLAG were plated into wells
1294 of a glass-bottom 384 well plate (6007558, PerkinElmer) and allowed to adhere
1295 for 2 hours. Cells were fixed by incubating with 4% paraformaldehyde for 30min,
1296 washed with PBS with .1% TritonX-100 (PBT) 3x 5min each, blocked in 5%
1297 Normal Goat Serum (NGS) in PBT for 1hr at room temperature, and incubated in
1298 primary antibodies diluted in PBT-NGS overnight at 4˚C on a rocker. Wells were
1299 washed in PBT, incubated with secondary antibodies and DAPI and washed in
1300 PBS. Plates were imaged on an IN Cell Analyzer 6000 (GE) using a 20x or 60x
1301 objective. Images were processed using Fiji software.
1302
1303 List of antibodies and chemicals used for tissue staining: rat anti-Elav (1:50,
1304 DSHB, 7E8A10), goat anti-HRP 647 (1:400, Jackson Immunoresearch, 123-605-
1305 021), mouse anti-ATP5α (1:500, Abcam, ab14748), DAPI (1:1000, Thermo
1306 Fisher, D1306), rabbit anti-FLAG (1:1000, Sigma, F7425), mouse anti-FasII
1307 (1:25, DSHB, 1D4), mouse anti-brp (1:25, DSHB, nc82), mouse anti-Dlg1 (1:250,
1308 DSHB, 4F3), anti-mouse 633 (1:500, A-21052, Molecular Probes), mouse
1309 monoclonal anti-Rh1 (1:50, DSHB 4C5), Phalloidin conjugated with
1310 Alexa 488 (1:250, Invitrogen A12379).
1311
1312 **Transmission electron microscopy (TEM) of adult photoreceptors**
1313
1314 TEM of *Drosophila* adult retinae were performed following standard electron
1315 microscopy procedures using a Ted Pella Bio Wave processing microwave with
1316 vacuum attachments. Briefly, whole heads were dissected in accordance to
1317 preserve the brain tissue. The tissue was covered in 2% paraformaldehyde, 2.5%
1318 Glutaraldehyde, in 0.1 M Sodium Cacodylate buffer at pH 7.2. After dissection,
1319 the heads were incubated for 48hrs in the fixative on a rotator at 4˚C. The pre-
1320 fixed heads were washed with 3X millipore water followed by secondary fixation
1321 with 1% aqueous osmium tetroxide, and rinsed again 3X with millipore water. To
1322 dehydrate the samples, concentrations from 25%–100% of Ethanol were used,
1323 followed by Propylene Oxide (PO) incubation. Dehydrated samples are infiltrated
1324 with gradual resin:PO concentrations followed by overnight infiltration with pure
1325 resin. The samples were embedded into flat silicone molds and cured in the oven
1326 at 62°C for 3-5 days, depending on the atmospheric humidity. The polymerized
1327 samples were thin-sectioned at 48-50 nm and stained with 1% uranyl acetate for
1328 14 minutes followed by 2.5% lead citrate for two minutes before TEM
1329 examination. Retina were viewed in a JEOL JEM 1010 transmission electron
1330 microscope at 80kV. Images were captured using an AMT XR-16 mid-mount 16
1331 mega-pixel digital camera in Sigma mode. Three animals per genotype per
1332 condition were used for TEM. At least 30 photoreceptors were used for organelle

1333 quantifications. Quantification of photoreceptor number, number of aberrant
1334 photoreceptors, and number of mitochondria per photoreceptor, was performed
1335 in Prism. Significance was calculated using a T-Test.
1336
1337 **Electrical recordings**
1338
1339 *Intracellular Recording from Larval NMJ*
1340 3rd instar larval NMJ recordings were performed as described previously (UGUR
1341 *et al.* 2017). Briefly, free moving larvae are dissected in HL3.1 buffer without
1342 Ca^{2+}. Recordings were performed by stimulating the segmental nerve innervating
1343 a hemisegment A3, Muscle 6/7 through a glass capillary electrode filled with
1344 HL3.1 with 0.75 mM Ca^{2+}. There were no differences in input resistance, time
1345 constant τ, and resting membrane potential among different genotypes tested.
1346 Repetitive stimulations were performed at 10Hz and were reported relative to the
1347 first excitatory junction potential (EJP). Data were processed with Mini Analysis
1348 Program by Synaptosoft, Clampfit, and Excel. At least 5 animals were used per
1349 each genotype per essay. Significance was calculated using a T-Test.
1350
1351 *Electroretinograms (ERGs)*
1352 ERGs were recorded according to (JAISWAL *et al.* 2015). Briefly, flies were
1353 immobilized on a glass slide with glue. Glass recording electrodes, filled with 100
1354 mM NaCl, were placed on the surface of the eye to record field potential. Another
1355 electrode placed on the humerals served as a grounding electrode. Before
1356 recording ERGs, flies were adjusted to darkness for three minutes. Their
1357 response to light was measured in 1sec. intervals for 30 sec. To test if the flies
1358 can recover from repetitive stimulation, we recorded ERGs after 30 sec. and
1359 1min constant darkness following repetitive stimulation. Data were processed
1360 with AXON-pCLAMP8.1. At least 6 animals were used per each genotype per
1361 essay. Significance was calculated using a T-Test.
1362
1363 **Measurement of ATP levels from larvae**
1364
1365 Ten 3rd instar larvae were snap frozen with liquid nitrogen in a 1.5 mL centrifuge
1366 tube. Following freezing, samples were homogenized in 100 µl of 6 M guanidine-
1367 HCl in extraction buffer (100 mM Tris and 4 mM EDTA, pH 7.8) to inhibit
1368 ATPases, and boiled for 3 min. The samples were centrifuged to remove cuticle.
1369 Supernatant was serially diluted with extraction buffer and protein concentration
1370 was measured using a BCA kit (Thermo Fischer, 23227). For each genotype,
1371 ATP levels were measured from equal protein amounts using an Invitrogen ATP
1372 detection kit (Invitrogen, A22066) according to their protocol. N=3 experiments,
1373 biological triplicates per genotype per experiment. Significance was calculated
1374 using a T-Test.
1375
1376 **Supplemental Information titles and legends**
1377

1378 **Supplemental Figure 1: Related to Figure 1. A.** Comparison of gene and
1379 transcript structure of the *sloth1* and *sloth2* open reading frames. A common
1380 primer pair is used to distinguish genomic from cDNA (transcript) template by
1381 PCR. Sequence of *sloth1-2* genomic and *sloth1-2* transcript region provided. **B.**
1382 DNA gel image of PCR fragments amplified from indicated template samples.
1383 Predicted spliced transcript containing both sloth1 and sloth2 open reading
1384 frames is amplified from cDNA generated from adult flies, 3rd instar larvae, and
1385 S2R+ cells.
1386
1387 **Supplemental Figure 2: Related to Figure 2. A.** Extended gene structure of
1388 *sloth1* and *sloth2* and genetic reagents. **B.** Sequence analysis of KO, dKO, and
1389 Gal4-KI alleles. **C.** (Left) Diagram of HDR knock-in of Gal4 into the *sloth1-sloth2*
1390 locus. (Right) DNA gel confirming Gal4 knock-in by PCR primers that flank the
1391 homology arms. Expected DNA fragment size in parenthesis.
1392
1393 **Supplemental Figure 3. Related to Figure 4.** Traces of electrical recordings
1394 from 3rd instar larval NMJ in *dKO*, and *dKO+genomic rescue* animals. Graph on
1395 right is a quantification of the excitatory junction potential (EJP) for indicated
1396 genotypes. Significance was calculated with a T-Test compared to the *yw* control
1397 sample. Error bars show mean with SD. N ≥ 5 larvae per genotype.
1398
1399 **Supplemental Figure 4. Related to Figure 5.** Confocal microscopy images of
1400 3rd instar larval NMJ at muscle 6/7 segment A2. Antibodies or fluorescent
1401 proteins (green) mark synaptic components and anti-HRP (red) marks neurons.
1402 Comparison of wild-type to dKO. Graph shows quantification of synaptic bouton
1403 number by anti-Dlg1 staining. Significance of dKO bouton number was calculated
1404 with a T-test compared to WT. Error bars show mean with SD. N ≥ 7 NMJs (each
1405 from a different animal).
1406
1407 **Supplemental Figure 5. Related to Figure 5. A-C.** Transmission electron
1408 microscopy (TEM) images of sectioned adult eye photoreceptors from indicated
1409 genetic backgrounds with accompanying quantification of photoreceptor number
1410 and aberrant photoreceptors. Scalebar is 2μm. Filled red arrows indicate dead or
1411 dying photoreceptors. Open red arrows indicate unhealthy photoreceptors. Error
1412 bars show mean with SD. **A.** Animals were 4 weeks old and raised in a 12hr
1413 light/dark cycle. **B.** Animals were 1-3 days old and raised in a 12hr light/dark
1414 cycle. **C.** Animals were 4 weeks old and raised in the dark.
1415
1416 **Supplemental Figure 6. Related to Figure 5.** Confocal microscopy of adult eye
1417 photoreceptors stained with phalloidin (green) and anti-Rh1 (red). Animals were
1418 4 weeks old and raised in the dark. Arrows indicate photoreceptors with higher
1419 levels of Rh1.
1420
1421 **Supplemental Figure 7. Related to Figure 6.** Confocal microscopy of 3rd instar
1422 larval brain with antibody staining. Anti-Sloth1 or Anti-Sloth2 (green),
1423 mitochondria labeled with anti-ATP5alpha (red), and nuclei labeled with DAPI

1424 (blue). Wild-type (*yw*) or *sloth1/2* KO. **A.** Zoom out of entire brain showing region
1425 imaged in panels B and C. Scale bar 100μm. **B.** Results using two independent
1426 anti-Sloth1 antibodies (#1 and #2). Scale bar 20μm. **C.** Results using two
1427 independent anti-Sloth2 antibodies (#1 and #2). Scale bar 20μm**.**
1428
1429 **Supplemental Figure 8. Related to Figure 6.** SDS-PAGE and western blotting
1430 using anti-Sloth1 and anti-Sloth2 antibodies of cell and mitochondrial lysates.
1431 Two independent (#1 and #2) anti-Sloth1 and Anti-Sloth2 antibodies were tested.
1432 Arrowheads indicated expected band, asterisks indicate unrelated band(s).
1433 Tricine gels were used. **A.** S2R+ whole cell lysates isolated from indicated
1434 genotypes. Rhodamine-Actin used as loading control. **B.** S2R+ mitochondrial
1435 lysates isolated from indicated genotypes. Anti-ATP5alpha used as loading
1436 control. Mitochondrial control = ATP5alpha, cytoplasmic control = alpha-tubulin.
1437 **C.** S2R+ fractions isolated from wild-type S2R+ cells. WCL = Whole Cell Lysate,
1438 cyto. = cytoplasmic lysate, mito. = mitochondrial lysate. Blots were stripped and
1439 reprobed after detection of each antigen. **D.** Mitochondrial lysates isolated from
1440 3rd instar larvae or adult thorax mitochondrial isolation of indicated genotypes.
1441 "da>" indicates da-Gal4 crossed with attP40 (wild-type), RNAi (UAS-shRNA-
1442 sloth1/2), OE (UAS-sloth1/2 transcript).
1443
1444 **Supplemental Figure 9. Related to Figure 7. A.** Sequence analysis of single
1445 KO S2R+ clones for *sloth1* (clone 2F8) and *sloth2* (clone 3A7). sgRNA and PAM
1446 site indicated by grey boxes. **B.** PCR genotyping of four independently derived
1447 single cell dKO S2R+ clones. **C-D.** Seahorse mitochondrial stress test
1448 quantification of **C.** ATP production and **D.** Proton leak. Significance of KO lines
1449 was calculated with a T-test compared to S2R+. Error bars show mean with SD.
1450 ** P≤0.01, *** P≤0.001, **** P≤0.0001. N=6 for each genotype. **E.** Confocal
1451 images of 3rd instar larval ventral nerve cord (VNC), axon bundles, and
1452 neuromuscular junction (NMJ). *MN-Gal4 UAS-mitoGFP* (*MN>mitoGFP*) (GFP)
1453 expresses mitochondrial-localized GFP in motor neurons. Neurons are stained
1454 with anti-HRP (magenta).
1455
1456 **Supplemental Figure 10. Related to Figure 7. A-B.** TEM images of sectioned
1457 adult photoreceptors. **A.** Adult flies are 4 weeks old and raised on a 12hr
1458 light/dark cycle. Mitochondria are indicated with red dots. **B.** Adult flies are 3 days
1459 old and raised in a 12hr light/dark cycle.
1460
1461 **Supplemental File 1.** Genomic sequence of *sloth1-sloth2* homologs in *D.*
1462 *melanogaster*, *S. urceolata*, *P. marinus*, and *C. intestinalis*
1463
1464 **Supplemental File 2.** Oligo and dsDNA sequences
1465
1466 **Supplemental File 3.** Gateway cloning plasmid list
1467
1468 **Supplemental File 4.** Raw gel and western images
1469

References:

Alloway, P. G., L. Howard and P. J. Dolph, 2000 The formation of stable rhodopsin-arrestin complexes induces apoptosis and photoreceptor cell degeneration. Neuron 28: 129-138.

Anderson, D. M., K. M. Anderson, C. L. Chang, C. A. Makarewich, B. R. Nelson *et al.*, 2015 A micropeptide encoded by a putative long noncoding RNA regulates muscle performance. Cell 160: 595-606.

Antonicka, H., Z. Y. Lin, A. Janer, M. J. Aaltonen, W. Weraarpachai *et al.*, 2020 A High-Density Human Mitochondrial Proximity Interaction Network. Cell Metab 32: 479-497 e479.

Basrai, M. A., P. Hieter and J. D. Boeke, 1997 Small open reading frames: beautiful needles in the haystack. Genome Res 7: 768-771.

Bergendahl, L. T., L. Gerasimavicius, J. Miles, L. Macdonald, J. N. Wells *et al.*, 2019 The role of protein complexes in human genetic disease. Protein Sci 28: 1400-1411.

Bi, P., A. Ramirez-Martinez, H. Li, J. Cannavino, J. R. McAnally *et al.*, 2017 Control of muscle formation by the fusogenic micropeptide myomixer. Science 356: 323-327.

Blumenthal, T., 2004 Operons in eukaryotes. Brief Funct Genomic Proteomic 3: 199-211.

Bosch, J. A., N. H. Tran and I. K. Hariharan, 2015 CoinFLP: a system for efficient mosaic screening and for visualizing clonal boundaries in Drosophila. Development 142: 597-606.

Brand, A. H., and N. Perrimon, 1993 Targeted gene expression as a means of altering cell fates and generating dominant phenotypes. Development 118: 401-415.

Brent, J. R., K. M. Werner and B. D. McCabe, 2009 Drosophila larval NMJ dissection. J Vis Exp.

Busch, J. D., M. Cipullo, I. Atanassov, A. Bratic, E. Silva Ramos *et al.*, 2019 MitoRibo-Tag Mice Provide a Tool for In Vivo Studies of Mitoribosome Composition. Cell Rep 29: 1728-1738 e1729.

Calvo, S. E., K. R. Clauser and V. K. Mootha, 2016 MitoCarta2.0: an updated inventory of mammalian mitochondrial proteins. Nucleic Acids Res 44: D1251-1257.

Casson, S. A., P. M. Chilley, J. F. Topping, I. M. Evans, M. A. Souter *et al.*, 2002 The POLARIS gene of Arabidopsis encodes a predicted peptide required for correct root growth and leaf vascular patterning. Plant Cell 14: 1705-1721.

Cavener, D. R., 1987 Comparison of the consensus sequence flanking translational start sites in Drosophila and vertebrates. Nucleic Acids Res 15: 1353-1361.

Chen, C. L., Y. Hu, N. D. Udeshi, T. Y. Lau, F. Wirtz-Peitz *et al.*, 2015 Proteomic mapping in live Drosophila tissues using an engineered ascorbate peroxidase. Proc Natl Acad Sci U S A 112: 12093-12098.

Chen, J., A. D. Brunner, J. Z. Cogan, J. K. Nunez, A. P. Fields *et al.*, 2020 Pervasive functional translation of noncanonical human open reading frames. Science 367: 1140-1146.

Chng, S. C., L. Ho, J. Tian and B. Reversade, 2013 ELABELA: a hormone essential for heart development signals via the apelin receptor. Dev Cell 27: 672-680.

1516 Chugunova, A., E. Loseva, P. Mazin, A. Mitina, T. Navalayeu *et al.*, 2019 LINC00116
1517 codes for a mitochondrial peptide linking respiration and lipid metabolism.
1518 Proc Natl Acad Sci U S A 116**:** 4940-4945.
1519 Couso, J. P., and P. Patraquim, 2017 Classification and function of small open reading
1520 frames. Nat Rev Mol Cell Biol 18**:** 575-589.
1521 Crosby, M. A., L. S. Gramates, G. Dos Santos, B. B. Matthews, S. E. St Pierre *et al.*, 2015
1522 Gene Model Annotations for Drosophila melanogaster: The Rule-Benders. G3
1523 (Bethesda) 5**:** 1737-1749.
1524 Dennerlein, S., S. Poerschke, S. Oeljeklaus, C. Wang, R. Richter-Dennerlein *et al.*, 2021
1525 Defining the interactome of the human mitochondrial ribosome identifies
1526 SMIM4 and TMEM223 as respiratory chain assembly factors. Elife 10.
1527 Fricker, L. D., 2005 Neuropeptide-processing enzymes: applications for drug
1528 discovery. AAPS J 7**:** E449-455.
1529 Fukasawa, Y., J. Tsuji, S. C. Fu, K. Tomii, P. Horton *et al.*, 2015 MitoFates: improved
1530 prediction of mitochondrial targeting sequences and their cleavage sites. Mol
1531 Cell Proteomics 14**:** 1113-1126.
1532 Galindo, M. I., J. I. Pueyo, S. Fouix, S. A. Bishop and J. P. Couso, 2007 Peptides encoded
1533 by short ORFs control development and define a new eukaryotic gene family.
1534 PLoS Biol 5**:** e106.
1535 Garcia, C. J., J. Khajeh, E. Coulanges, E. I. Chen and E. Owusu-Ansah, 2017 Regulation
1536 of Mitochondrial Complex I Biogenesis in Drosophila Flight Muscles. Cell Rep
1537 20**:** 264-278.
1538 Golpich, M., E. Amini, Z. Mohamed, R. Azman Ali, N. Mohamed Ibrahim *et al.*, 2017
1539 Mitochondrial Dysfunction and Biogenesis in Neurodegenerative diseases:
1540 Pathogenesis and Treatment. CNS Neurosci Ther 23**:** 5-22.
1541 Gratz, S. J., F. P. Ukken, C. D. Rubinstein, G. Thiede, L. K. Donohue *et al.*, 2014 Highly
1542 specific and efficient CRISPR/Cas9-catalyzed homology-directed repair in
1543 Drosophila. Genetics 196**:** 961-971.
1544 Guo, X., A. Chavez, A. Tung, Y. Chan, C. Kaas *et al.*, 2018 High-throughput creation
1545 and functional profiling of DNA sequence variant libraries using CRISPR-Cas9
1546 in yeast. Nat Biotechnol 36**:** 540-546.
1547 Hardie, R. C., and P. Raghu, 2001 Visual transduction in Drosophila. Nature 413**:**
1548 186-193.
1549 Hoskins, R. A., J. M. Landolin, J. B. Brown, J. E. Sandler, H. Takahashi *et al.*, 2011
1550 Genome-wide analysis of promoter architecture in Drosophila melanogaster.
1551 Genome Res 21**:** 182-192.
1552 Hsu, P. Y., and P. N. Benfey, 2018 Small but Mighty: Functional Peptides Encoded by
1553 Small ORFs in Plants. Proteomics 18**:** e1700038.
1554 Jaiswal, M., N. A. Haelterman, H. Sandoval, B. Xiong, T. Donti *et al.*, 2015 Impaired
1555 Mitochondrial Energy Production Causes Light-Induced Photoreceptor
1556 Degeneration Independent of Oxidative Stress. PLoS Biol 13**:** e1002197.
1557 Kann, O., and R. Kovacs, 2007 Mitochondria and neuronal activity. Am J Physiol Cell
1558 Physiol 292**:** C641-657.
1559 Karginov, T. A., D. P. H. Pastor, B. L. Semler and C. M. Gomez, 2017 Mammalian
1560 Polycistronic mRNAs and Disease. Trends Genet 33**:** 129-142.

1561 Katsir, L., K. A. Davies, D. C. Bergmann and T. Laux, 2011 Peptide signaling in plant
1562 development. Curr Biol 21**:** R356-364.
1563 Kumar, S., Y. Yoshida and M. Noda, 1993 Cloning of a cDNA which encodes a novel
1564 ubiquitin-like protein. Biochem Biophys Res Commun 195**:** 393-399.
1565 Liu, X., K. Salokas, F. Tamene, Y. Jiu, R. G. Weldatsadik *et al.*, 2018 An AP-MS- and
1566 BioID-compatible MAC-tag enables comprehensive mapping of protein
1567 interactions and subcellular localizations. Nat Commun 9**:** 1188.
1568 Magny, E. G., J. I. Pueyo, F. M. Pearl, M. A. Cespedes, J. E. Niven *et al.*, 2013 Conserved
1569 regulation of cardiac calcium uptake by peptides encoded in small open
1570 reading frames. Science 341**:** 1116-1120.
1571 Makarewich, C. A., K. K. Baskin, A. Z. Munir, S. Bezprozvannaya, G. Sharma *et al.*,
1572 2018 MOXI Is a Mitochondrial Micropeptide That Enhances Fatty Acid beta-
1573 Oxidation. Cell Rep 23**:** 3701-3709.
1574 Mudge, J. M., J. Ruiz-Orera, J. R. Prensner, M. A. Brunet, F. Calvet *et al.*, 2022
1575 Standardized annotation of translated open reading frames. Nat Biotechnol
1576 40**:** 994-999.
1577 Murari, A., S. K. Rhooms, N. S. Goparaju, M. Villanueva and E. Owusu-Ansah, 2020 An
1578 antibody toolbox to track complex I assembly defines AIF's mitochondrial
1579 function. J Cell Biol 219.
1580 Nelson, B. R., C. A. Makarewich, D. M. Anderson, B. R. Winders, C. D. Troupes *et al.*,
1581 2016 A peptide encoded by a transcript annotated as long noncoding RNA
1582 enhances SERCA activity in muscle. Science 351**:** 271-275.
1583 Ni, J. Q., R. Zhou, B. Czech, L. P. Liu, L. Holderbaum *et al.*, 2011 A genome-scale shRNA
1584 resource for transgenic RNAi in Drosophila. Nat Methods 8**:** 405-407.
1585 Nickless, A., J. M. Bailis and Z. You, 2017 Control of gene expression through the
1586 nonsense-mediated RNA decay pathway. Cell Biosci 7**:** 26.
1587 Papp, B., C. Pal and L. D. Hurst, 2003 Dosage sensitivity and the evolution of gene
1588 families in yeast. Nature 424**:** 194-197.
1589 Pauli, A., M. L. Norris, E. Valen, G. L. Chew, J. A. Gagnon *et al.*, 2014 Toddler: an
1590 embryonic signal that promotes cell movement via Apelin receptors. Science
1591 343**:** 1248636.
1592 Pearson, R. K., B. Anderson and J. E. Dixon, 1993 Molecular biology of the peptide
1593 hormone families. Endocrinol Metab Clin North Am 22**:** 753-774.
1594 Pellegrino, M. W., A. M. Nargund and C. M. Haynes, 2013 Signaling the mitochondrial
1595 unfolded protein response. Biochim Biophys Acta 1833**:** 410-416.
1596 Perkins, L. A., L. Holderbaum, R. Tao, Y. Hu, R. Sopko *et al.*, 2015 The Transgenic
1597 RNAi Project at Harvard Medical School: Resources and Validation. Genetics
1598 201**:** 843-852.
1599 Plaza, S., G. Menschaert and F. Payre, 2017 In Search of Lost Small Peptides. Annu
1600 Rev Cell Dev Biol 33**:** 391-416.
1601 Port, F., H. M. Chen, T. Lee and S. L. Bullock, 2014 Optimized CRISPR/Cas tools for
1602 efficient germline and somatic genome engineering in Drosophila. Proc Natl
1603 Acad Sci U S A 111**:** E2967-2976.
1604 Prelich, G., 2012 Gene overexpression: uses, mechanisms, and interpretation.
1605 Genetics 190**:** 841-854.

1606 Pueyo, J. I., E. G. Magny, C. J. Sampson, U. Amin, I. R. Evans *et al.*, 2016 Hemotin, a
1607 Regulator of Phagocytosis Encoded by a Small ORF and Conserved across
1608 Metazoans. PLoS Biol 14**:** e1002395.
1609 Richter, D. J., P. Fozouni, M. B. Eisen and N. King, 2018 Gene family innovation,
1610 conservation and loss on the animal stem lineage. Elife 7.
1611 Saghatelian, A., and J. P. Couso, 2015 Discovery and characterization of smORF-
1612 encoded bioactive polypeptides. Nat Chem Biol 11**:** 909-916.
1613 Sandoval, H., C. K. Yao, K. Chen, M. Jaiswal, T. Donti *et al.*, 2014 Mitochondrial fusion
1614 but not fission regulates larval growth and synaptic development through
1615 steroid hormone production. Elife 3.
1616 Sardiello, M., F. Licciulli, D. Catalano, M. Attimonelli and C. Caggese, 2003
1617 MitoDrome: a database of Drosophila melanogaster nuclear genes encoding
1618 proteins targeted to the mitochondrion. Nucleic Acids Res 31**:** 322-324.
1619 Savojardo, C., N. Bruciaferri, G. Tartari, P. L. Martelli and R. Casadio, 2020 DeepMito:
1620 accurate prediction of protein sub-mitochondrial localization using
1621 convolutional neural networks. Bioinformatics 36**:** 56-64.
1622 Snyder, S. H., and R. B. Innis, 1979 Peptide neurotransmitters. Annu Rev Biochem
1623 48**:** 755-782.
1624 Sopko, R., D. Huang, N. Preston, G. Chua, B. Papp *et al.*, 2006 Mapping pathways and
1625 phenotypes by systematic gene overexpression. Mol Cell 21**:** 319-330.
1626 Stapleton, M., J. Carlson, P. Brokstein, C. Yu, M. Champe *et al.*, 2002 A Drosophila full-
1627 length cDNA resource. Genome Biol 3**:** RESEARCH0080.
1628 Stein, C. S., P. Jadiya, X. Zhang, J. M. McLendon, G. M. Abouassaly *et al.*, 2018
1629 Mitoregulin: A lncRNA-Encoded Microprotein that Supports Mitochondrial
1630 Supercomplexes and Respiratory Efficiency. Cell Rep 23**:** 3710-3720 e3718.
1631 Suzuki, K., T. Hashimoto and E. Otaka, 1990 Yeast ribosomal proteins: XI. Molecular
1632 analysis of two genes encoding YL41, an extremely small and basic ribosomal
1633 protein, from Saccharomyces cerevisiae. Curr Genet 17**:** 185-190.
1634 Szklarczyk, R., M. A. Huynen and B. Snel, 2008 Complex fate of paralogs. BMC Evol
1635 Biol 8**:** 337.
1636 Taylor, J. S., and J. Raes, 2004 Duplication and divergence: the evolution of new
1637 genes and old ideas. Annu Rev Genet 38**:** 615-643.
1638 Thompson, S. R., 2012 So you want to know if your message has an IRES? Wiley
1639 Interdiscip Rev RNA 3**:** 697-705.
1640 Thul, P. J., L. Akesson, M. Wiking, D. Mahdessian, A. Geladaki *et al.*, 2017 A
1641 subcellular map of the human proteome. Science 356.
1642 Trevisan, T., D. Pendin, A. Montagna, S. Bova, A. M. Ghelli *et al.*, 2018 Manipulation of
1643 Mitochondria Dynamics Reveals Separate Roles for Form and Function in
1644 Mitochondria Distribution. Cell Rep 23**:** 1742-1753.
1645 Ugur, B., H. Bao, M. Stawarski, L. R. Duraine, Z. Zuo *et al.*, 2017 The Krebs Cycle
1646 Enzyme Isocitrate Dehydrogenase 3A Couples Mitochondrial Metabolism to
1647 Synaptic Transmission. Cell Rep 21**:** 3794-3806.
1648 Usui, S., L. Yu and C. A. Yu, 1990 The small molecular mass ubiquinone-binding
1649 protein (QPc-9.5 kDa) in mitochondrial ubiquinol-cytochrome c reductase:
1650 isolation, ubiquinone-binding domain, and immunoinhibition. Biochemistry
1651 29**:** 4618-4626.

1652 Van Der Kelen, K., R. Beyaert, D. Inze and L. De Veylder, 2009 Translational control
1653 of eukaryotic gene expression. Crit Rev Biochem Mol Biol 44**:** 143-168.
1654 Veitia, R. A., S. Bottani and J. A. Birchler, 2008 Cellular reactions to gene dosage
1655 imbalance: genomic, transcriptomic and proteomic effects. Trends Genet 24**:**
1656 390-397.
1657 Verstreken, P., C. V. Ly, K. J. Venken, T. W. Koh, Y. Zhou *et al.*, 2005 Synaptic
1658 mitochondria are critical for mobilization of reserve pool vesicles at
1659 Drosophila neuromuscular junctions. Neuron 47**:** 365-378.
1660 Viswanatha, R., Z. Li, Y. Hu and N. Perrimon, 2018 Pooled genome-wide CRISPR
1661 screening for basal and context-specific fitness gene essentiality in
1662 Drosophila cells. Elife 7.
1663 Wang, J. W., E. S. Beck and B. D. McCabe, 2012 A modular toolset for recombination
1664 transgenesis and neurogenetic analysis of Drosophila. PLoS One 7**:** e42102.
1665 Wu, C. F., and F. Wong, 1977 Frequency characteristics in the visual system of
1666 Drosophila: genetic dissection of electroretinogram components. J Gen
1667 Physiol 69**:** 705-724.
1668 Xue, Z., M. Ren, M. Wu, J. Dai, Y. S. Rong *et al.*, 2014 Efficient gene knock-out and
1669 knock-in with transgenic Cas9 in Drosophila. G3 (Bethesda) 4**:** 925-929.
1670 Yamamoto, S., M. Jaiswal, W. L. Charng, T. Gambin, E. Karaca *et al.*, 2014 A drosophila
1671 genetic resource of mutants to study mechanisms underlying human genetic
1672 diseases. Cell 159**:** 200-214.
1673 Yanagawa, S., J. S. Lee and A. Ishimoto, 1998 Identification and characterization of a
1674 novel line of Drosophila Schneider S2 cells that respond to wingless
1675 signaling. J Biol Chem 273**:** 32353-32359.
1676 Yang, L., and A. Veraksa, 2017 Single-Step Affinity Purification of ERK Signaling
1677 Complexes Using the Streptavidin-Binding Peptide (SBP) Tag. Methods Mol
1678 Biol 1487**:** 113-126.
1679 Yeasmin, F., T. Yada and N. Akimitsu, 2018 Micropeptides Encoded in Transcripts
1680 Previously Identified as Long Noncoding RNAs: A New Chapter in
1681 Transcriptomics and Proteomics. Front Genet 9**:** 144.
1682 Zhang, S., B. Reljic, C. Liang, B. Kerouanton, J. C. Francisco *et al.*, 2020 Mitochondrial
1683 peptide BRAWNIN is essential for vertebrate respiratory complex III
1684 assembly. Nat Commun 11**:** 1312.
1685 Zhou, R., I. Hotta, A. M. Denli, P. Hong, N. Perrimon *et al.*, 2008 Comparative analysis
1686 of argonaute-dependent small RNA pathways in Drosophila. Mol Cell 32**:** 592-
1687 599.
1688

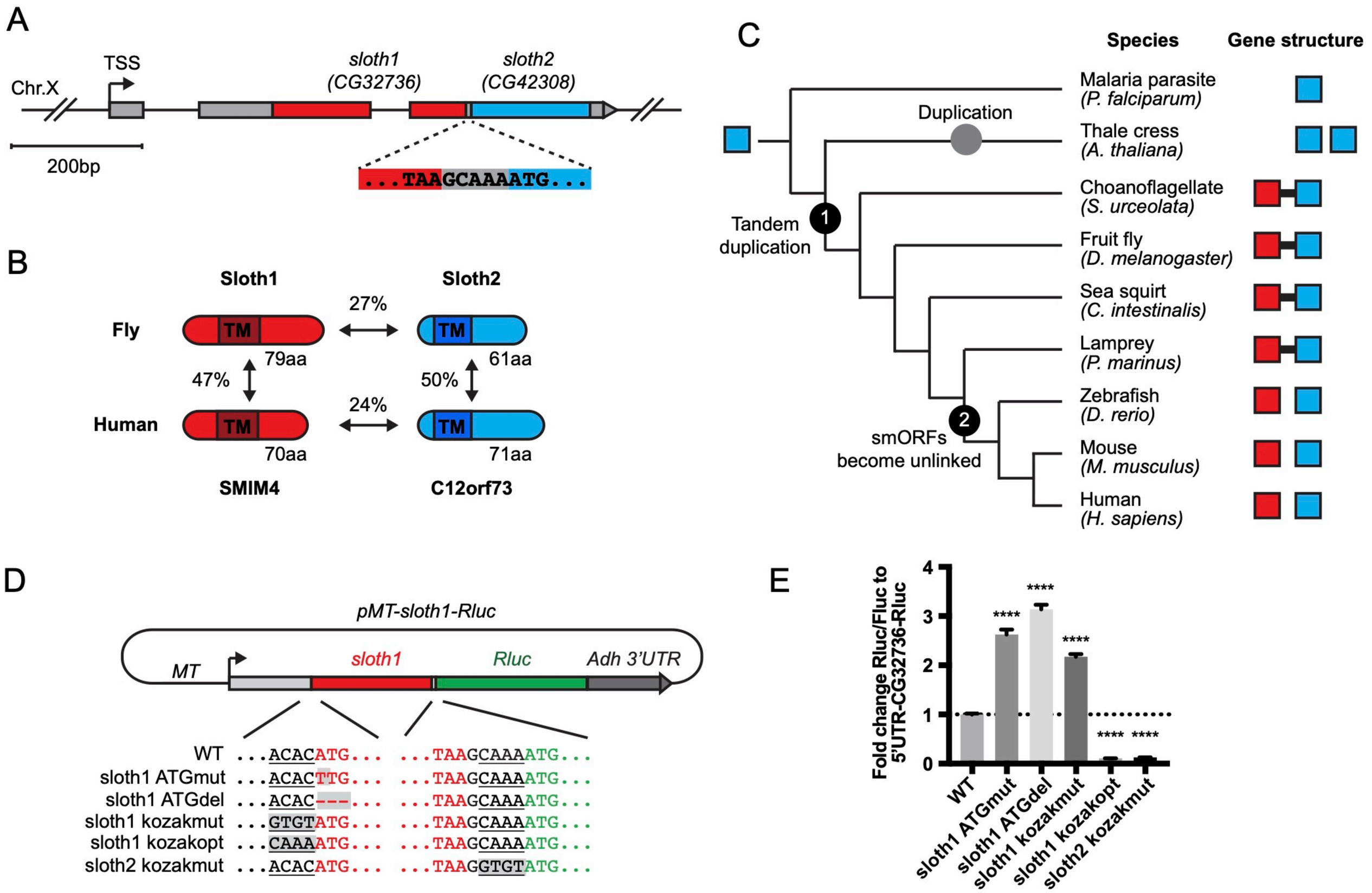
A
TSS
Chr.X
sloth1
(CG32736)
sloth2
(CG42308)
200bp
...TAAGCAAAATG...
B
Sloth1
Sloth2
Fly
Human
TM
79aa
61aa
70aa
71aa
27%
47%
50%
24%
SMIM4
C12orf73
C
Species
Gene structure
Duplication
Tandem
duplication
smORFs
become unlinked
Malaria parasite
(P. falciparum)
Thale cress
(A. thaliana)
Choanoflagellate
(S. urceolata)
Fruit fly
(D. melanogaster)
Sea squirt
(C. intestinalis)
Lamprey
(P. marinus)
Zebrafish
(D. rerio)
Mouse
(M. musculus)
Human
(H. sapiens)
D
pMT-sloth1-Rluc
MT
sloth1
Rluc
Adh 3'UTR
WT ...ACACATG... ...TAAGCAAAATG...
sloth1 ATGmut ...ACACTTG... ...TAAGCAAAATG...
sloth1 ATGdel ...ACAC---... ...TAAGCAAAATG...
sloth1 kozakmut ...GTGTATG... ...TAAGCAAAATG...
sloth1 kozakopt ...CAAAATG... ...TAAGCAAAATG...
sloth2 kozakmut ...ACACATG... ...TAAGGTGTATG...
E
Fold change Rluc/Fluc to
5'UTR-CG32736-Rluc
****
WT
sloth1 ATGmut
sloth1 ATGdel
sloth1 kozakmut
sloth1 kozakopt
sloth2 kozakmut

Figure 1

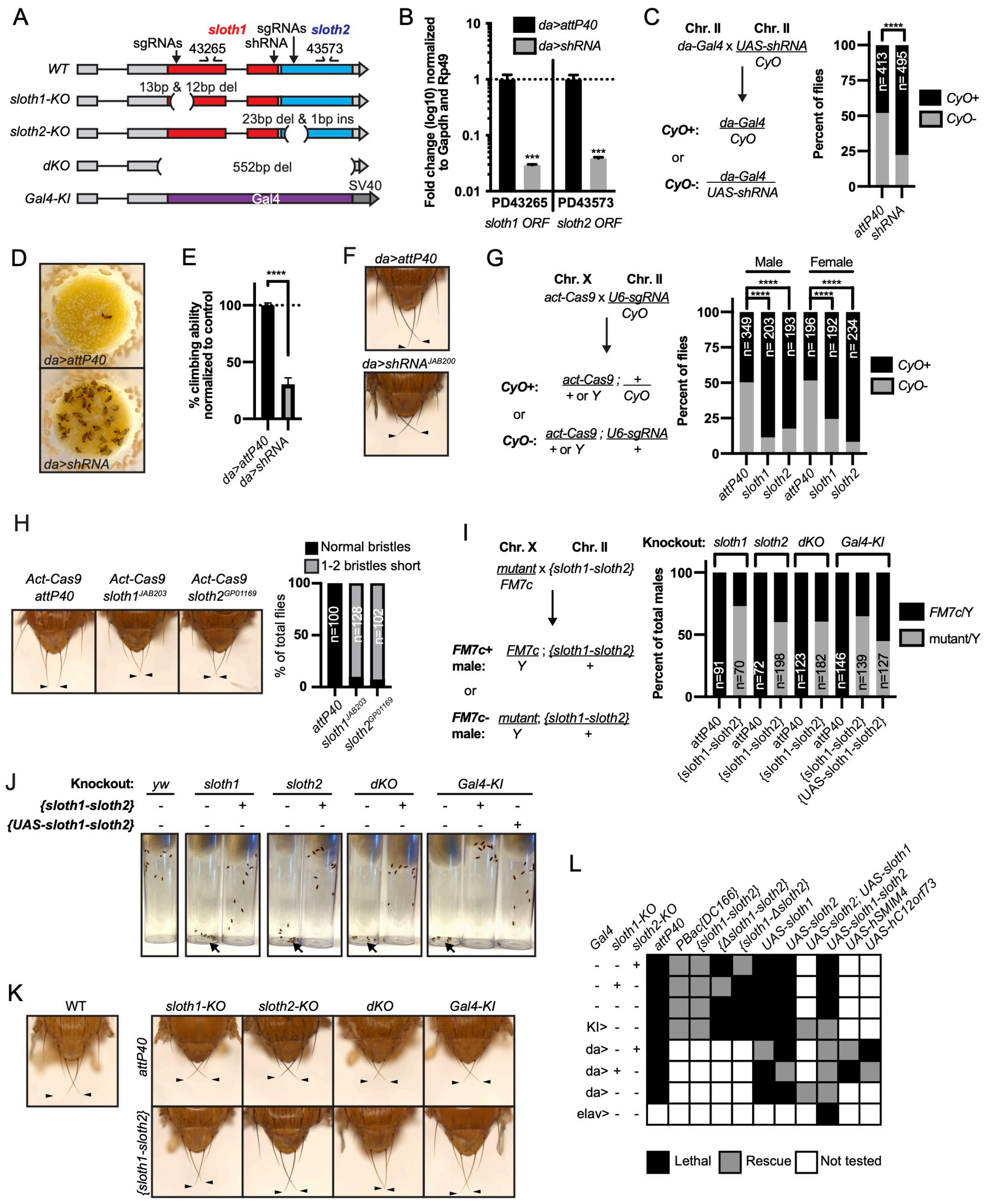
A
sloth1
sgRNAs
sloth2
sgRNAs
43265
shRNA
43573
WT
13bp & 12bp del
sloth1-KO
23bp del & 1bp ins
sloth2-KO
dKO
552bp del
SV40
Gal4-KI
Gal4
B
da>attP40
da>shRNA
Fold change (log10) normalized to Gapdh and Rp49
10
1
0.1
0.01
***
PD43265
PD43573
sloth1 ORF
sloth2 ORF
C
Chr. II
Chr. II
da-Gal4 x UAS-shRNA
CyO
CyO+:
da-Gal4
CyO
or
CyO-:
da-Gal4
UAS-shRNA
Percent of flies
****
n= 413
n= 495
CyO+
CyO-
attP40
shRNA
D
da>attP40
da>shRNA
E
% climbing ability normalized to control
100
50
0
****
da>attP40
da>shRNA
F
da>attP40
da>shRNA^JAB200
G
Chr. X
Chr. II
act-Cas9 x U6-sgRNA
CyO
CyO+:
act-Cas9 ; +
+ or Y
CyO
or
CyO-:
act-Cas9 ; U6-sgRNA
+ or Y
+
Male
Female
Percent of flies
n= 349
n= 203
n= 193
n= 196
n= 192
n= 234
attP40
sloth1
sloth2
H
Act-Cas9 attP40
Act-Cas9 sloth1^JAB203
Act-Cas9 sloth2^GP01169
Normal bristles
1-2 bristles short
% of total flies
n=100
n=128
n=102
I
Chr. X
Chr. II
mutant x {sloth1-sloth2}
FM7c
FM7c+ male:
FM7c ; {sloth1-sloth2}
Y
+
or
FM7c- male:
mutant; {sloth1-sloth2}
Y
+
Knockout: sloth1 sloth2 dKO Gal4-KI
Percent of total males
FM7c/Y
mutant/Y
n=91
n=70
n=72
n=198
n=123
n=182
n=146
n=139
n=127
attP40
{sloth1-sloth2}
{UAS-sloth1-sloth2}
J
Knockout: yw sloth1 sloth2 dKO Gal4-KI
{sloth1-sloth2}
{UAS-sloth1-sloth2}
K
WT
sloth1-KO
sloth2-KO
dKO
Gal4-KI
attP40
{sloth1-sloth2}
L
Gal4
sloth1-KO
sloth2-KO
attP40
PBac{DC166}
{sloth1-sloth2}
{Δsloth1-sloth2}
{sloth1-Δsloth2}
UAS-sloth1
UAS-sloth2
UAS-sloth2; UAS-sloth1
UAS-sloth1-sloth2
UAS-hSMIM4
UAS-hC12orf73
Kl>
da>
elav>
Lethal
Rescue
Not tested

Figure 2

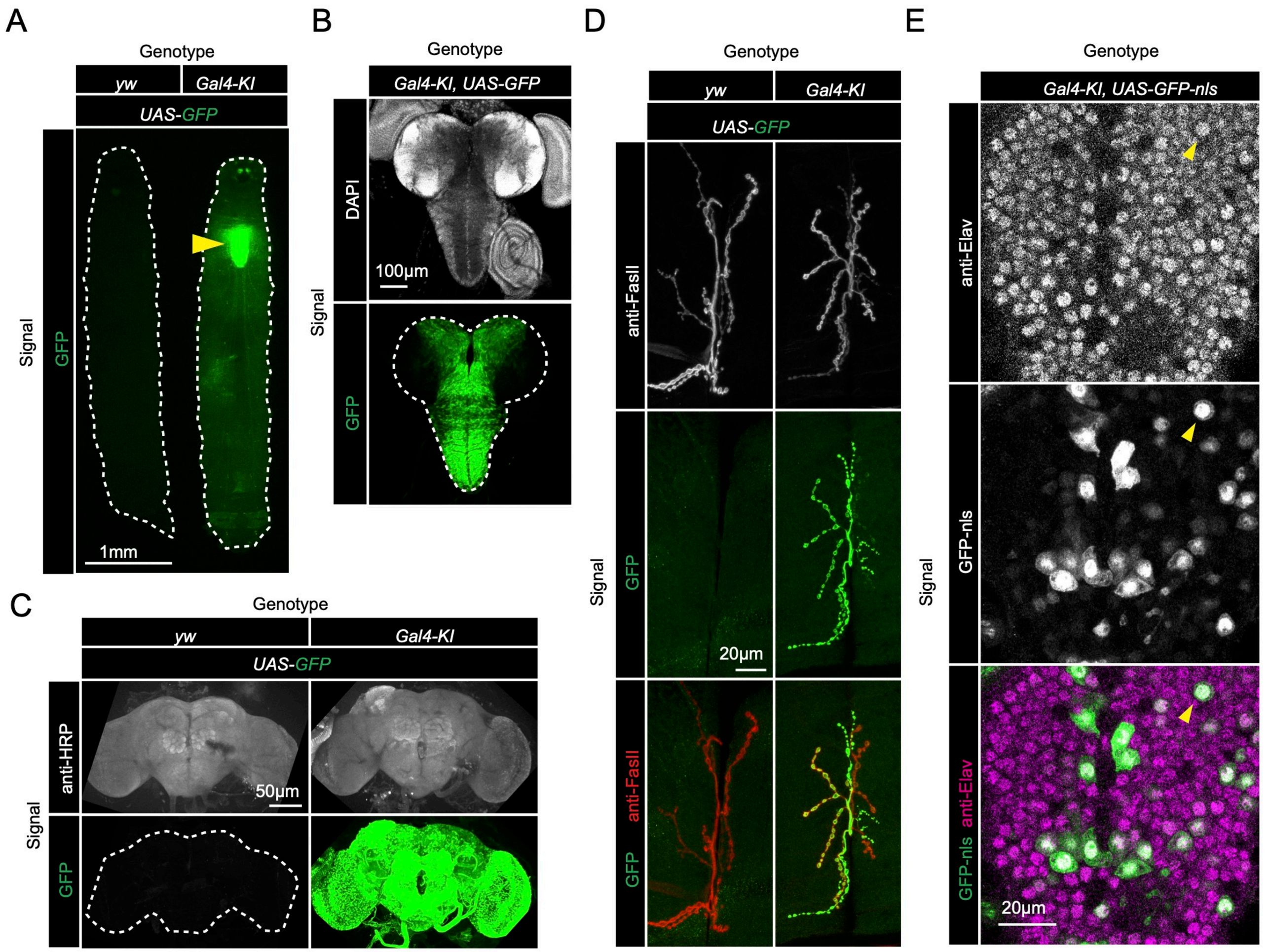
A
Genotype
yw
Gal4-KI
UAS-GFP
Signal
GFP
1mm
B
Genotype
Gal4-KI, UAS-GFP
DAPI
100µm
Signal
GFP
C
Genotype
yw
Gal4-KI
UAS-GFP
anti-HRP
50µm
Signal
GFP
D
Genotype
yw
Gal4-KI
UAS-GFP
anti-FasII
Signal
GFP
20µm
anti-FasII
GFP
E
Genotype
Gal4-KI, UAS-GFP-nls
anti-Elav
Signal
GFP-nls
anti-Elav
GFP-nls
20µm

Figure 3

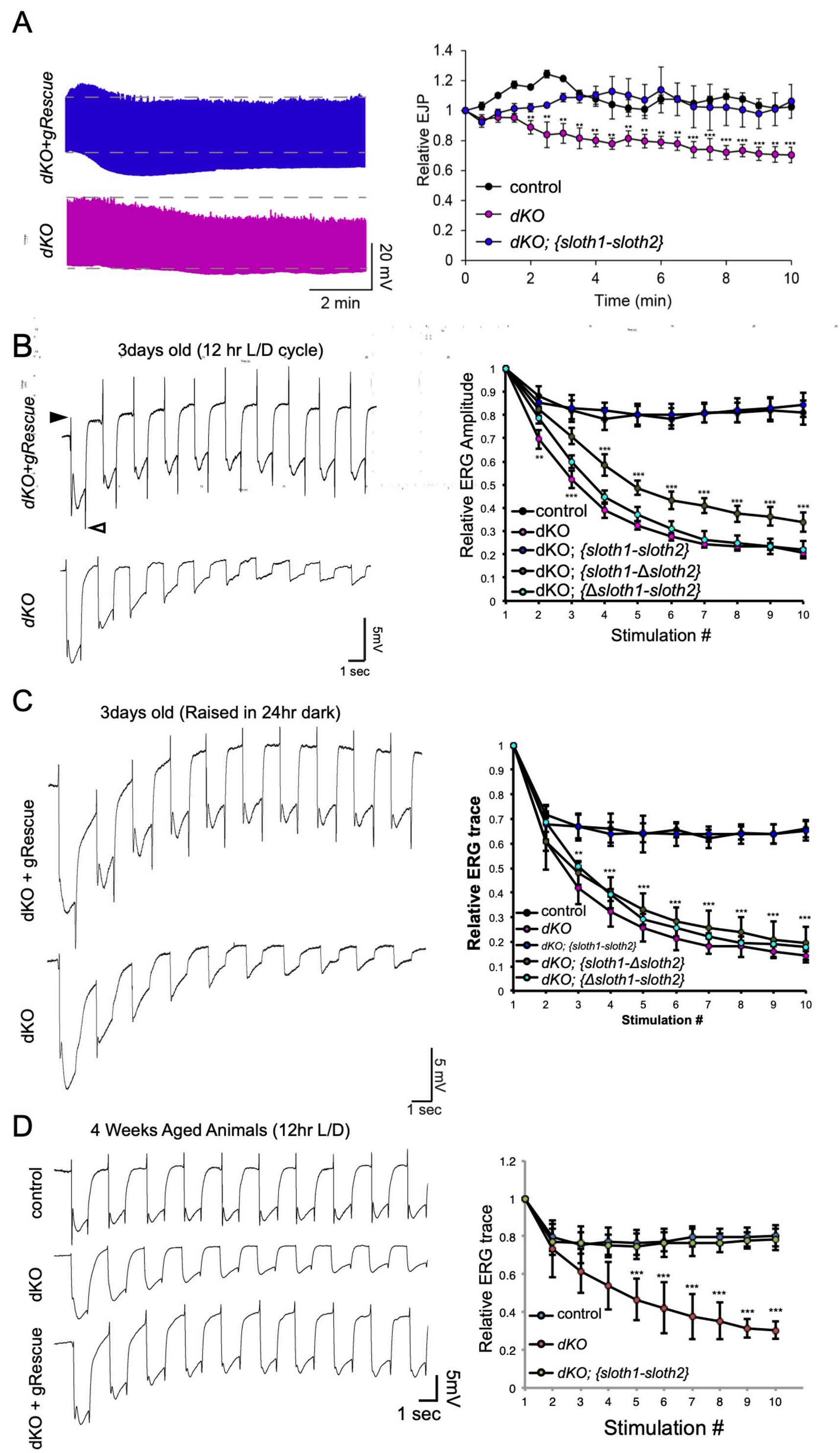
A
dKO+gRescue
dKO
20 mV
2 min
Relative EJP
control
dKO
dKO; {sloth1-sloth2}
Time (min)
B
3days old (12 hr L/D cycle)
dKO+gRescue
dKO
5mV
1 sec
Relative ERG Amplitude
control
dKO
dKO; {sloth1-sloth2}
dKO; {sloth1-Δsloth2}
dKO; {Δsloth1-sloth2}
Stimulation #
C
3days old (Raised in 24hr dark)
dKO + gRescue
dKO
5 mV
1 sec
Relative ERG trace
control
dKO
dKO; {sloth1-sloth2}
dKO; {sloth1-Δsloth2}
dKO; {Δsloth1-sloth2}
Stimulation #
D
4 Weeks Aged Animals (12hr L/D)
control
dKO
dKO + gRescue
5mV
1 sec
Relative ERG trace
control
dKO
dKO; {sloth1-sloth2}
Stimulation #

Figure 4

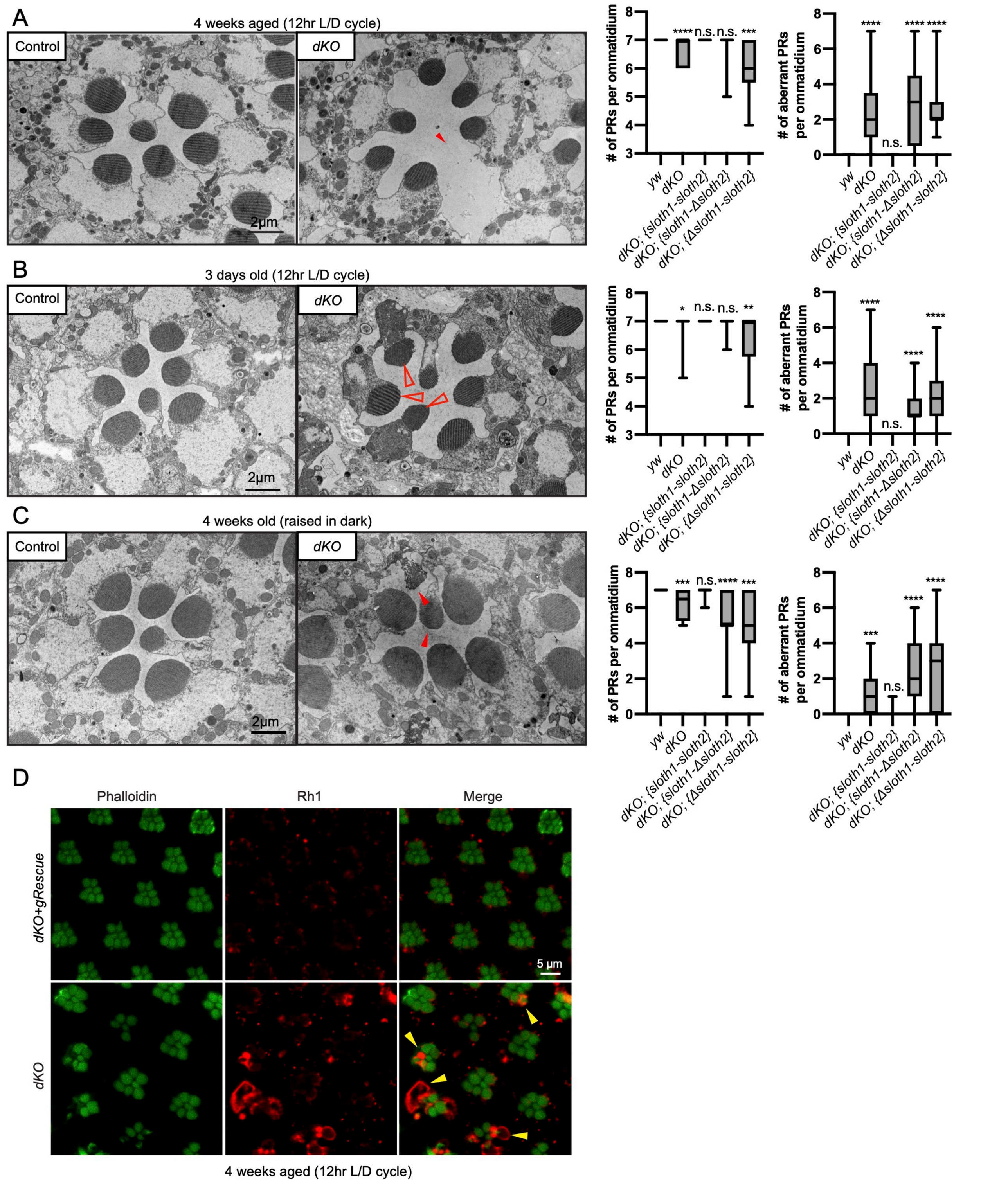
A
4 weeks aged (12hr L/D cycle)
Control
dKO
2μm
B
3 days old (12hr L/D cycle)
Control
dKO
2μm
C
4 weeks old (raised in dark)
Control
dKO
2μm
D
Phalloidin
Rh1
Merge
dKO+gRescue
dKO
5 μm
4 weeks aged (12hr L/D cycle)
# of PRs per ommatidium
# of aberrant PRs per ommatidium
yw
dKO
dKO; {sloth1-sloth2}
dKO; {sloth1-Δsloth2}
dKO; {Δsloth1-sloth2}
****
n.s.
***
*
**

Figure 5

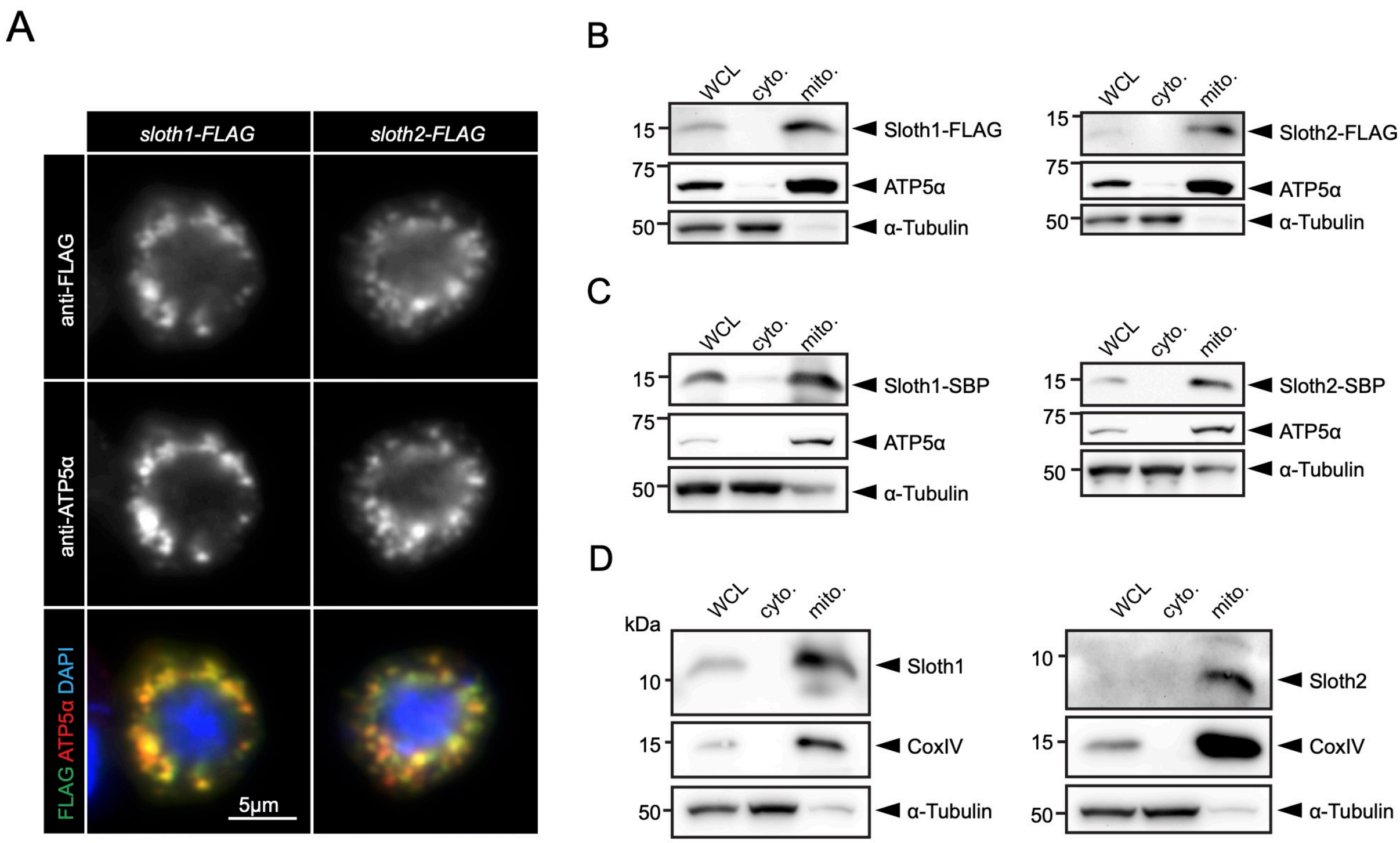
A
sloth1-FLAG
sloth2-FLAG
anti-FLAG
anti-ATP5α
FLAG ATP5α DAPI
5μm
B
WCL
cyto.
mito.
15
75
50
Sloth1-FLAG
ATP5α
α-Tubulin
Sloth2-FLAG
C
Sloth1-SBP
Sloth2-SBP
D
kDa
10
Sloth1
Sloth2
CoxIV

Figure 6

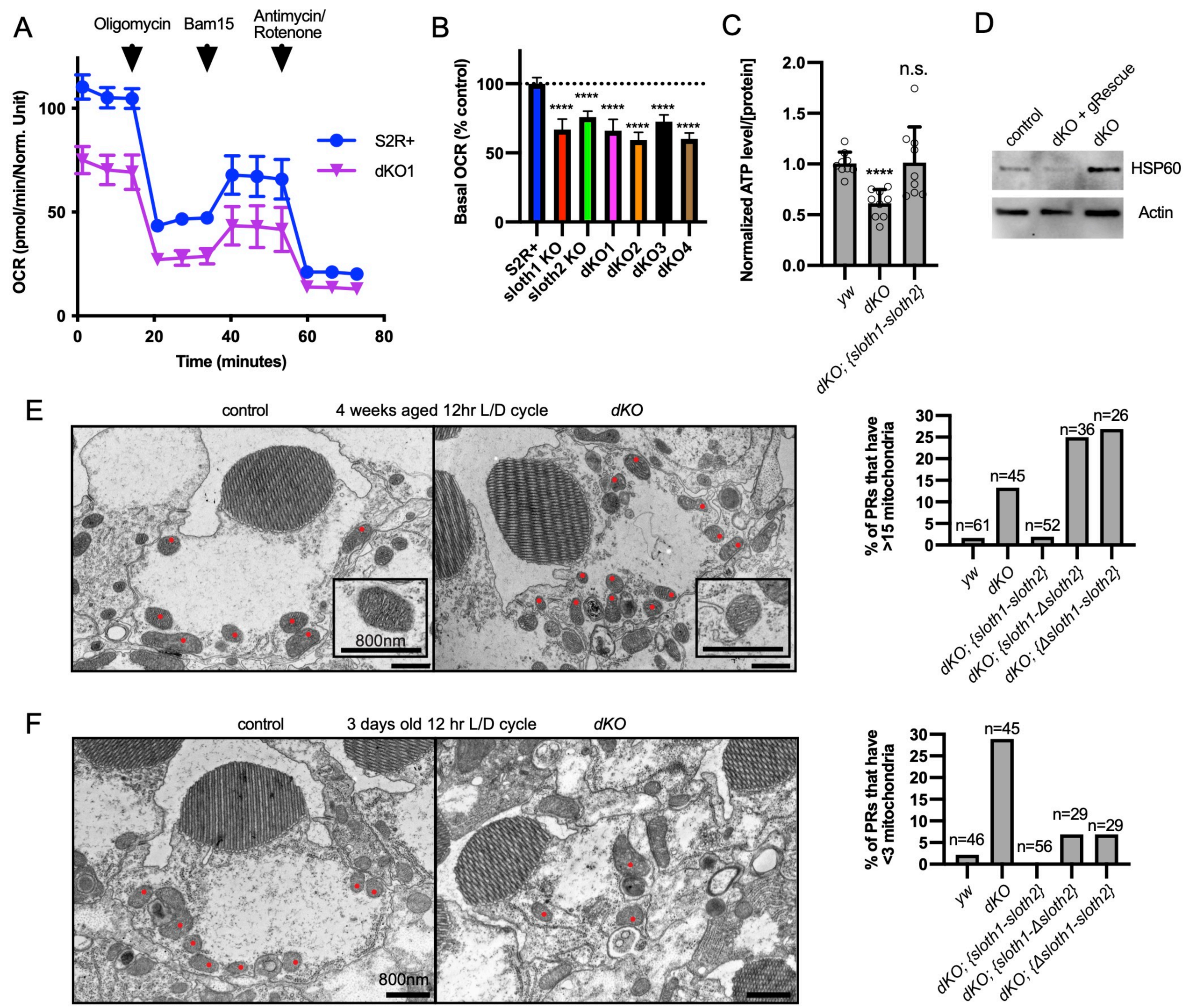
A
Oligomycin
Bam15
Antimycin/
Rotenone
OCR (pmol/min/Norm. Unit)
Time (minutes)
S2R+
dKO1
B
Basal OCR (% control)
S2R+
sloth1 KO
sloth2 KO
dKO1
dKO2
dKO3
dKO4
C
Normalized ATP level/[protein]
n.s.
yw
dKO
dKO; {sloth1-sloth2}
D
control
dKO + gRescue
dKO
HSP60
Actin
E
control
4 weeks aged 12hr L/D cycle
dKO
800nm
% of PRs that have >15 mitochondria
n=61
n=45
n=52
n=36
n=26
dKO; {sloth1-Δsloth2}
dKO; {Δsloth1-sloth2}
F
control
3 days old 12 hr L/D cycle
dKO
800nm
% of PRs that have <3 mitochondria
n=46
n=45
n=56
n=29
n=29

Figure 7

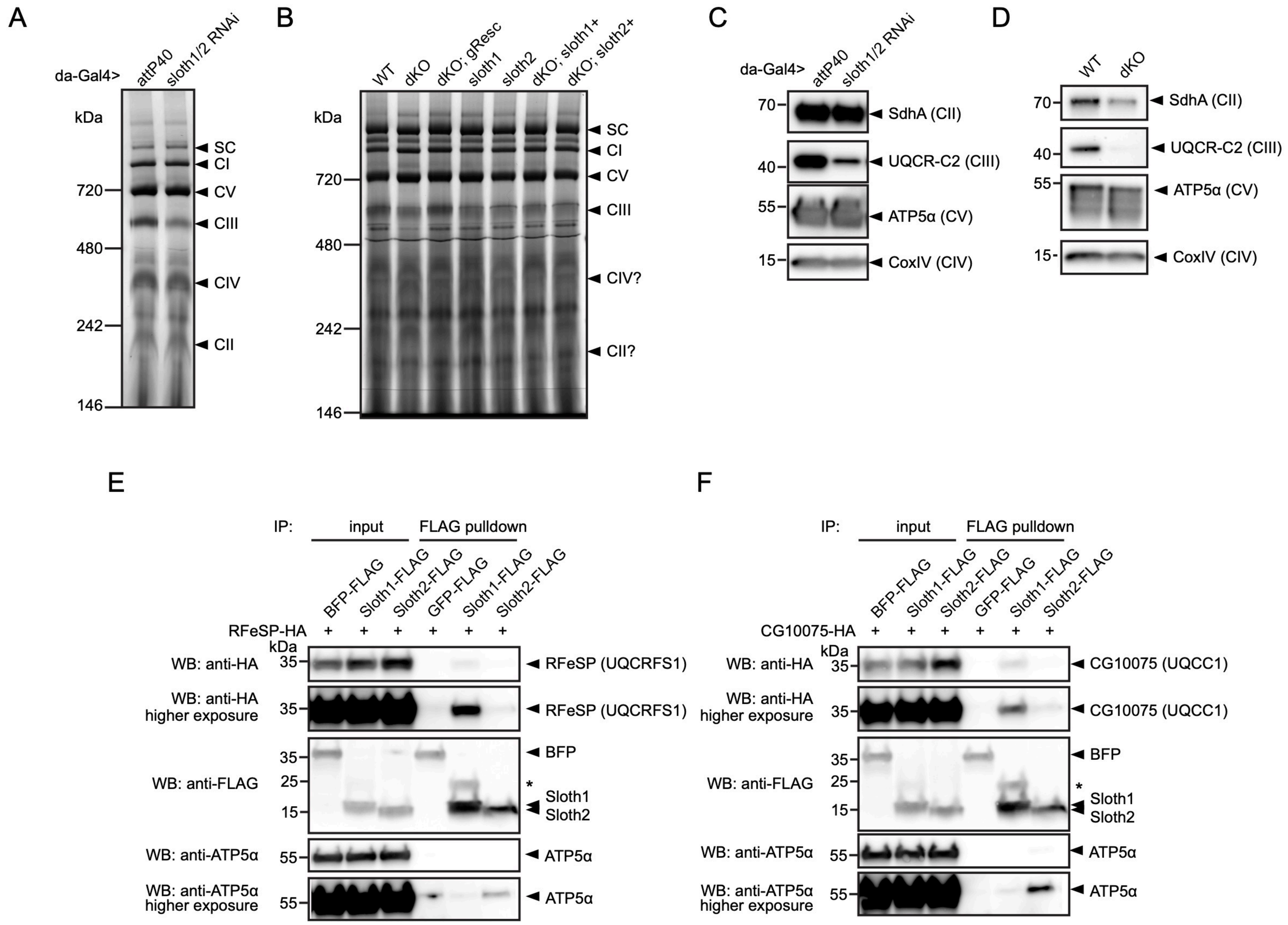
A
da-Gal4>
attP40
sloth1/2 RNAi
kDa
720
480
242
146
SC
CI
CV
CIII
CIV
CII
B
WT
dKO
dKO; gResc
sloth1
sloth2
dKO; sloth1+
dKO; sloth2+
kDa
720
480
242
146
SC
CI
CV
CIII
CIV?
CII?
C
da-Gal4>
attP40
sloth1/2 RNAi
70
40
55
15
SdhA (CII)
UQCR-C2 (CIII)
ATP5α (CV)
CoxIV (CIV)
D
WT
dKO
70
40
55
15
SdhA (CII)
UQCR-C2 (CIII)
ATP5α (CV)
CoxIV (CIV)
E
IP:
input
FLAG pulldown
BFP-FLAG
Sloth1-FLAG
Sloth2-FLAG
GFP-FLAG
Sloth1-FLAG
Sloth2-FLAG
RFeSP-HA
kDa
WB: anti-HA
35
RFeSP (UQCRFS1)
WB: anti-HA higher exposure
35
RFeSP (UQCRFS1)
WB: anti-FLAG
35
25
15
BFP
*
Sloth1
Sloth2
WB: anti-ATP5α
55
ATP5α
WB: anti-ATP5α higher exposure
55
ATP5α
F
IP:
input
FLAG pulldown
BFP-FLAG
Sloth1-FLAG
Sloth2-FLAG
GFP-FLAG
Sloth1-FLAG
Sloth2-FLAG
CG10075-HA
kDa
WB: anti-HA
35
CG10075 (UQCC1)
WB: anti-HA higher exposure
35
CG10075 (UQCC1)
WB: anti-FLAG
35
25
15
BFP
*
Sloth1
Sloth2
WB: anti-ATP5α
55
ATP5α
WB: anti-ATP5α higher exposure
55
ATP5α

Figure 8

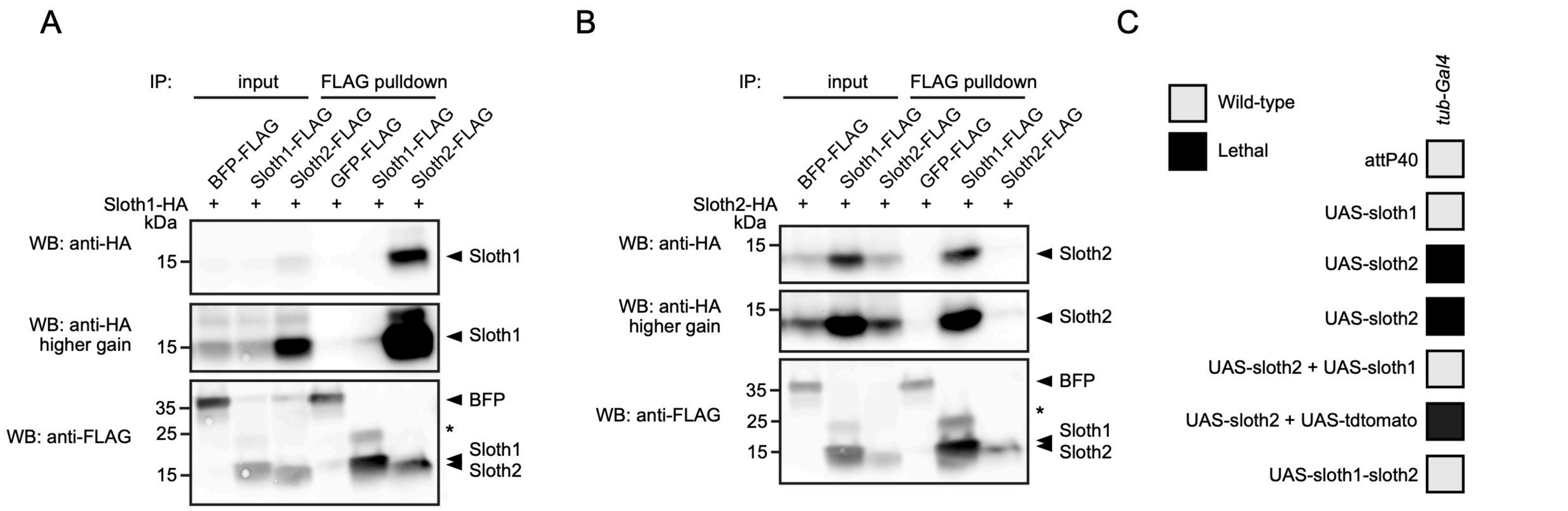
A
IP:
input
FLAG pulldown
BFP-FLAG
Sloth1-FLAG
Sloth2-FLAG
GFP-FLAG
Sloth1-FLAG
Sloth2-FLAG
Sloth1-HA
kDa
WB: anti-HA
15
Sloth1
WB: anti-HA higher gain
15
Sloth1
35
25
15
WB: anti-FLAG
BFP
*
Sloth1
Sloth2
B
IP:
input
FLAG pulldown
BFP-FLAG
Sloth1-FLAG
Sloth2-FLAG
GFP-FLAG
Sloth1-FLAG
Sloth2-FLAG
Sloth2-HA
kDa
WB: anti-HA
15
Sloth2
WB: anti-HA higher gain
15
Sloth2
35
25
15
WB: anti-FLAG
BFP
*
Sloth1
Sloth2
C
Wild-type
Lethal
tub-Gal4
attP40
UAS-sloth1
UAS-sloth2
UAS-sloth2
UAS-sloth2 + UAS-sloth1
UAS-sloth2 + UAS-tdtomato
UAS-sloth1-sloth2

Figure 9

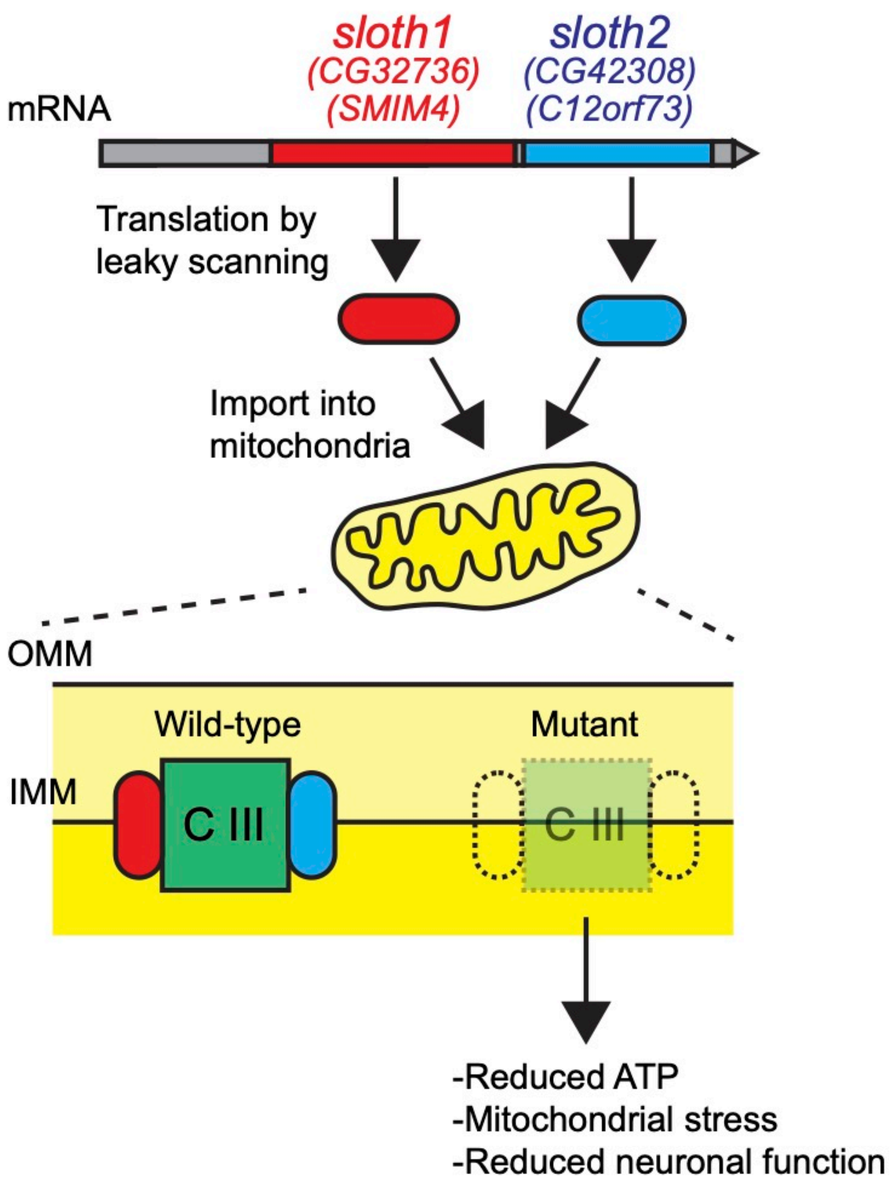
sloth1
(CG32736)
(SMIM4)
sloth2
(CG42308)
(C12orf73)
mRNA
Translation by
leaky scanning
Import into
mitochondria
OMM
IMM
Wild-type
Mutant
C III
C III
-Reduced ATP
-Mitochondrial stress
-Reduced neuronal function

Figure 10

A

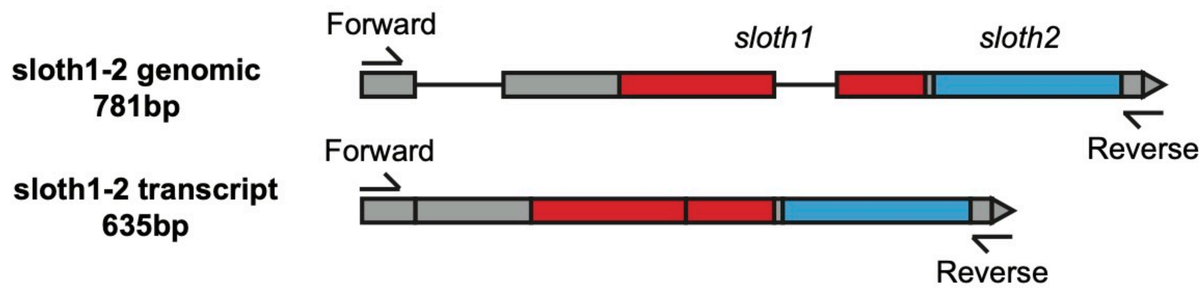


```
Forward   AATCGAACAGCTGATTGCTG
Reverse   CTTAAATAGCTTTAGTCACCAATAACTTG
```

Key
Underlined – primer binding site
lowercase – intron
UPPERCASE – exon
RED – sloth1 coding sequence
BLUE – sloth 2 coding sequence

sloth1-2 genomic
781bp

AATCGAACAGCTGATTGCTGCGAACCGGAACAAATGGAAATTGTATCGTGAGgcaagtggagtttccccttttacttttggcaaat
aataaataaacaaaggaacaagcctaaacattttcaattaaaccatatacagAACTAACGCACACATGTGACGGAGGCAATACAC
AAACACGGCACCTTTGAATCTCGCCTTAAAATTGGCGAAACCAACACGGAATTATATAACCGCCGGCTGAAAACACATGAGTCCG
TACAGCGGATCCGTGCGTCGTCTGCTGGACAGTTGGCCAGGAAAGAAGCGCTTCGGTGTCTACCGCTTCCTGCCGCTCTTCTTTT
TACTGGGCGCCGGCCTGGAATTCTCCATGATCAATTGGACAGTGGGCGAGACCAATTTCTgtgagactgctacgcttaaaacctt
actttatttactaatacggaatcttttccatgcagACCGCACTTTTAAGCGCCGCCAGGCGAAGAACTACGTGGAAGAGCAGCA
GCATCTGCAGGCGCGAGCCGCGAATAACACCAACTAAGCAAAATGCCCGCCGGAGTTTCCTGGGGCCAGTACCTGAAATTCCTCG
GCTGTGCCCTGGCATCCATGATGGCCGGATCGCAGGCTGTTCACCTTTACTATAAGCCTCTGGAGGACTTGCGCGTCTACATCGA
ACAGGAGCAACACAGCACACAGGTGGATCCCACCGCAAAGCCACCGGAATCTGCATAACACTGTGTACTAGACAAGTTATTGGTG
ACTAAAGCTATTTAAG

sloth1-2 transcript
635bp

AATCGAACAGCTGATTGCTGCGAACCGGAACAAATGGAAATTGTATCGTGAGAACTAACGCACACATGTGACGGAGGCAATACAC
AAACACGGCACCTTTGAATCTCGCCTTAAAATTGGCGAAACCAACACGGAATTATATAACCGCCGGCTGAAAACACATGAGTCCG
TACAGCGGATCCGTGCGTCGTCTGCTGGACAGTTGGCCAGGAAAGAAGCGCTTCGGTGTCTACCGCTTCCTGCCGCTCTTCTTTT
TACTGGGCGCCGGCCTGGAATTCTCCATGATCAATTGGACAGTGGGCGAGACCAATTTCTACCGCACTTTTAAGCGCCGCCAGGC
GAAGAACTACGTGGAAGAGCAGCAGCATCTGCAGGCGCGAGCCGCGAATAACACCAACTAAGCAAAATGCCCGCCGGAGTTTCCT
GGGGCCAGTACCTGAAATTCCTCGGCTGTGCCCTGGCATCCATGATGGCCGGATCGCAGGCTGTTCACCTTTACTATAAGCCTCT
GGAGGACTTGCGCGTCTACATCGAACAGGAGCAACACAGCACACAGGTGGATCCCACCGCAAAGCCACCGGAATCTGCATAACAC
TGTGTACTAGACAAGTTATTGGTGACTAAAGCTATTTAAG

B

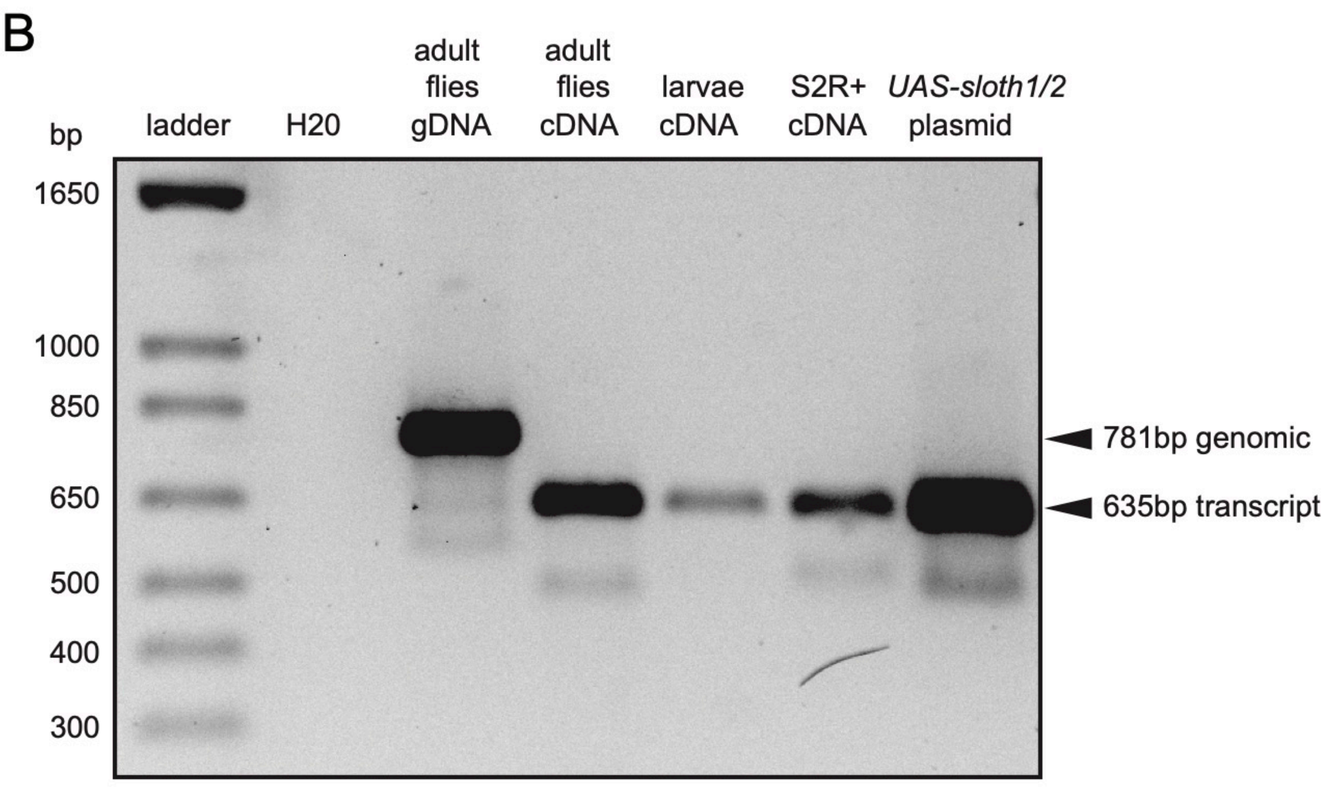

Figure 1-figure supplement 1

Figure 2-figure supplement 1

A

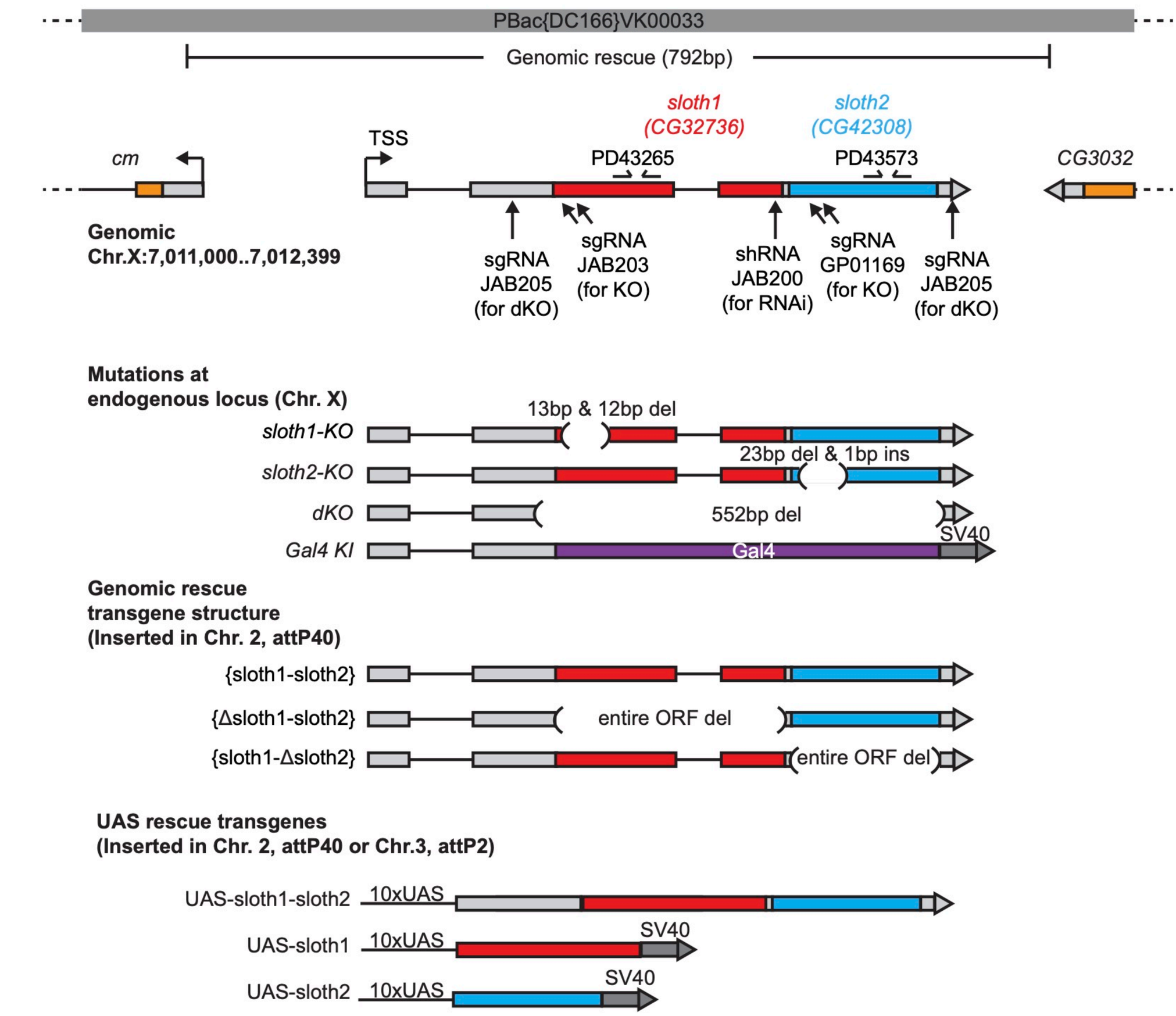

B

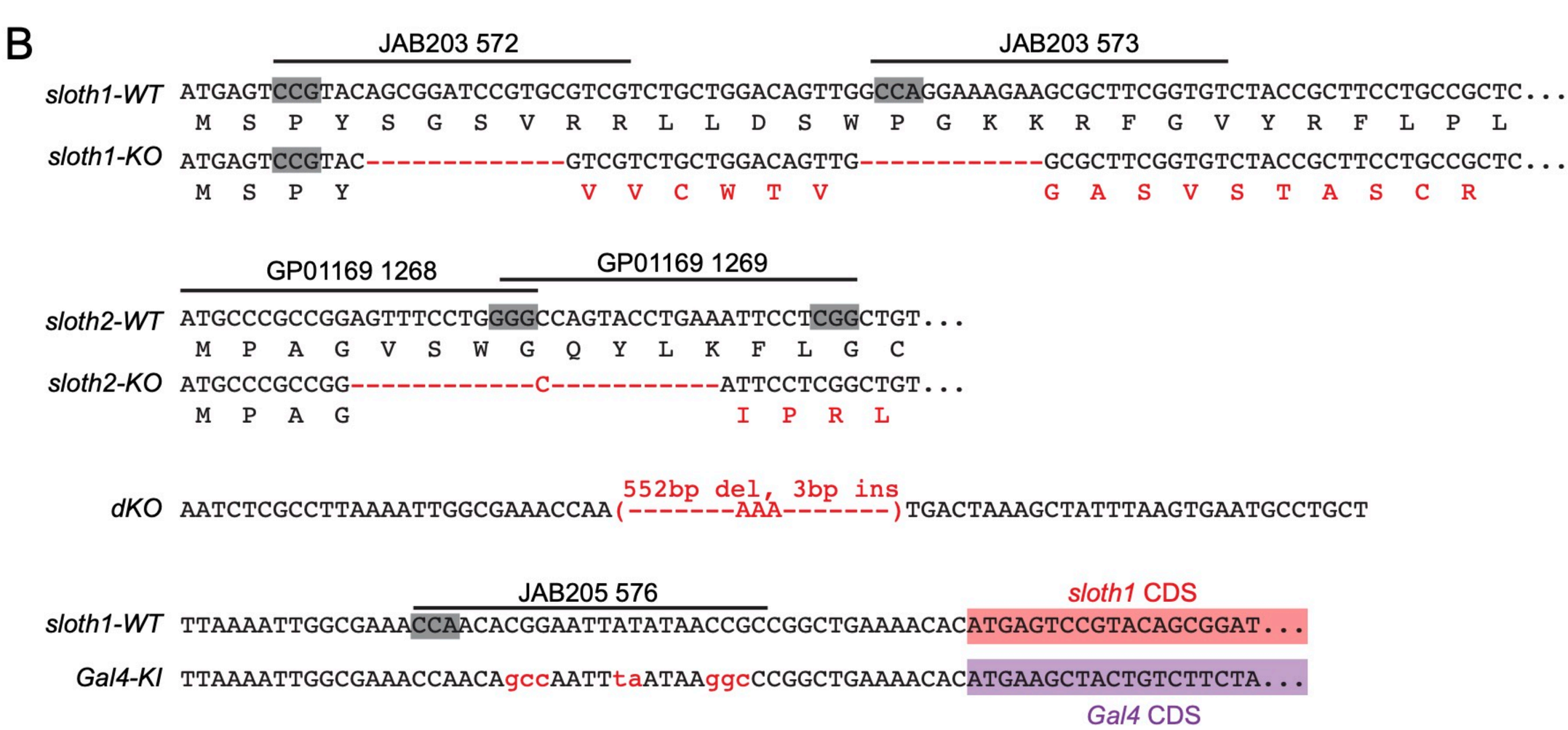

C

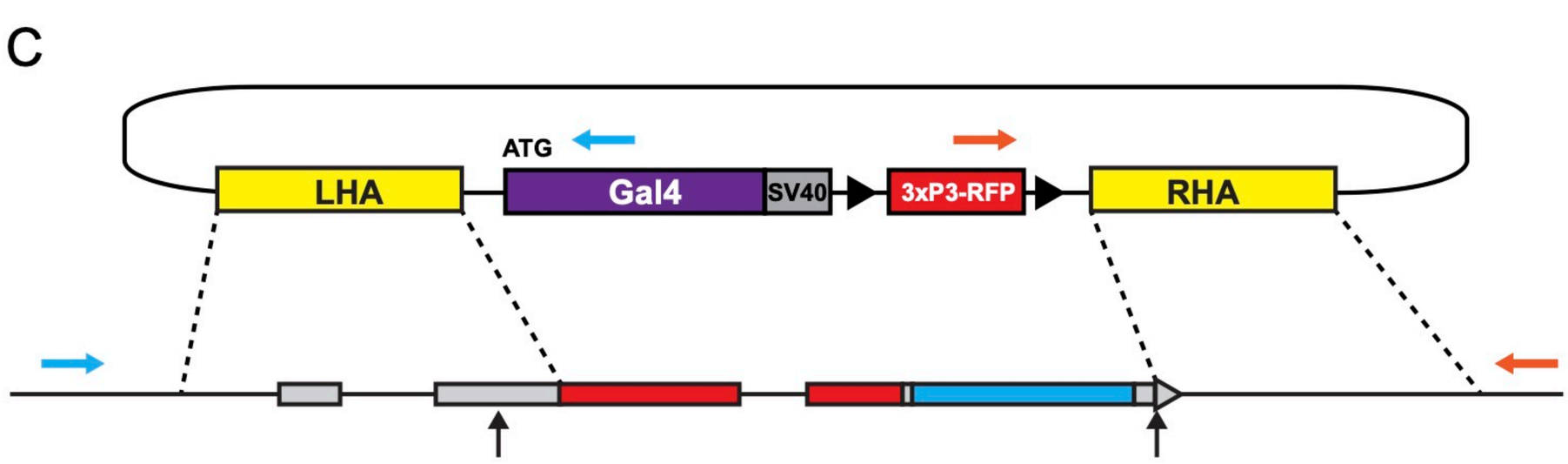

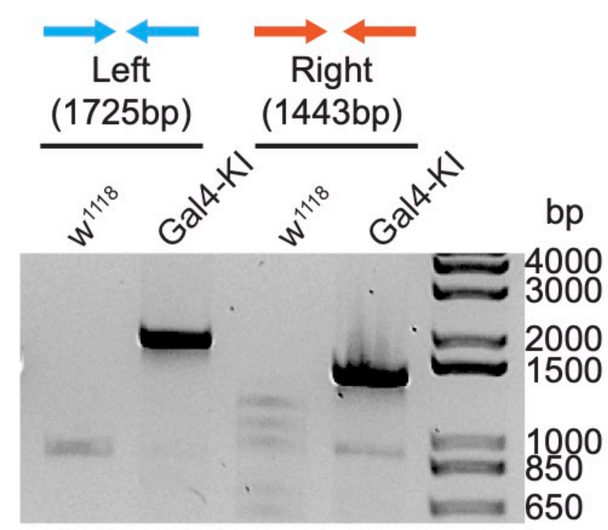

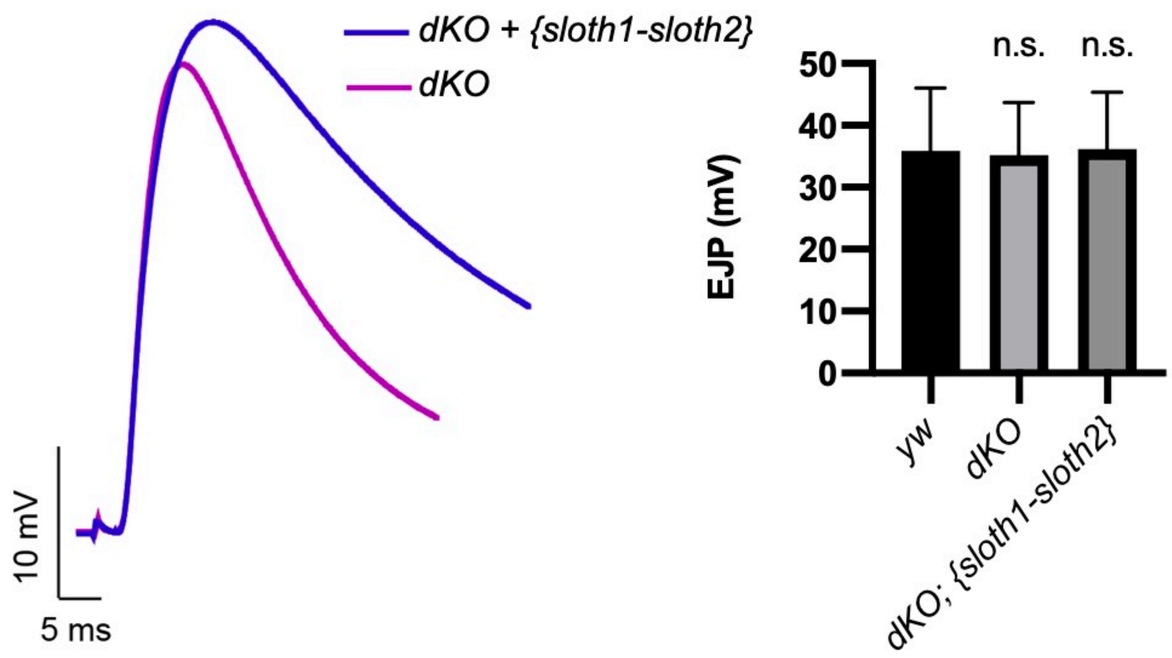

Figure 4-figure supplement 1

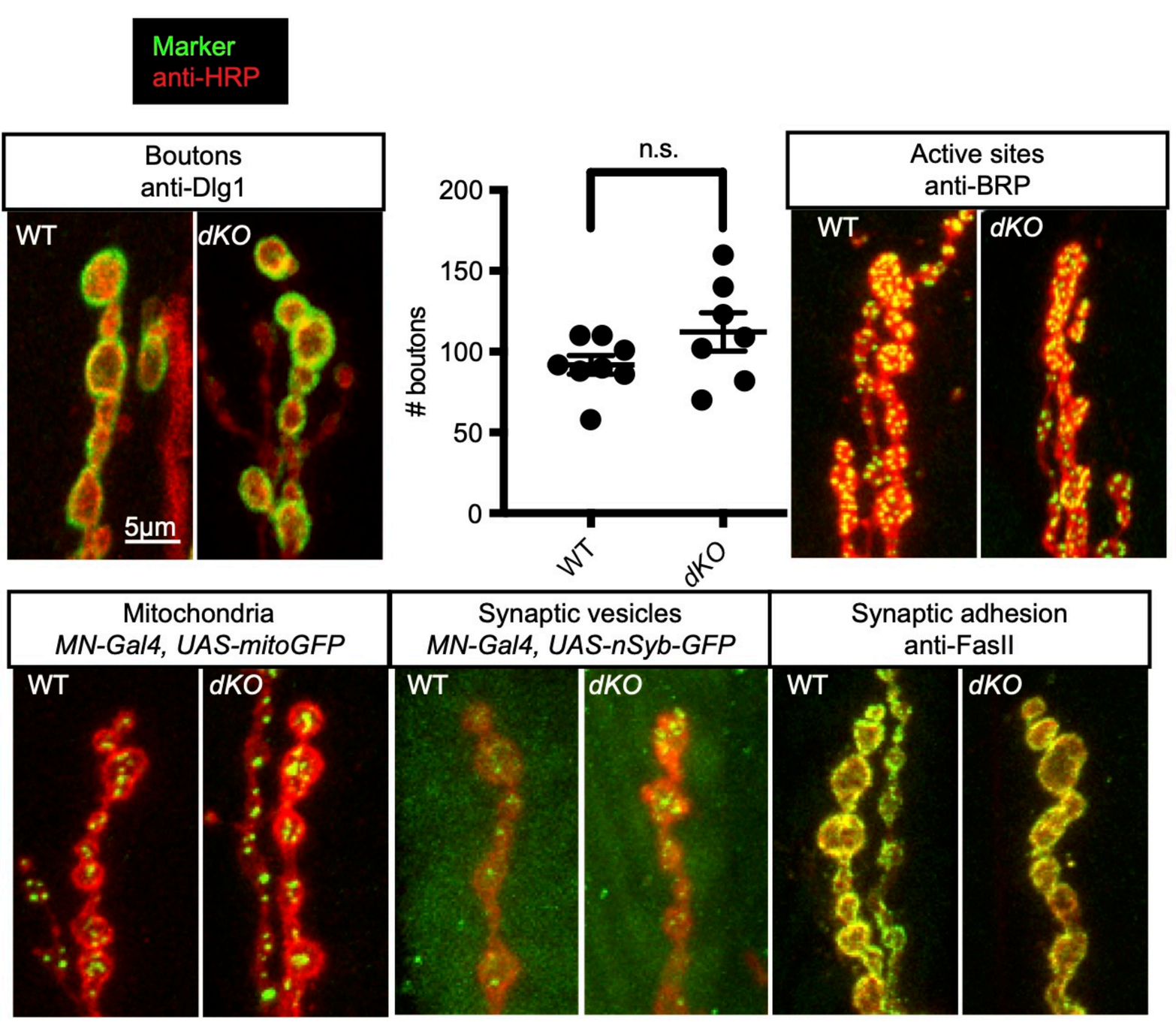

Figure 5-figure supplement 1

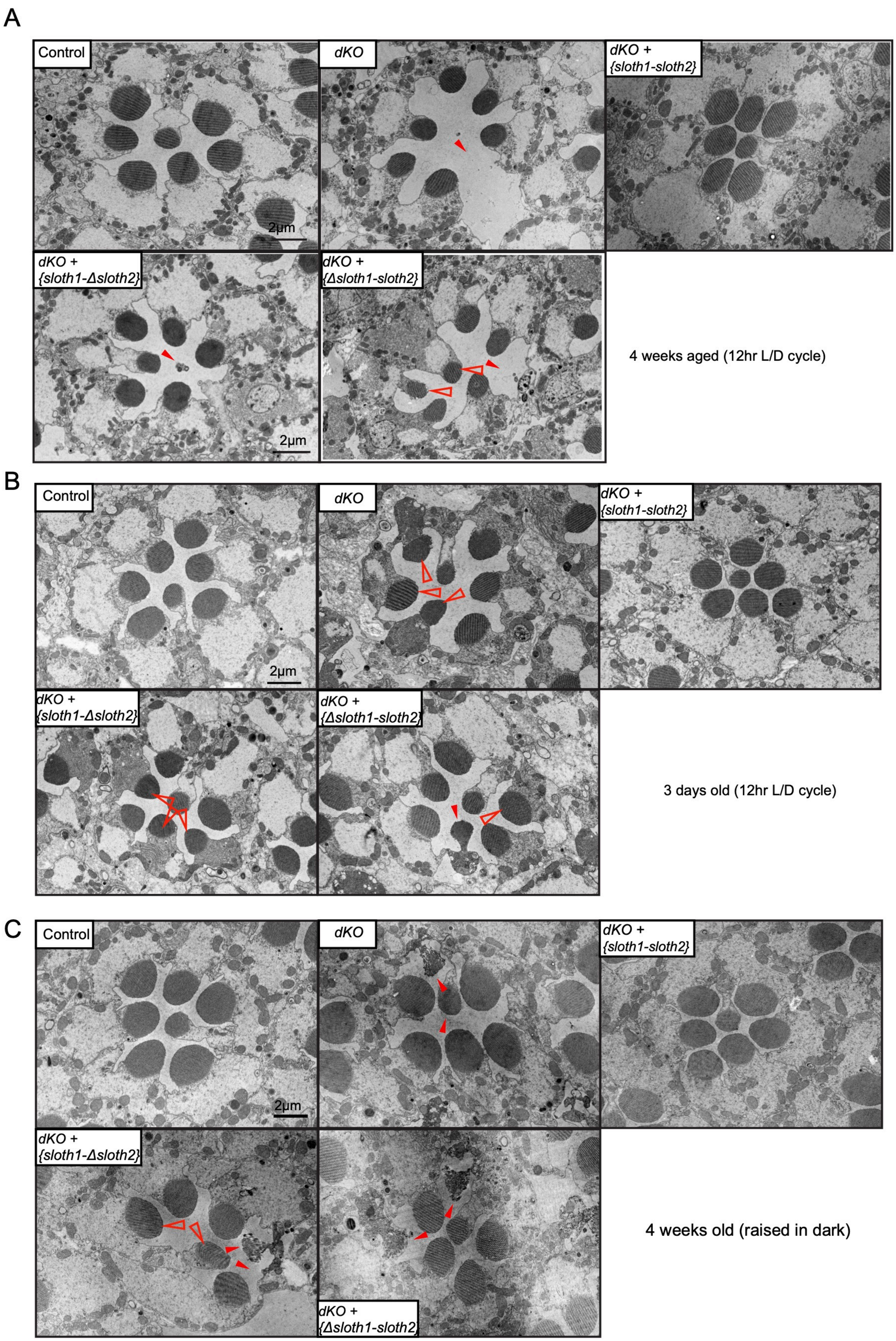

Figure 5-figure supplement 2

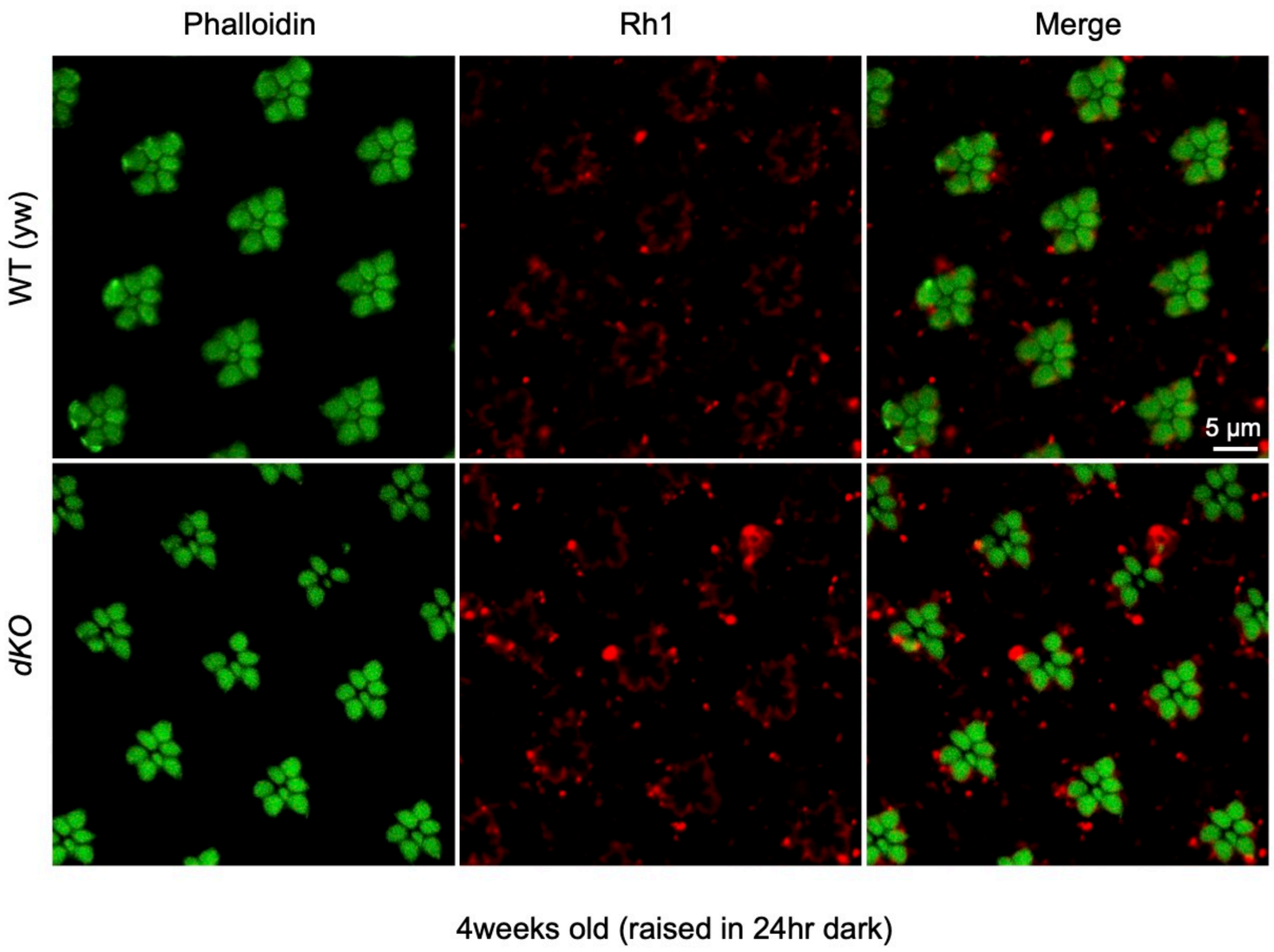

Figure 5-figure supplement 3

A

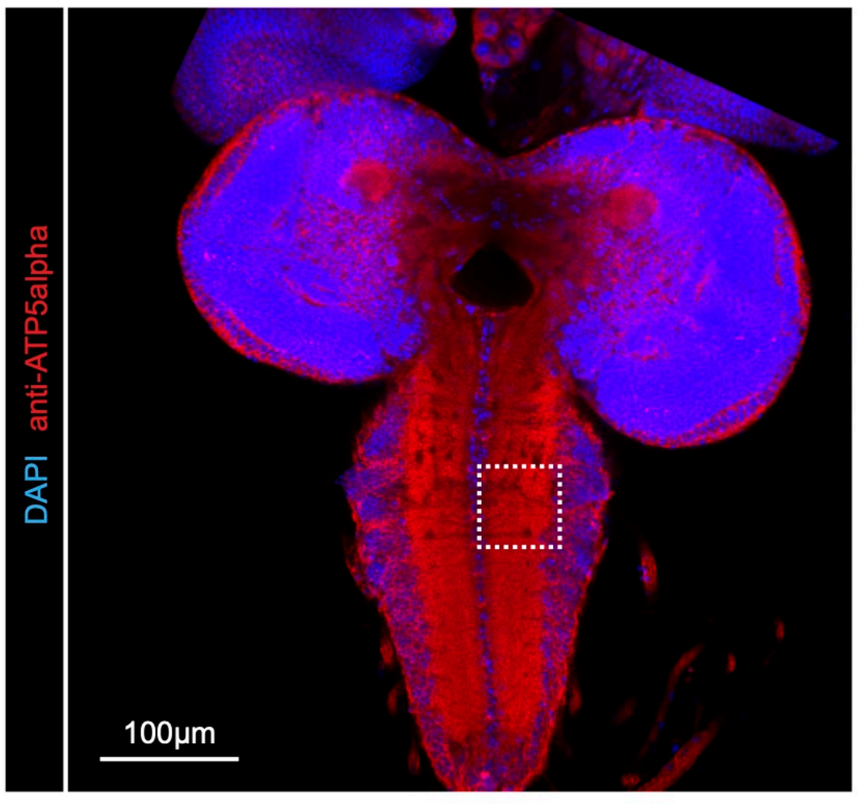

B

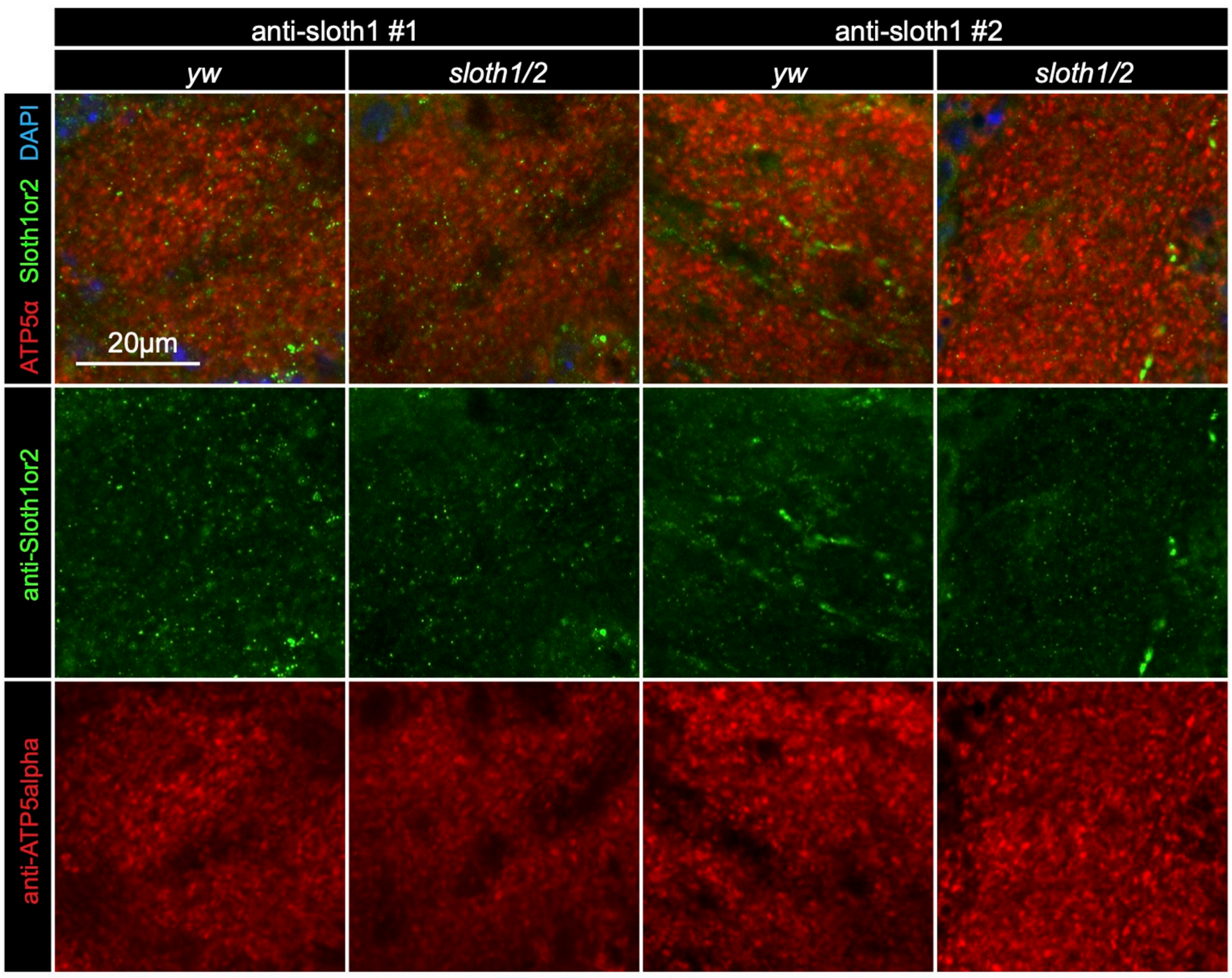

C

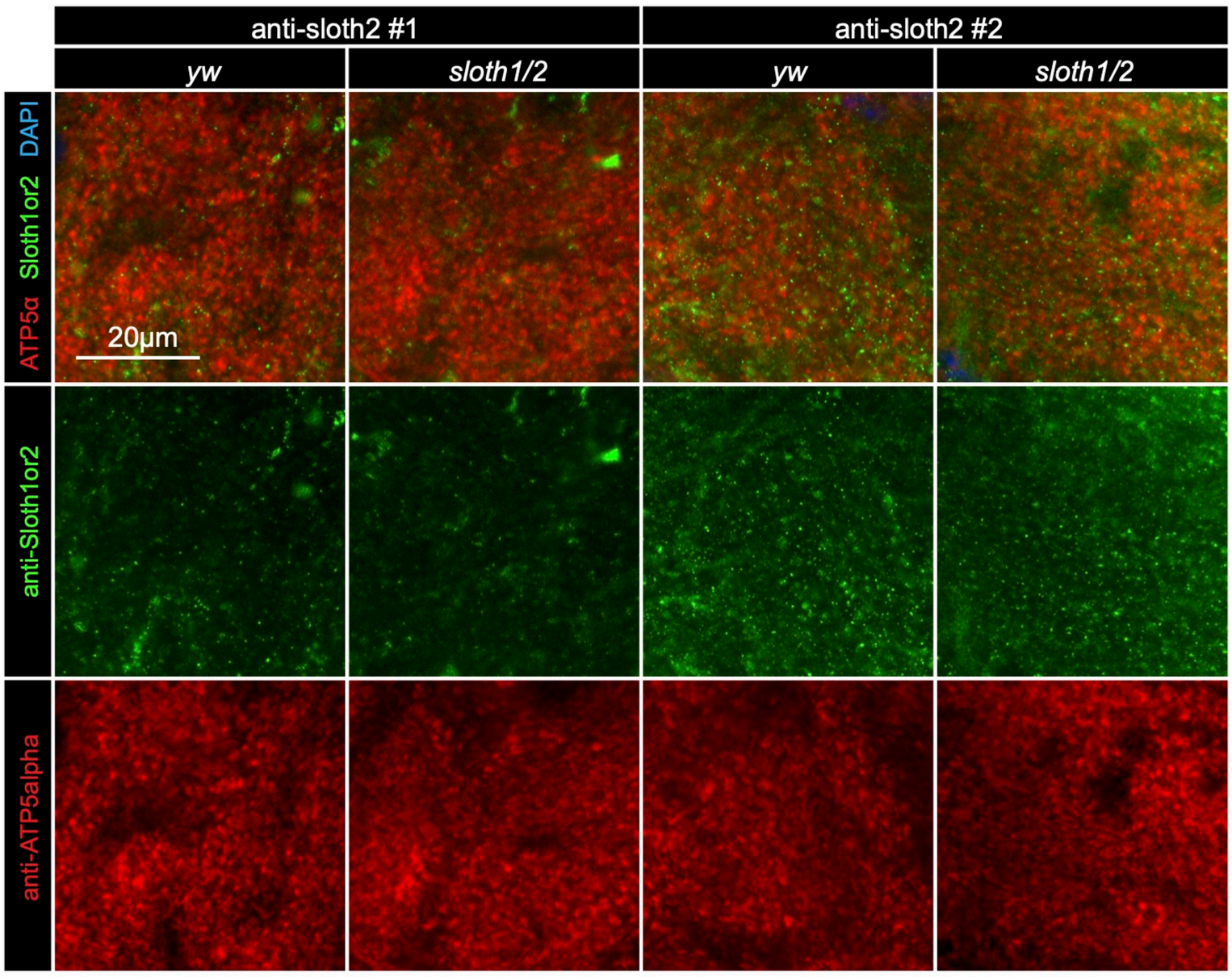

Figure 6-figure supplement 1

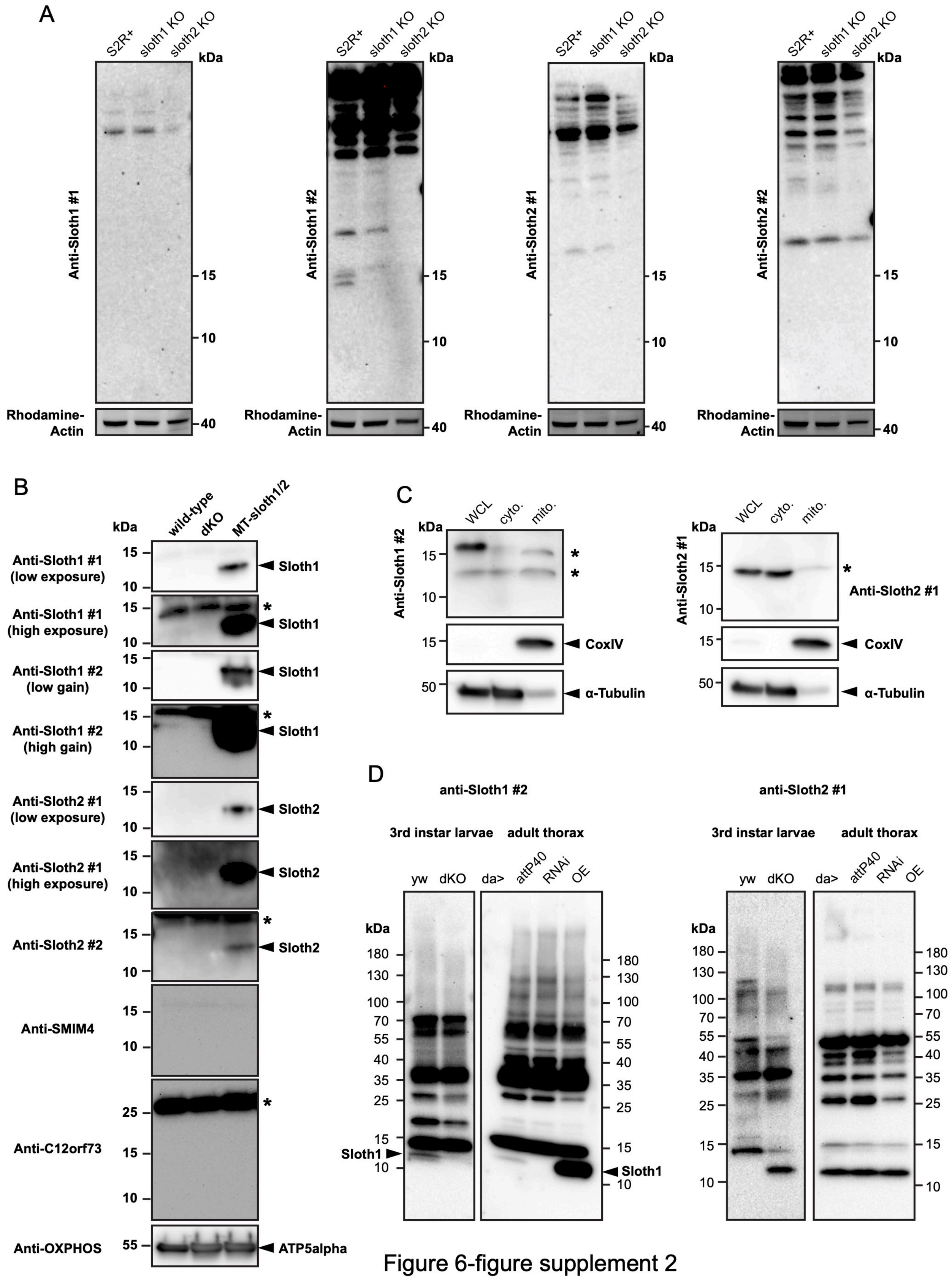

Figure 6-figure supplement 2

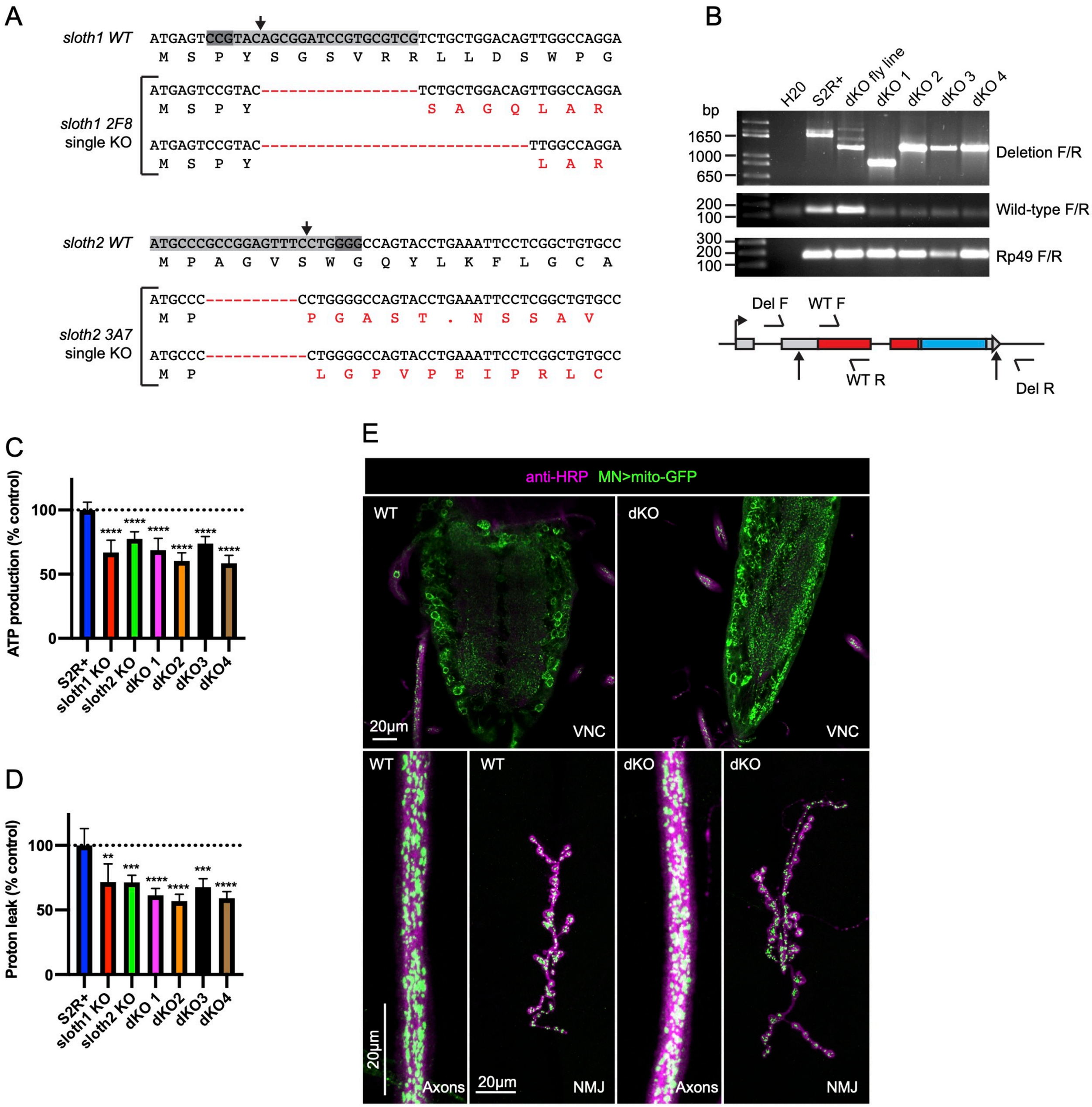

Figure 7-figure supplement 1

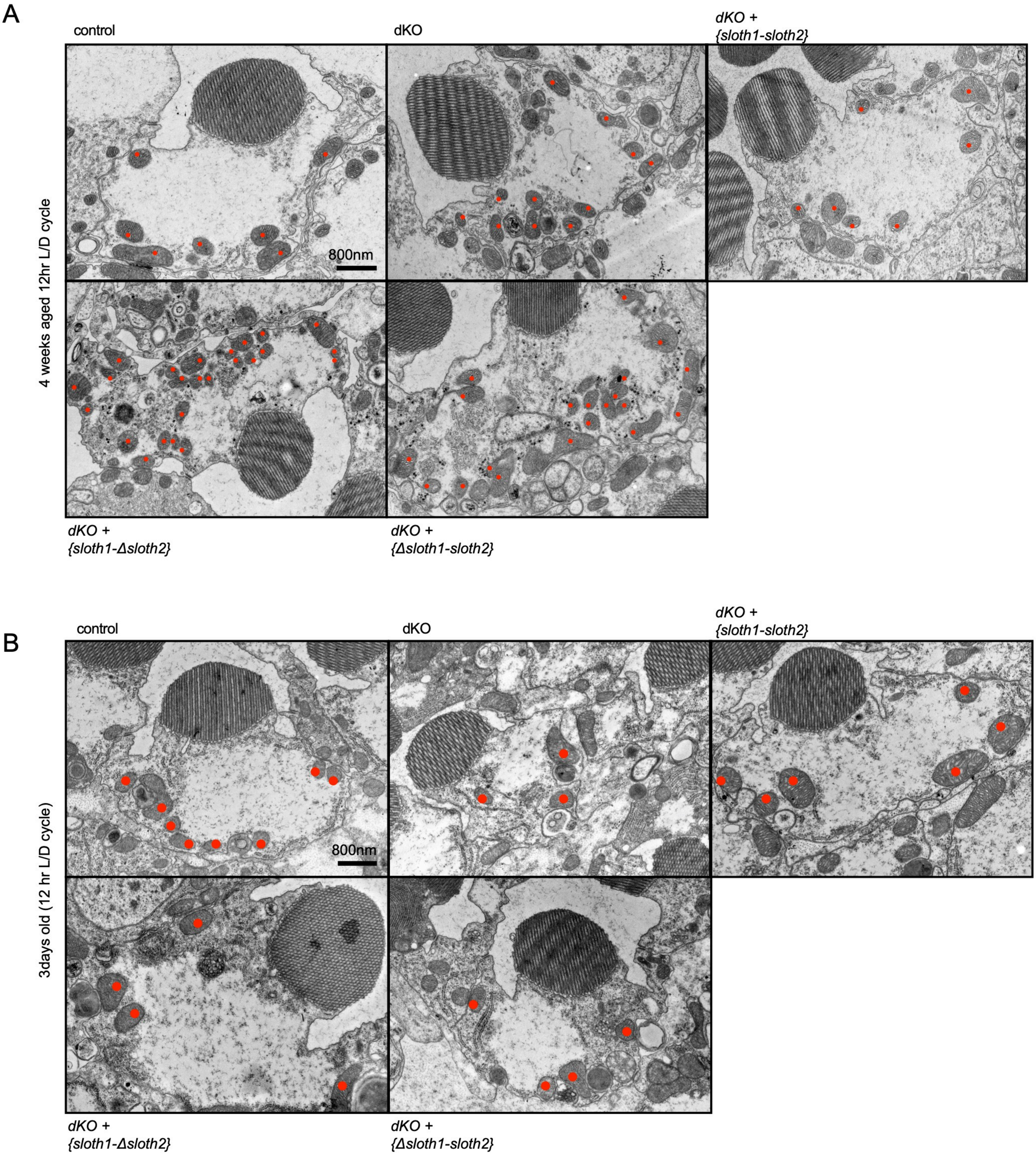

Figure 7-figure supplement 2